Electrochemical Energy Reviews (2023) 6:24
https://doi.org/10.1007/s41918-023-00192-8

REVIEW ARTICLE

Emerging Atomic Layer Deposition for the Development of High-Performance Lithium-Ion Batteries

Sina Karimzadeh[1] · Babak Safaei[1,2] · Chris Yuan[3] · Tien-Chien Jen[1]

Received: 14 June 2022 / Revised: 16 November 2022 / Accepted: 4 April 2023 / Published online: 12 July 2023

Abstract

With the increasing demand for low-cost and environmentally friendly energy, the application of rechargeable lithium-ion batteries (LIBs) as reliable energy storage devices in electric cars, portable electronic devices and space satellites is on the rise. Therefore, extensive and continuous research on new materials and fabrication methods is required to achieve the desired enhancement in their electrochemical performance. Battery active components, including the cathode, anode, electrolyte, and separator, play an important role in LIB functionality. The major problem of LIBs is the degradation of the electrolyte and electrode materials and their components during the charge−discharge process. Atomic layer deposition (ALD) is considered a promising coating technology to deposit uniform, ultrathin films at the atomic level with controllable thickness and composition. Various metal films can be deposited on the surface of active electrodes and solid electrolyte materials to tailor and generate a protective layer at the electrode interface. In addition, synthesis of microbatteries and novel nanocomplexes of the cathode, anode, and solid-state electrolyte to enhance the battery performance can all be attained by ALD. Therefore, the ALD technique has great potential to revolutionize the future of the battery industry. This review article provides a comprehensive foundation of the current state of ALD in synthesizing and developing LIB active components. Additionally, new trends and future expectations for the further development of next-generation LIBs via ALD are reported.

Keywords Atomic layer deposition · Li-ion batteries · Electrodes · Solid-state electrolytes · Separators

Abbreviations

LIBs	Lithium-ion batteries
ALD	Atomic layer deposition
PEALD	Plasma-enhanced ALD
ALE	Atomic layer epitaxy
CVD	Chemical vapor deposition
PVD	Physical vapor deposition
PLD	Pulse laser deposition
SSEs	Solid-state electrolytes
TSSB	Thin-film solid-state batteries
GPC	Growth rate per cycle
TFELs	Electroluminescent hashtags
TMA	Trimethylaluminum
LCO	$LiCoO_2$
LMO	$LiMnO_2$
LNO	$LiNiO_2$
LFP	$LiFePO_4$
LMR	$Li_{1.2}Mn_{0.6}Ni_{0.2}O_2$
NMC	$LiNiMnCoO_2$
NMC811	$LiNi_{0.8}Mn_{0.1}Co_{0.1}O_2$
NMC333	$LiNi_{1/3}Mn_{1.3}Co_{1.3}O_2$
NMC532	$LiNi_{0.5}Mn_{0.3}Co_{0.2}O_2$
NMC662	$LiNi_{0.6}Mn_{0.2}Co_{0.2}O_2$
NCA	$LiNi_{0.8}Co_{0.15}Al_{0.05}O_2$
LNMO	$LiNi_{0.5}Mn_{1.5}O_4$
LTO	Lithium titanate
$LiTaO_3$	Lithium tantalate
TMO	Transition metal oxide

✉ Tien-Chien Jen
tjen@uj.ac.za

Sina Karimzadeh
skarimzadeh@uj.ac.za

Babak Safaei
babak.safaei@emu.edu.tr

Chris Yuan
chris.yuan@case.edu

[1] Department of Mechanical Engineering Science, University of Johannesburg, Johannesburg 2006, Gauteng, South Africa

[2] Department of Mechanical Engineering, Eastern Mediterranean University, Famagusta, North Cyprus Via Mersin 10, Turkey

[3] Department of Mechanical and Aerospace Engineering, Case Western Reserve University, Cleveland, OH 44106, USA

LLOs	Li-rich layered oxides
PO_x	Trimethyl phosphate
VOTP	Vanadium (V) oxytripropoxide
Li(thd)	Lithium triethylborohydride
LiCp	Lithium pentamethylcyclopentadienide
LiHMDS	Hexamethyldisilazane
Li(hfac)	Lithium hexafluoroacetylacetone
LiTMSO	Lithium trimethylsilanolate
GO	Graphene oxide
GF	Graphene foam
LLCZN	Garnet ($Li_7La_{2.75}Ca_{0.25}Zr_{1.75}Nb_{0.25}O_{12}$)
LPO	Li_3PO_4
NMC	$LiNi_{0.76}Mn_{0.14}Co_{0.10}O_2$
TMP	Trimethyl phosphate
LiO^tBu	Lithium *tert*-butoxide
TEOS	Tetraethylorthosilane
TDMASn	Tetrakis(dimethylamino)tin (IV)
TDMA-Al	Tris(dimethylamido)aluminum(III)
Ta(OEt)	Tantalum(V) ethoxide
$Nb(OEt)_5$	Niobium(V) ethoxide
LNO	Lithium niobium oxide
TiI_4	Titanium tetraiodide
TGA	Thermogravimetric analysis
SEM	Scanning electron microscopy
TEM	Transmission electron microscopy
XPS	X-ray photoelectron spectroscopy
EIS	Electrochemical impedance spectroscopy
TTIP	Titanium isopropoxide
DEPA	Diethyl phosphoramidate plasma
CE	Coulombic efficiency
DEZ	Diethylzinc
ZTB	Zirconium tert-butoxide
Hfac	Hexafluoroacetylacetone
TDMAT	Tetrakis(dimethylamino)titanium
SSA	Specific surface area
SEI	Solid electrolyte interface
CFP	CNT network/carbon fiber paper
VTIP	Vanadyl triisopropoxide
$RuCp_2$	Bis(cyclopentadienyl)ruthenium
$Mo(CO)_6$	Molybdenum hexacarbonyl
$Hf(NMe_2)_4$	Tetrakis(dimethylamino)hafnium
NC	Nitrogen-doped carbon
TDMA-Al	Tris(dimethylamido)aluminum (III)
OLEs	Organic liquid electrolytes
EMC	Ethyl methyl carbonate
DEC	Diethyl carbonate
DMC	Dimethyl carbonate
LAGP	Lithium aluminum germanium phosphate
PVDF-HFP	Polyvinylidene fluoride-hexafluoropropylene
R2R	Roll-to-roll
PP	Polypropylene
PE	Polyethylene
TEOS	Tetraethoxysilane
$Ta(OEt)_5$	Tantalum(V) ethoxide
TIB	Titanium monoboride
$Al_2(NMe_2)_6$	Tris(dimethylamino)aluminum dimer
APTES	(3-Aminopropyl)triethoxysilane
BDEAS	Bis(diethylamino)silane
$Mg[EtCp]_2$	Bis(ethylcyclopentadienyl)magnesium
AAO	Anodic aluminum oxide
LPZ	Lithium polyphosphazene
OER	Oxygen evolution reaction
HER	Hydrogen evolution reaction
PET	Polyethylene terephthalate
TPA	Dicarboxylic acid

1 Introduction

Currently, with the progress in high-performance energy storage systems and the increase in the demand for their application in electric and hybrid electric vehicles (EVs and HEVs) [1], electronic devices, aerospace applications, etc., high power density, high energy density, and reliability concepts are being presented [2-4]. Expanding the use of LIB technology can be one of the most effective solutions to convert solar and wind energy and decrease the dependence on the use of fossil fuels, thereby alleviating air pollution and global warming [5, 6]. Rechargeable batteries have been adopted in various applications for more than 100 years, and thus far, lithium-ion batteries (LIBs) have been considered ideal and reliable power storage devices with a long service life and a high gravimetric/volumetric energy density, making them the commonest commercial battery type. However, LIBs are insufficient in many aspects to fully supply the energy of high-power EVs. Therefore, in-depth research is being conducted on improvement and development of the next generation of LIBs.

To achieve ideal performance, several factors must be considered in designing LIBs, such as the implementation of three-dimensional (3D) porous materials, including nanofibers and nanotubes, and layered structures to engineer the surface valence state. An increase in the area of the electrode–electrolyte interface facilitates the diffusion of active Li ions for faster transfer and improved reaction [7]. In this regard, the application of methods such as coating is an effective way to reduce costs by utilizing less expensive materials and to improve the stability, energy density, power density, self-discharge mitigation, energy capacity, and charge/discharge rate as well as increase the lifespan and safety [8].

Atomic layer deposition (ALD) is an exclusive deposition technique that provides a conformal ultrathin film on the substrate based on alternation of reactant and precursor exposure in a reactor, and its self-limiting feature enables

controllable precise film growth and composition at the atomic level. ALD is a promising technology in modern industries that require high-aspect-ratio structures such as thin-film solid-state batteries and semiconductors in microelectronics [9]. ALD was first used by Suntola et al. [10] in 1970 in Finland and was first implemented as atomic layer epitaxy (ALE) in the production of electroluminescent hashtags (TFELs) with the introduction of a ZnS thin film. Other applications, such as in the development of semiconductors, fuel cells, catalysts, batteries, capacitors, drug delivery devices, and dental and orthopedical implants, have been widely investigated in academic research institutes and industries [11-14]. In addition, ALD has the potential to enable additional scientific research in the future due to the discovery of novel precursors. Numerous scientific studies on ALD have been published [15-18]. However, ALD can only deposit inorganic materials. A technique similar to ALD, developed in the 1990s, to deposit organic polymers such as polyamine, polyamide, polyurethane, polythiurea, polyimide, polyester, polyimide amide, polyurea, and hybrid films including integration of metal atoms such as superstructures and nanolaminates, can be realized by adopting a combination of ALD and molecular layer deposition (MLD) [19]. Organic−inorganic hybrids were made possible by combining ALD precursors with all-organic precursors in the 2000s.

The attractive possibility of realizing new functions is provided by hybrid materials, which permit the utilization of the material properties of both their organic and inorganic components. Hybrid materials in the form of thin films have the potential to provide breakthroughs in a number of technological application areas. Notably, synthesizing organic and inorganic building blocks at the molecular scale is challenging because different preparation conditions are needed to form organic and inorganic networks.

ALD is a unique coating method that can be used for LIBs development, and its application lies in (i) design and fabrication of nanostructured LIB components, (ii) tailoring of the interface between the components, and (iii) modification of the electrochemical properties of LIB active components (Fig. 1). In addition, compared to traditional wet chemical techniques, ALD surface deposition results in a more uniform surface coating, without excessive harmful reactants. Therefore, LIB application at the industry level can easily be scaled up via ALD.

In general, the components of LIB cells include the following: the positive electrode (the cathode) is in the form of lithium metal oxides (such as $LiCoO_2$, $LiMnO_2$, and $LiFePO_4$) that commonly have layered, spinel, and olivine structures [20]. The negative electrode (the anode) material, made of graphite, silicon, etc., is layered or porous [21]. The electrolyte is in the form of a gel or in the solid state (such as $LiFP_6$, Li_2SiO_3, and $LiTaO_3$) [22], and the separating insulating layer is conductive for Li ions [23]. To

Fig. 1 Application of ALD in LIB advancement

provide a sense to the reader of the variety of crystal structures exhibiting fast ion conduction, some typical crystal structures depicted in Fig. 2 are discussed in this section. Generally, the diffusion topology in ion conductors can be identified based on the dimensionality, for instance, one-dimensional (1D) in tavorites and olivine $LiMPO_4$ (Fig. 2g, h), two-dimensional (2D) in layered $LiCoO_2$ and graphite (Fig. 2a, j, respectively), and 3D in the spinel, garnet, natrium superionic conductor (NASICON) [24], thiophosphate ($Li_{10}GeP_2S_1$) and antiperovskites (Fig. 2b, c, d, f, i, respectively). Notably, such classifications have inherent subjectivity; for instance, $Li_{10}GeP_2S_{12}$ (Fig. 2c) could be considered either a 3D or pseudo-1D conductor. However, diffusion dimensionality has prominent significance for the macroscopic conductivity in materials, as do the ion migration barriers. Accordingly, infiltration paths with ion diffusion activation barriers of < 600 meV (~ 58 kJ mol^{-1}) are favorable for electrode applications, whereas activation barriers have to be < 300 meV (~ 29 kJ mol^{-1}) for solid electrolyte applications [25].

Figure 3 presents a schematic diagram of the components and working principles of LIBs. During charge, through the utilization of an external electrical potential, Li ions in the structure of the cathode are deintercalated, and these ions are intercalated by transferring and passing through the electrolyte into the anode. Due to these displacements of Li ions, an electron current from the cathode to the anode is generated. This current is conducted through current collectors, which are mainly made of aluminum in the cathode and copper in the anode. During discharge, these displacements of ions and electrons are reversed. Therefore, the materials incorporated in the structure of electrodes, as well as their

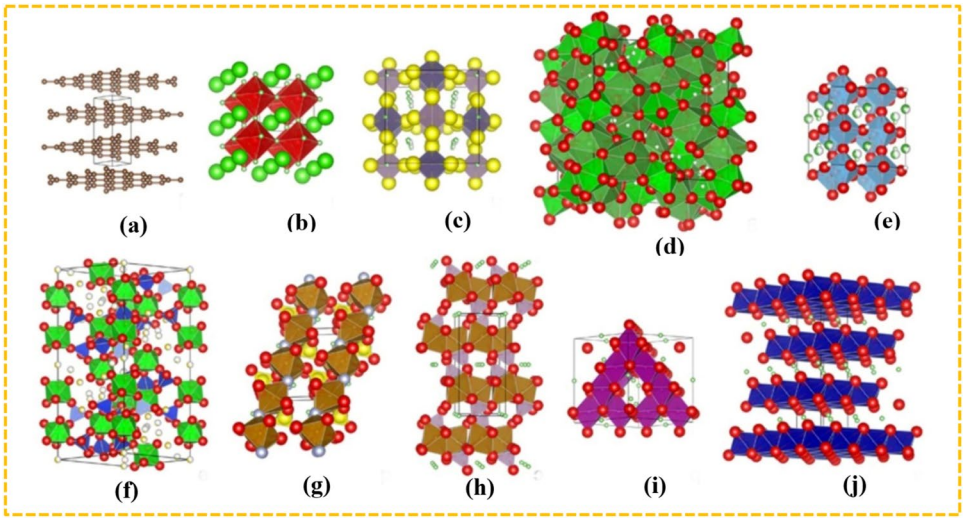

Fig. 2 Crystal structures of **a** layered graphite, **b** antiperovskite Li_3OCl, **c** thiophosphate $Li_{10}GeP_2S_{12}$, **d** garnet $Li_7La_3Zr_2O_{12}$, **e** $Na_3Zr_2Si_2PO_{12}$ perovskite $Li_{3x}La_{2/3-x}TiO_3$, **f** NASICON, **g** tavorite $LiFeSO_4F$, **h** olivine $LiFePO_4$, **i** spinel $LiMn_2O_4$ and **j** layered $LiCoO_2$. Reprinted with permission from Ref. [25]. Copyright © 2016, Zhi Deng et al.

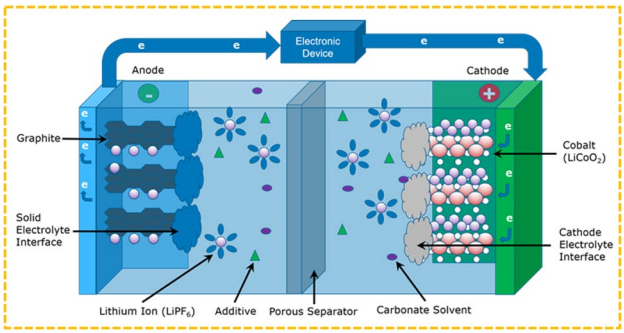

Fig. 3 Schematic illustration of the working principle of rechargeable LIBs. Reprinted with permission from Ref. [28]. Copyright © 2021, SHUTTERSTOCK

modification methods, significantly affect the electrochemical performance, such as the voltage and specific capacity, of LIBs [26, 27].

To date, extensive research has been conducted at industrial and laboratory scales on improving the electrode materials of LIBs as well as their capacity, stability, and safety and decreasing their production cost. However, further research and efficient theories are required to alleviate or completely resolve the problems and shortcomings in batteries. To address these challenges in LIBs, researchers around the world have continuously investigated effective solutions, including discovering nanostructured electrode materials, optimizing components, and applying novel methods in designing LIB cell configurations. One of these solutions is surface coating and surface modification of electrode materials. Recently, many extensive and promising studies on coating electrodes have been performed to improve the performance of LIBs [29, 30]. Different materials and methods have been applied for coating, considering the inherent properties of electrode materials and their application and development [29, 31]. Typically, coating of electrode materials can be achieved by two methods: doping and surface coating. The doping method is efficient in changing the physical morphological properties of materials by manipulating the crystalline configuration at the atomic scale with the aim of tailoring the bandgap, cation ordering, defect concentration, and charge distribution [32, 33]. Surface coating, by introducing a layer of a material with a certain thickness on the electrode surface, can significantly change the electrochemical properties of LIBs and improve their thermal stability, mechanical robustness, rate capability, ion transport, and capacity retention [34, 35]. Additionally, the coated layer can act as a protective or sacrificial layer to inhibit side reactions of the electrode material with the electrolyte [36]. Several studies have been performed to determine how well surface coatings can improve the electrochemical performance of batteries [37-40].

Common and traditional methods for growing films on electrode surfaces, such as the sol–gel [41], hydrothermal [42], mechanical mixing [43], chemical vapor deposition (CVD) [44], pulsed laser deposition (PLD) [45], ball milling [46], physical vapor deposition (PVD) [47], and wet chemistry [48] methods, have been implemented. These methods can face serious challenges in obtaining a uniform, smooth and pinhole-free surface with high film thickness, lack control of the film thickness, which can significantly affect the transmission of ions and electrons, and lack high precision in atomic deposition on the surface. For example, from the chemical point of view, in the PVD and sol–gel methods, the intermolecular strength among film and electrode surface atoms is not sufficiently strong since coating particles are randomly dispersed, and the film uniformity is not favorable due to the limited fluid dynamics of particles [49]. Additionally, in the CVD method, the high temperature of deposition (above 300 °C), especially in cases where

the coefficients of thermal expansion for the electrode and coating materials are different, results in the generation of stress and cracks on the film surface and therefore induces mechanical instability [50]. Moreover, poor material junctions and grain boundaries could result in inefficient charge transport and yield charge scattering. In the face of the above challenges, the emerging and promising method of ALD has been introduced with its multiple advantages and significant improvement and developments in super-thin deposition with atomic precision [51]. Due to the special capabilities and features of this technology, it is not only successfully applied in the preparation of cathode and anode electrodes as well as electrolytes of LIBs but also applied for modification of the electrode surface at the atomic scale in a controllable manner to tailor the electrochemical properties. This strategy has been considered a promising method to solve emerging problems in advanced electrical energy storage devices by producing complex nanostructured materials and/or surface modification.

Based on several advantages of ALD, this technology has been applied for developments in many industries, such as in LIBs, catalysts, drug delivery and discovery, fuel cells, microelectronics, supercapacitors, semiconductors, and photovoltaics, and has been successful and efficient [14, 52-54]. Therefore, the practical energy density, structural stability, reaction kinetics, and mass transfer diffusion of ALD-fabricated materials can be significantly enhanced. Schematics of thin film deposition on heterogeneous substrates using CVD, PVD, sol–gel, and ALD for comparison are illustrated in Fig. 4. Furthermore, Table 1 compares the different surface coating methods with respect to their advantages and disadvantages. Due to the increasing popularity of ALD for LIBs, here, we discuss the latest developments and progress in the ALD strategy for advanced LIBs regarding the ever-expanding studies. After the introduction section, the working principle, mechanism, and attributes of ALD are reviewed. Unique engineering of electrode–electrolyte interface junctions on the basis of ALD provides extraordinary synergistic influences on the electrochemical properties and improves the

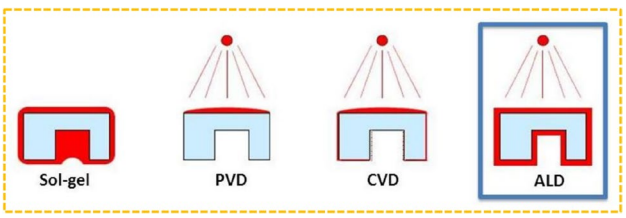

Fig. 4 Schematics of thin film deposition on complex surfaces by the sol–gel, PVD, CVD, and ALD methods. Reprinted with permission from Ref. [55]. Copyright © 2010, Peter M. Martin. Published by Elsevier Inc. All rights reserved

structural stability of solid-state electrolytes (SSEs) and electrode materials.

The Scopus database (Web of Science) was used to collect the documents to be reviewed in this article. While doing so, two sets of keyword strings, "Atomic Layer Deposition" and "Lithium-ion Battery," were applied. As a result of using the aforesaid two keyword search strings, 1 201 document results reported from 2000 to 2022 emerged in Scopus. Note that documents were obtained from this database (Scopus) on November 5, 2022. Statistical allocations of documents by year and region are shown in Figs. 5 and 6, respectively. Figure 5 depicts the allocation of documents reported between 2000 and 2022, both years inclusive. Evidently, there were few documents reported before 2010. Furthermore, the graph shows that the applications of LIBs recently, i.e., within the last decade, captured the attention of researchers, and as a result, numerous studies were proposed and investigated.

In the earlier years of development, i.e., from 2010 to 2016, approximately 15 documents were reported in 2010, 25 documents in 2012, 48 documents in 2013, 59 documents in 2014, and 93 and 82 documents in 2015 and 2016, respectively. Subsequently, from 2017 to date (2022), there was a drastic increase in the number of reported studies. This evidently shows that the applications of high-performance LIBs have recently attracted substantially greater scholarly interest because of their spontaneous advantages in several fields of study. However, a decrease in the number of studies reported in 2022 is found, which can be due to the impact of the COVID-19 pandemic. In addition, Fig. 6 illustrates the number of publications based on the region in the last decade.

Therefore, in the current review, we provide a general description of the fundamentals and characteristics of ALD processes and identify four widely used lithium precursors following this introduction. In the following section, we succinctly discuss the working mechanism of LIBs and briefly discuss the advantages of ALD. Then, the latest developments and advancements realized with ALD lying in three aspects are specified and highlighted: (i) designing and synthesizing nanostructured LIB components, (ii) tailoring the interface to optimize the surface and interfacial surroundings of LIB components, and (iii) modifying LIB materials. Meanwhile, we focus on some successful case studies that used ALD to resolve LIB issues. Then, we summarize the most exciting studies for the creation of full cells of 3D thin-film solid-state batteries (TSSBs) and the accomplishments realized with ALD in the design of nanostructured components. Finally, we focus on the paramount importance of ALD in next-generation LIBs along with its prospective applications in LIBs for future research. Additionally, renovation of the

Table 1 Comparison of different surface coating methods in terms of their advantages, disadvantages, and applications; 1 Å = 1×10^{-10} m

Surface coating method	Coating accuracy	Advantages	Disadvantages	Application
ALD	1 Å	Uniform coating Precise and adjustable deposition thickness Highly reactive precursor High film density Low temperature and stress Excellent adhesion Great stoichiometry	Expensive Complicated preparation process High material waste rate Slow deposition rate Fewer precursors available than in CVD	Electronic chips Sensors Fuel cells Batteries Solar cells Drug delivery HER & OER catalysts Wear resistance
CVD	10 Å	Various precursor availability High deposition rate Good reproducibility Simple	Less reactive precursors Not suitable for polymers and very thin films Requires a high substrate temperature	Sensors Batteries Integrated circuits Optoelectronics Semiconductors Wear resistance Catalysts Powder production
PVD	0.1 μm	Safer than CVD (no toxic material) Low temperature Thin coating Low cost Relatively fast process	Nonuniform deposition Requires an annealing time Low deposition rate No stoichiometry Compressive stress	Semiconductors Optical devices Wear resistance Nanocomposites Aluminized PET film for food packaging Solar cells
PLD	0.1 μm	Simple deposition process Low substrate temperature Versatile Short test period High deposition rate	Small area deposition Slow deposition rate Impurities	Optoelectronics Orthopedics & biomedical devices Luminescence Superconductors
Sol–gel	1 μm	High adhesive strength Low cost Simple to perform No need for a conductive substrate Low temperature	Nonuniform deposition Nonadjustable coating High temperature required to synthesis anatase nanocrystals	Pharmaceuticals Separators Batteries Biosensors Electronics Optical devices Energy devices
RF Sputtering	1 nm	High purity Precise control of the film thickness and surface roughness High deposition rate	High operational cost Possible microfilm cracks Li loss during heat treatment Unsatisfactory ionic conductivity	Batteries Wear protection Sensors Optical devices Semiconductors Solar cells Biomedical devices
Hydrothermal	1 μm	Dense morphology Simple Low cost Versatile Environmentally friendly	Long production time Severe conditions	Crystal synthesis Batteries Photocatalysts Wear resistance Sensors Solar cells
Ball Milling	0.1 mm	Low cost Easy procedure Suitable for scale up production	Discontinuous coating layer Nonuniform coating on particles Easy to pollute and collapse the sample	Powder manufacturing Batteries Hydrogen storage Solar cells Nanocomposites

ALD reactor design to increase its manufacturing capability and the chance of using this approach to develop future energy storage devices are discussed.

2 Principles of ALD

ALD is characterized by sequential gas phase chemical reactions with a solid substrate, and film growth is

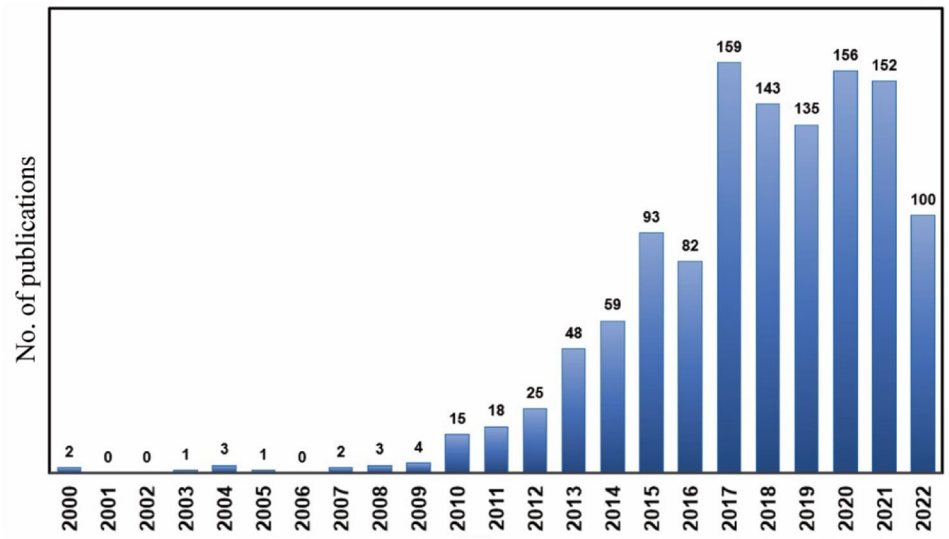

Fig. 5 Demonstration of the publication number per year from 2000 to 2022

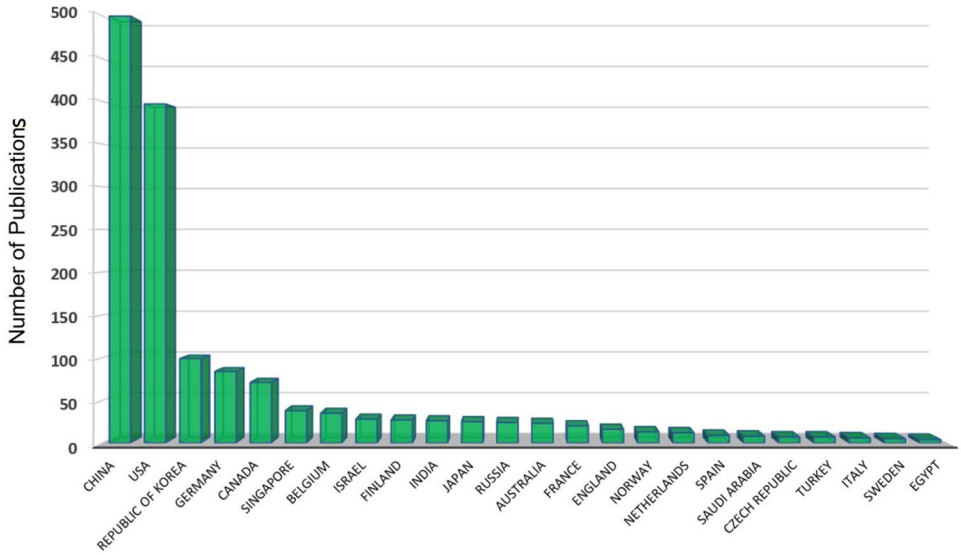

Fig. 6 Demonstration of the publication number per country in the last decade (from 2012 to 2022). The following keywords were used in the Web of Science search: lithium-ion battery and atomic layer deposition

accomplished by exposure to sequential precursors and reactors. ALD has the capability to coat various kinds of materials at the angstrom level in terms of film thickness and composition, with the film having the characteristics of being sequential, uniform, self-limiting, pinhole-free, and without cracks. ALD is a particular type of CVD that has no limitations, such as steady-state film growth and the simultaneous presence of precursors and high operating temperatures, which are common in CVD. The ALD process is usually performed at room temperature or below 350 °C. The low working temperature for coating in this method has the great advantage of being able to use brittle and high-temperature sensitive materials such as inorganic compounds, polymers, drug molecules, and precursors that become unstable at high temperatures [56, 57]. Many various materials can be deposited by the ALD method, including elements, metal oxides, nitrides, fluorides, sulfides, selenides, phosphides, tellurides and metal–organic frameworks (MOFs) [58-62], each of which can be used in various applications according to their properties. ALD is a widely used approach in the manufacture of microelectronic and semiconductor devices, electrodes and nanomaterials to shrink the size and boost the performance [63]. Nevertheless, ALD has some limitations, including a low growth rate and expensive equipment and precursors. Therefore, determining the optimal conditions for each ALD experiment is important.

Figure 7 illustrates the general deposition process of two precursors as sources on a substrate by ALD. The ALD process is carried out cyclically, and the precursors are kept separate during the reaction; thus, the precursor reactions are divided into two individual half-reactions. A typical ALD cycle consists of the following four steps: exposure of the first precursor-purging and exposure of the second

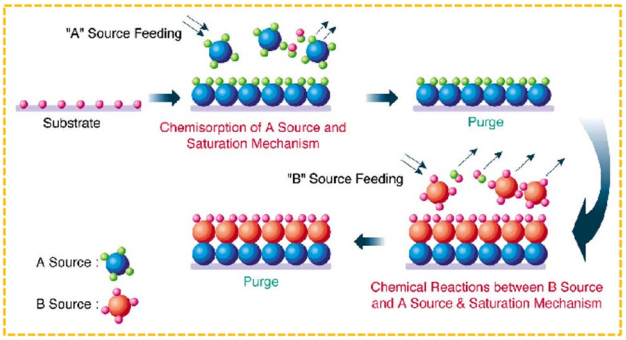

Fig. 7 Schematic representation of the general ALD binary reaction mechanism. Reprinted with permission from Ref. [64]. Copyright © 2012, Physics & High Technology

precursor-purging. The host substrate is in solid form and consists of a monolayer to multilayer surface that was previously activated with functional groups such as hydroxyl and oxide groups. This substrate is subsequently exposed to precursors or reactants, which usually include two, three, or four reactants. To reach gas saturation levels, precursor molecules can only interact with a limited number of surface sites on the substrate. The film growth process terminates after the surface sites are consumed. The reactor is then prepared for the subsequent precursor injection by purging away any remaining reactants and side products from the chamber through an inert gas such as nitrogen or argon. Then, by repeating this cycle, the film consisting of deposited atoms grows on the surface of the substrate to the desired thickness. Each deposition cycle has two half-cycles, the first of which is the time it takes for the surface to be exposed to the precursor. The second is the time it takes to evacuate residual products from the chamber (purging time). The time required to carry out an ALD cycle is the sum of these two time values.

Generally, in ALD, one monolayer of the film or less will be produced in one ALD cycle, which indicates the growth rate per cycle (GPC) of the ALD process. The GPC is calculated by dividing the thickness of the deposited film by the number of cycles (nm cycle^{-1}). The GPC is affected by a variety of factors, including the amount of precursor flux that reaches the substrate, reaction temperature, pulse and purge duration of reactants and the nature of the reactions between the surface and the precursor in the form of chemisorption. As mentioned, the GPC of the film and surface reactions of the precursor can be significantly affected by the temperature. An ideal ALD process follows the ALD window, in which the GPC is constant as a function of temperature and there is no GPC dependence on the temperature range (Fig. 8a). At low temperatures, the GPC can either increase owing to adsorption of the multilayer precursor or decrease due to limited reaction kinetics. However, at the high temperature end, the GPC can increase due to the decomposition of precursors or unwanted reactions [65]. At this point, the GPC can also decrease due to the low sticking constant of precursors, insufficient active sites, or precursor desorption.

The self-limiting feature of ALD is attributed to the limited reaction between the precursor and active sites of the surface, which react until the saturation limit is achieved or steric hindrance of precursors prevents further adsorption on the substrate. Successful film growth is highly dependent on the surface chemistry of the substrate because in some cases, the occurrence of other phenomena, such as diffusion or etching, is probable [66]. For instance, the surfaces of

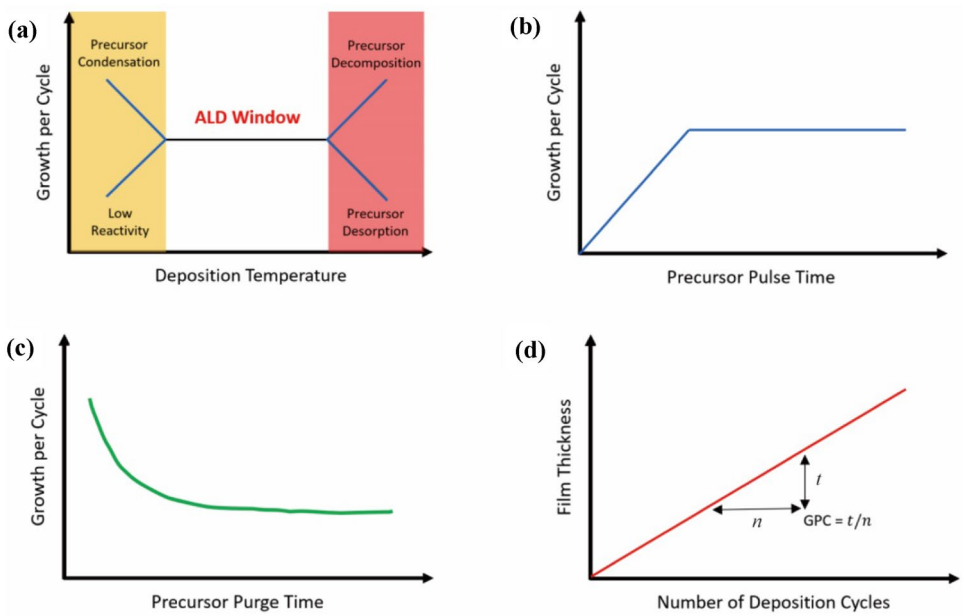

Fig. 8 Schematic demonstration of ALD features: **a** ALD window of the GPC independence from the deposition temperature, **b** GPC versus precursor pulse time, **c** GPC versus precursor purge time, and **d** film thickness versus the number of deposition cycles

carbonaceous materials such as carbon nanotubes (CNTs) and graphene are inactive until they are subjected to special treatment to create active surface groups to enable controlled deposition. Avoiding such pretreatment might lead to poor conformality and have an impact on the self-limiting tendency of a normal ALD cycle. Therefore, an increase in the precursor dose or pulse time will not lead to a higher GPC rate (Fig. 8b). Additionally, the purge time between precursor pulses should be sufficiently long to prevent excess precursor from adhering to the surface or remaining in the gas phase when the second precursor is introduced (Fig. 8c). By relying on the self-limiting behavior of ALD, control of the film thickness and good uniformity and conformality are achievable. Thus, after reaching a constant GPC, the desired film thickness can be controlled by the number of deposition cycles (Fig. 8d).

ALD is classified into two variants based on how the deposition reaction receives energy. Thermal ALD and plasma-enhanced ALD (PEALD) are two commonly used types of ALD that will be introduced in the following section.

2.1 Thermal ALD

Thermal ALD is a method in which heating generates the energy needed for surface reactions, and deposition is generally carried out at temperatures from 150 to 350 °C, at which chemisorption occurs between the precursor and the surface. This method has the ability to accurately control the thickness regardless of the surface geometry or chamber design. The precursor molecule can be considered ML_n, where M indicates a metal atom, L denotes the ligand surrounding M and *n* is the quantity of L. Trimethylaluminum (TMA) is one of the most well-known precursors with the chemical formula $Al(CH_3)_3$ for the fabrication of Al_2O_3 films with the assistance of the H_2O coreactant [67, 68]. First, with the ligand exchange reaction, the substrate surface with –OH is exposed to TMA, and TMA chemically dissociates with the chemisorption process, which can be defined as Eq. (1).

$$S@OH + Al(CH_3)_3(g) \rightarrow S@O@Al(CH_3)_2 + CH_4(g) \quad (1)$$

$$S@O@Al(CH_3)_2 + 2H_2O(g) \rightarrow S@O@Al(OH)_2 + 2CH_4(g) \quad (2)$$

where S@ OH denotes the substrate surface with OH functional groups.

After saturation, the remaining TMA and byproducts are purged away by inert gas. The H_2O vapor then reacts with the $Al(CH_3)_2$ group to form a hydroxylated Al_2O_3 surface and CH_4 byproduct, which is described as Eq. (2). By repeating the above four steps, the desired thickness of the Al_2O_3 film will be formed. Notably, despite the low reactivity of water vapor, it is the most conventional reactant for the oxidation of substrate surfaces in thermal ALD. Additionally, it can withstand high temperatures without decomposition.

2.2 Plasma ALD

Generally, the deposition temperature of ALD is in the range from100 to 350 °C, and the precursor reaction with the coreactant requires a certain amount of activation energy. In some cases, this temperature range is not desired when thermally fragile substrates are utilized, such as polymers in flexible electronics and drug powders. PEALD is a new ALD concept, in which reactive radicals such as ions and electrons are generated in the source gas during reaction with the assistance of plasma power. In the case of depositing single-element films such as semiconductors and metals that are not deliverable by thermal ALD, PEALD fulfils this need with the assistance of radicals. In other words, PEALD promotes the reaction process through the assistance of energetic species and radicals to reduce the precursors. The main advantage of PEALD is depositing films at low temperatures, even at ambient temperature, compared to thermal ALD. Therefore, it provides wider precursor and substrate material selection for growing thin films, utilizes less reactive metal and is thus cost effective. In PEALD, the stoichiometry of the process can be controlled, and impurities such as carbon contamination can be mitigated, improving the quality of thin films, with better density and less resistivity [69]. Another advantage of PEALD is decreasing the injection and purge time during the deposition cycle, especially for low-temperature processes, and it often has a better growth rate. Moreover, it removes the limitation of using water as the coreactant in thermal ALD by alternating it with other coreactants. The coreactants in PEALD are generally remote ozone O_3, oxygen O_2, nitrogen N_2 and mixed N_2/H_2 gases that are highly reactive. NH_3 and H_2S are commonly used as hybrids for nitrides and sulfides [70]. Additionally, despite the toxicity of H_2Se, it is also rarely used to produce a selenide layer [71]. Notably, the utilization of such toxic reagents requires a reactor with high design and safety standards to safely discharge the residual products. The coreactant molecules are typically ionized and dissociated by free electrons in the plasma, producing highly reactive species such as radicals (e.g., O or H, depending on the reactant gas). Hornsveld et al. [72] deposited a lithium carbonate (Li_2CO_3) film via an O_2 coreactant through PEALD. As a result, a wider range from substrate materials and precursors that are thermally fragile can be used in this method.

2.3 Lithium Precursors

Typically, ALD precursors contain metal atoms that are surrounded by organic ligands in the form of solid, liquid, or gaseous chemicals and held in a bubbler. The temperature of the bubbler is adjusted according to the chemical properties of the precursors. An ideal precursor needs to have high reactivity and lose all of its weight during reaction with the active sites of the substrate in one step at lower temperatures. Therefore, it can be characterized as a precursor with reasonable thermal stability and high volatility, which impacts the growth mechanism [73]. In addition, to select a proper precursor for an ALD study, a few physical properties should be taken into consideration, including the ALD conditions, material of interest, final application, reactivity to other reactants, and desired film features such as the electrical conductivity, current leakage, dielectric constant, photochemical activity, impermeability, antibacterial activity, and adsorption capacity. Therefore, selecting a suitable lithium precursor is crucial for the desired growth of lithium-containing films for LIB applications. In 2009, Putkonen et al. [74] researched the lithium precursors LiO^{t}Bu, Li(thd), LiCp, lithium dicyclohexylamide, and *n*-BuLi. Their research proved that LiO^{t}Bu and Li(thd) are more suitable and stabler precursors when used with H_2O and O_3 coreactants, respectively. In later years, other precursors such as lithium hexamethyldisilazane [LiHMDS, Li(N(SiMe$_3$)$_2$)] along with O_3 were introduced for the growth of lithium silicate films [75]. In other studies, this precursor was used for depositing Li_3N and Li_2CO_3 [76]. Thermogravimetric analysis (TGA) is a helpful tool for analyzing the volatility and stability of a precursor at a given temperature [77, 78]. For example, Hämäläinen et al. [75] proved that the Li (thd), LiO^{t}Bu, Li(N(SiMe$_3$)$_2$), and Li(hfac) precursors were sublimated without significant residues, indicating the suitability of these precursors. In another study, Meng et al. [79] reported that $LiOSiMe_3$ and lithium trifluoroacetate have good volatility potential as lithium precursors in ALD. Additionally, comparing them showed that $LiOSiMe_3$ is a more suitable option for ALD at temperatures above 300 °C. Other lithium precursors are lithium acetate, lithium benzoate, and lithium trimethylsilanolate (LiTMSO) [80-82]. Finally, thus far, four lithium precursors, i.e., $LiOSiMe_3$, Li(N(SiMe$_3$)$_2$), Li(thd), and LiO^{t}Bu, have been widely used since they are stable and high volatility precursors for the ALD process. Figure 9 shows the chemical structure of these four Li precursors.

3 ALD Application in the Development of LIB Components

Benefiting from the ability of ALD to deposit simple and complex metal oxides on each tiny particle, the generation of powder nanocoatings on the cathode and anode electrodes in LIBs is becoming increasingly popular, as it has proven to improve the lifetime of batteries, boost the battery capacity and significantly enhance safety [83]. ALD technology provides the most accurate, great performing, scalable, reproducible, and inexpensive coating method to mitigate undesired reactions and improve the battery efficiency. When batteries are stored for long periods of time or operated in various conditions, adverse reactions occur within the structure inside the batteries that cause battery damage and degradation and affect the battery performance. Due to ALD, most of these unfavorable reactions, such as the loss of lithium ions, transition metal dissolution, formation of dendrites on the cathode surface, formation of a solid electrolyte interface (SEI) layer, and the Jahn–Teller effect can be alleviated or eliminated by introducing a passivation surface [84]. Both anode and cathode materials and SSEs in 2D and 3D geometries have been successfully deposited by ALD [85, 86].

ALD coatings on a broad range from materials, including cathodes, anodes, SSEs, and separators, can improve the LIB performance in different applications. Overall, depending on the application, ALD can stabilize materials. These effects can result in higher capacity, higher voltage operation, less impedance creation across cycling, less gas production, improved safety, and longer cycle life and lifespan. Currently, numerous companies utilize ALD coatings for their particular electrode and SSE compounds, using high manufacturing ALD systems that can process 3 to 30 t of powder per day [87]. The advantages of ALD have been seen for the following cathode powder materials: NCM (811, 721, 622, 532), LCO, NCA, LMO (spinel and non-spinel types),

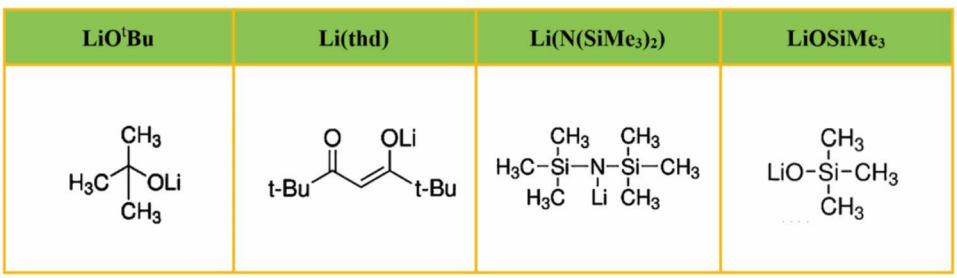

Fig. 9 Chemical structure of four different lithium precursors

and LMNO [88-92]. Additionally, anode powder materials include synthetic graphite, natural graphite, Si/C composites [93], silicon, and lithium titanate (LTO) [94-97]. In Ni-rich cathode materials, a higher Ni concentration results in lower stability and, more importantly, lower quality of the surface coating [98-100]. However, for Ni-rich materials, ALD coatings provide the most enhancement in comparison with other conventional coating methods [101]. Meanwhile, ALD coating of anode materials, even just a few deposition cycles, can significantly improve the voltage performance and cell cycle life. Nevertheless, applying an ALD coating on a combination of cathode and anode materials such as in LCO/graphite cells has even more benefits, including better capacity retention over the cycle life and a higher specific discharge capacity [91]. Aluminum oxide is the most preferred choice for many chemical processes and can improve battery performance parameters [102, 103]. Currently, many companies are looking for new materials and advanced coating mechanisms, such as those intended to improve the Li-ion conductivity and mobility. Advanced ALD coatings, including lithium metal oxides, metal fluorides and metal phosphates, are often suitable for LIBs and all-solid-state battery cells and may also be considered for hybrid oxide/carbon coatings, organic polymer coatings, sulfur coatings, etc. In the following section, we discuss the state-of-the-art LIB components, including the cathode, anode, electrolyte, and separator, and then review the importance of ALD for enhanced LIB performance.

3.1 Cathode Materials

One key component of LIBs that has been extensively researched is the positive battery electrode (the cathode). The LIB cathode electrode is the heaviest and most expensive component of lithium batteries compared to the anode and electrolyte components. Cathode materials are generally composed of transition metal oxides that can be oxidized by elimination of Li and transition to a higher valence state, i.e., reduction occurs at the cathode [104]. The stability of the cathode structure in the discharge and intercalation of Li is among the most critical factors affecting the performance of LIBs. Ideal cathode materials must possess the following properties: high reversibility of the intercalation/deintercalation of Li^+ ions through a stable process, high potential energy, the lowest possible Fermi level, low cost, high thermal stability and perfect compatibility with electrolytes to solve explosion problems [105]; however, fast Li^+ ion diffusion, high electronic conductivity involving ionic and electronic conductivity, environmental friendliness, and an easy synthesis method are also important. Fabrication of cathode materials with all of the above desirable properties is complicated and challenging. The properties of LIB cathodes can be classified based on their morphology and structure. Conventional LIB cathode materials include transition metal oxide-based compounds that have layered structures, such as $LiCoO_2$, spinel structures, such as $LiMn_2O_4$, and olivine structures, such as $LiFePO_4$. For high-energy systems, layered cathode materials are more favorable [106], and for low-energy systems, which require high stability and long life along with low cost, spinel and olivine cathode materials are generally preferred [107]. These cathode materials have presented high performance during charge/discharge cycling.

LCO was the first lithium-ion cathode material, which was introduced to the market by Sony in 1991 [108]. Because of its high capacity and good cyclability, it is still the most popular cathode for LIBs [109]. However, it has disadvantages such as toxicity, expense, and scarcity and suffers from capacity fading during frequent charge−discharge cycles such that its structural arrangement changes from monoclinic to hexagonal, resulting in an approximately 50% decrease in the practical capacity [110]. The theoretical specific capacity of LCO is 274 mAh g^{-1}; however, practically, only 50% of it is effective. In other words, only half of the lithium ions can electrochemically intercalate and be released from the structure of $Li_{1-x}CoO_2$ ($x=0.5$) to generate an electric current due to the instability of the structure at a high voltage of approximately 4.2 V versus Li^+/Li. This limitation is even severer for $x>0.5$ [111]. Numerous studies have been carried out to alleviate the drawbacks of LCO, for instance, nanofilm coating by metal oxides such as AL_2O_3 and TiO_2 as an artificial layer [112, 113].

Batteries based on Ni, i.e., $LiNiO_2$ (LNO), and Mn, i.e., $LiMnO_2$ (LMO), in the cathode are other layered battery types. Mn and Ni, which are abundant and nontoxic, can be considered environmentally friendly [114]. The materials of these batteries are inexpensive and have a lower production cost; therefore, these kinds of batteries have become popular among researchers. However, these batteries also have some limitations, such as the difficulty of fabricating pure forms and their low stability during charge compared to LCO [115]. Accordingly, in the deintercalation process, the layered structure becomes disordered and is converted to the spinel form, and then, Mn atoms disperse from the structure. These issues are a major obstacle to their widespread commercialization [116]. To mitigate these problems, extensive research has been conducted on the use of transition metal oxide materials, and various combinations have been developed, such as $LiNiMnCoO_2$ (NMC), $LiNi_{0.6}Mn_{0.2}Co_{0.2}O_2$ (NMC662), $LiNi_{0.5}Mn_{0.3}Co_{0.2}O_2$ (NMC532), $LiNi_{0.8}Mn_{0.1}Co_{0.1}O_2$ (NMC811), and $LiNi_{1/3}Mn_{1.3}Co_{1.3}O_2$ (NMC333) [117, 118]. These types of batteries have advantages such as high functional voltage, acceptable electrochemical stability, high thermal stability, good reversible capacity, cost effectiveness, and environmental friendliness. Despite their advantages, these

batteries still suffer from serious problems such as interfacial degradation and humidity vulnerability that drastically decrease their life [119, 120]. Another type of layered cathode material is Li-rich layered oxides (LLOs), which have a high capacity of 250–300 mAh g^{-1} [121]. However, they have some drawbacks, such as sudden Mn migration and loss of oxygen from the structure of the transition metal during primary charge, which result in significant voltage fading during cycling and irreversible capacity fade, resulting in a weak rate capability [122]. These limitations have also prevented the commercialization of these batteries. Cathodes with spinel-like materials such as $LiMn_2O_4$ have limitations such as the Jahn–Teller effect, which decreases their thermal stability [123], a relatively low discharge capacity (120 mAh g^{-1}), Mn migration, and oxygen loss, which require more research [124].

Future research on these novel frameworks will provide improved cathode materials for LIBs. In addition, their topics are still of interest to further improving the performance of the developed $LiFePO_4$/C cathode materials. Intercalation materials generally consist of M^{n+}, where M is a metal and $n+$ is the valence conversion of the metal M, and Li ions are regularized in the structure and surrounded by oxygen atoms in the octahedral and tetrahedral molecular geometry [125].

In 1980, Goodenough et al. [108] of Oxford University developed Li cathodes using transition metal oxides to increase the cell voltage. The concept of transition metal oxide intercalation depends on the charge/discharge reaction.

$$TMO_2 + xLi^+ + xe^- \rightleftharpoons Li_xTMO_2 \quad (3)$$

where "TM" is a transition metal such as Fe, Co, Ni, and Mn and the "x" value is in the range from 0 to 1 for monovalent cations.

The intercalation process can be considered to involve a metal network in which ions can deposit and migrate. Electrode materials act as hosts for Li and multivalent ions to maintain electroneutrality [126]. Cathode materials are divided into several categories according to their structure. Li-rich layered $Li_{1+x}M_{1-x}O_2$, layered $LiMO_2$, olivine $LiMPO_4$, spinel LiM_2O_4, silicate composite Li_2MSiO_4 and borate composite $LiMBO_3$, where M denotes a metal such as Fe, Mn, Ni, V, Co, Cr, and Cu, have been broadly researched [127-132]. Furthermore, many other cathode materials, such as MnO_2, V_2O_5, LiV_3O_8, and fluorides (FeF_3), have also been reported [133-136]. All of the above cathode materials have specific and different crystal structures (illustrated in Fig. 10) and present the desired capabilities and promising potential.

In Table 2, the practical properties of some commonly applied LIB cathode materials are summarized. Additionally, Fig. 11 presents the potential/capacity ranges of various

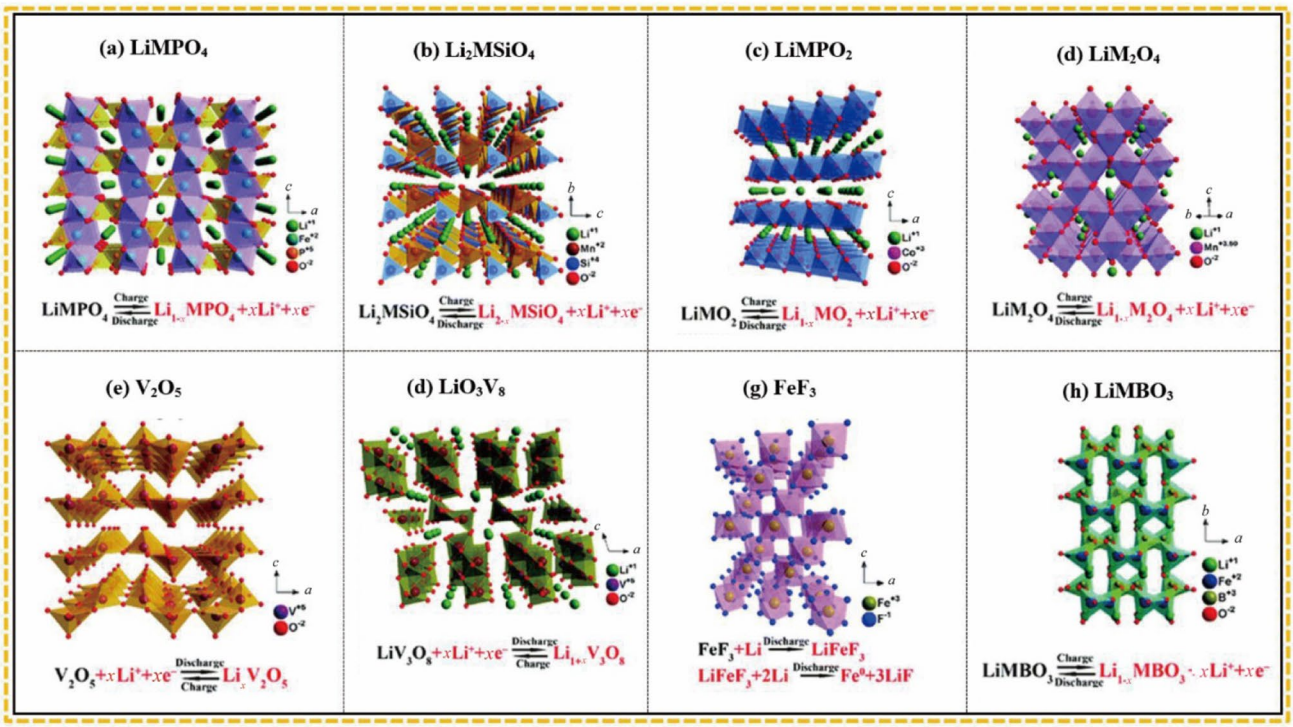

Fig. 10 Electrochemical reactions and crystal structures of different cathodes: **a** olivine $LiMPO_4$, **b** Li_2MSiO_4, **c** spinel LiM_2O_4, **d** layered LiM_2O_2, **e** V_2O_5, **f** LiV_3O_8, **g** FeF_3, and **h** $LiMBO_3$. Reprinted with permission from Ref. [137]. Copyright © 2016, Royal Society of Chemistry

Table 2 Practical properties of some common LIB cathode materials

Cathode material	Max specific capacity /(mAh g^{-1})	Average voltage /V	Specific energy /(Wh kg^{-1})	Description
$LiCoO_2$ [147]	140	3.90	520	Most common, toxic, expensive, and unsafe
$LiMn_2O_4$ [148]	120	4.05	450	Unstable at high temperatures, inexpensive, safe, Jahn–Teller issue, capacity fading
$LiFePO_4$ [149]	160	3.45	540	Good stability, safe, long life, inexpensive, low voltage, low conductivity, slow Li-ion diffusion
$LiNiPO_4$ [150]	110	5.10	800	High voltage, high stability, environmentally friendly, inexpensive, low conductivity,
$LiNi_{0.5}Mn_{1.5}O_4$ [151]	130	4.60	550	High voltage, safe, unstable at high voltages
$LiNi_{1/3}Mn_{1/3}Co_{1/3}O_2$ [152]	140–160	3.80	630	Fast voltage fading, low capacity rate, poor cycle life
$LiNi_{0.8}Co_{0.15}Al_{0.05}O_2$ [153]	200	3.73	720	High capacity, safe, Co free, oxygen release, thermal instability
V_2O_5 [154]	250	3.60	530	High energy and power density, low electron/lithium conductivity, poor rate capability and cycling stability
Sulfur [155]	1 675	2.10	2 447	Environmentally friendly, very low cost, high availability, high volume change, low conductivity, poor cyclability

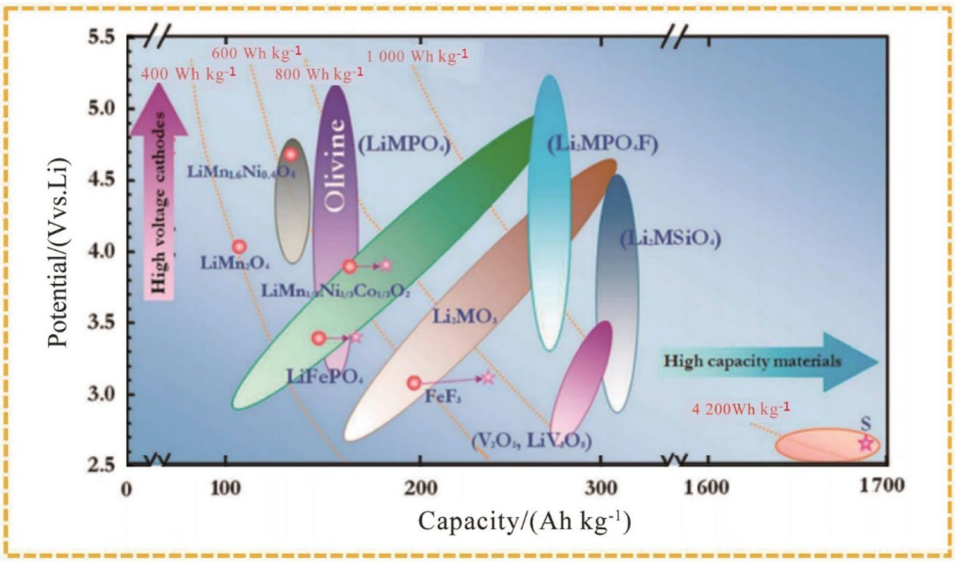

Fig. 11 Schematic representation of the potential versus capacity ranges for different cathode materials [156]. Copyright © 2011, Chemistry of Materials

cathode materials for comparison. The application of cathode materials has some common problems, including the production cost of solid-state materials through long and high heating processes, environmental impact and raw material cost of large-scale cells, sensitivity of the performance of the cathode to the stoichiometry, oxygen release, heat generation from the cathode in the fully charged condition, and weak practical capacity [138, 139]. Ultrahigh-energy cathodes provide inexpensive electric batteries for vehicles [140]. In the development of cathodes for next-generation LIBs, research is being conducted to reduce the production cost; some common examples include utilizing materials with high abundance, such as Fe or Ti with a stable tetravalent state [141, 142]. Additionally, applying expensive and rare elements in the form of doping, such as vanadium, niobium, molybdenum, yttrium, and tantalum, in the composition of cathode materials can significantly improve their performance [143, 144]. However, selection of the appropriate methods of fabrication, coating, and modification is also of great importance in the synthesis of electrode materials. Moreover, the byproducts (LiF, P_2O_5, etc.) formed from side reactions strongly attach to the surface of cathode materials, which highly inhibit Li^+ transmission [145, 146]. Thus, to boost the performance of the cathode in batteries, ALD coating is suggested as an impressive method to enhance the specific capacity, performance, energy density, safety, conductivity, lifetime, and cycling stability and mitigate the self-discharge and resistance of commercial cathode materials,

which can alleviate the cost of the battery for consumer products, EVs, and energy storage systems.

3.1.1 Fabrication of LIB Cathode Materials via ALD

Due to the extraordinary process of reaction-controlled deposition applied in ALD, cathode materials developed by this method can be classified into two categories of lithiated and unlithiated complexes. Over the past decade, lithiated complexes such as $LiCoO_2$, $LiMn_2O_4$, and $LiFePO_4$, as well as unlithiated transition metal materials such as $FePO_4$ and V_2O_5, have been developed through ALD [157-159]. To vary the stoichiometry of the lithiated cathodes, different subcycle deposition ratios are being used. Due to the feature of conformal ultrathin films, the electrode acts well at the interface between the electrolyte and current collector. As a result, the stress generated by the intercalation and deintercalation of Li ions in the cathode is reduced, thus making it mechanically more robust [160]. Additionally, the ALD thin film improves the electrochemical properties, resulting in excellent cyclability compared to bulk crystals, and thus, the high reversible capacity approximates the theoretical value [83, 161].

ALD can create conformal and homogenous thin layers on surfaces with a high-aspect-ratio topography while also offering atomic-scale adjustments of the target material composition, size, and thickness. The synthesis of quaternary cathode materials is consistently more difficult than that of binary and ternary materials due to their complex surface and structural chemistry [162]. The presence of Co, which is toxic in nature and increases production costs, in the structure of conventional $LiCoO_2$ (LCO) cathodes, first commercialized in 1980 [109], has forced researchers to conduct extensive research into the development of LCO structure derivatives such as $Li_{1.2}MnNiCo_{0.8}O_2$ (NMC) and $LiNi_{0.8}Co_{0.15}Al_{0.05}O_2$ (NCA), each of which has advantages and disadvantages in their application. The LCO cathode is a layered material fabricated through the ALD method using subcycles, LiO_2, and one or two binary oxides. Notten et al. [157] applied PEALD using the precursors Co_3O_4 ($CoCp_2$-O_2) and Li_2CO_3(LiO^tBu-O_2) at 325 °C to successfully obtain LCO cathode materials. Their evaluations showed that LCO cathodes fabricated with this method have good reversible electrochemical performance. In another study, research was performed to fabricate spinel structure $LiMn_2O_4$ by the ALD technique. To fabricate this type of cathode, Li(thd)-plasma O_3 and $Mn(thd)_3$-plasma O_3 precursors were used in alternative cycles at 225 °C. The results of the above research showed that the fabricated $LiMnO_4$ cathode possessed a high capacity of 230 mAh g^{-1} and a stable cycling performance of up to 1 000 cycles [163]. Notably, the structures fabricated by ALD can be combined with materials with unique electrochemical properties, such as V_2O_5, NbO_5, and $FePO_4$, to improve the performance of the cathode while taking into account its specific application [164-166]. Unlithiated $FePO_4$ cathodes with amorphous structures were fabricated via ALD. Sun et al. [167] implemented ALD to form a $FePO_4$ cathode by subcycle deposition of trimethyl phosphate-water and Fe_2O_3 (ferrocene-ozone) on nitrogenized CNTs at 200–350 °C. The results of their evaluation showed that as an LIB cathode, the fabricated cathode had a discharge capacity of 177 mAh g^{-1}. Hence, the $FePO_4$ structure in the form of a thin film or modification material can enhance the efficiency of solid-state LIBs.

V_2O_5 is another unlithiated cathode material that can be fabricated with ALD without the need for thermal posttreatment. Xie et al. [168] studied the structure of a 3D V_2O_5/TiO_2 cathode on a CNT surface, in which amorphous V_2O_5 and thin-film TiO_2 were grown on the CNT surface. To do so, VOTP, $TiCl_4$, and H_2O precursors were used. The discharge capacity of the 15-cycle TiO_2/50-cycle V_2O_5/CNT paper electrode was 400 mAh g^{-1}, which is nearly the theoretical value of V_2O_5. Moreover, the deposition of the TiO_2 film on the cathode solved the vanadium dissolution problem. In another study, Nilsen et al. [169] fabricated a V_2O_5 cathode structure for LIBs via ALD by using $VO(thd)_2$ and O_3 precursors at 215 °C. The results showed that 500-cycle deposition with a growth rate of 10 nm V_2O_5 led to the highest electrochemical performance. As shown in Fig. 12, thinner films had higher capacity retention at high C rates. ALD-500 was slightly influenced by higher discharge rates, with the capacity decreasing from 104 to 83 mAh g^{-1} at 1 and 10 C rates. At higher C rates, the capacity retention was decreased with increasing effective film thickness. ALD-500 with a surface controlled by [001]-plane V_2O_5 platelets showed the highest rate performance. The capacity remained stable for 650 cycles and first dropped to under 80% of its initial value after 1 530 cycles (represented by the gray region in Fig. 12c). Additionally, in another work, Sun et al. [159] utilized ALD and created a 33 nm-thick lithiated $FePO_4$ film on CNTs. They used $FeCp_2$-O_3-TMP-H_2O and LiO^tBu-H_2O precursors with sequences of 5 and 1, respectively (Fig. 13). Analysis showed that their fabricated cathode had excellent capacity retention of 70.5% up to 2 000 cycles. In addition, an increase in the current rate at 60 °C provided a high capacity of approximately 71 mAh g^{-1}.

Recently, the quaternary cathode material lithium nickel silicon oxide ($LiNiSiO_4$) was fabricated by using ALD [170]. To fabricate this structure, deposition of one layer of Li-Ni–O including subcycles of $LiN[(CH_3)_3Si]_2 + O_2$ plasma, $Ni(Cp)_2 + O_2$ plasma, NiO, and Li_2O was applied. Then, for the formation of $Li_{22}Si_5$ and $Li_2Si_2O_5$, annealing at 400–900 °C was performed. Analyses showed that the synthesized material could obtain a specific capacity of 20–26 μAh μm^{-1} cm^{-2} depending on the annealing temperature and

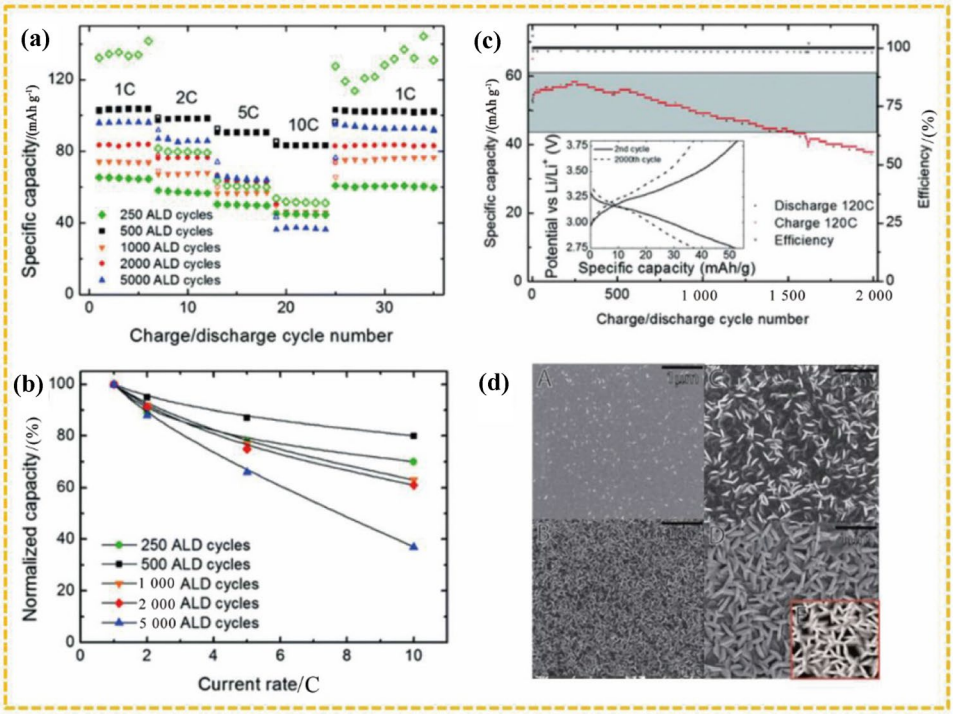

Fig. 12 **a** Rate performance of V_2O_5-deposited coin cells obtained with 250 to 5 000 ALD cycles. **b** Capacity retention following a second discharge, normalized to the 1 C capacity. **c** The gray band in the figure denotes the window with a capacity loss below 80% of the initial capacity (55 mAh g^{-1} at 120 C). The coulombic efficiency was approximately 100%. Inset: the charge−discharge plot of the 2nd and 2 000th cycles. **d** SEM images of configurations fabricated with various ALD cycles (500, 1 000, 2 000, 5 000) on silicon substrates. Reprinted with permission from Ref. [169]. Copyright © 2014, Royal Society of Chemistry

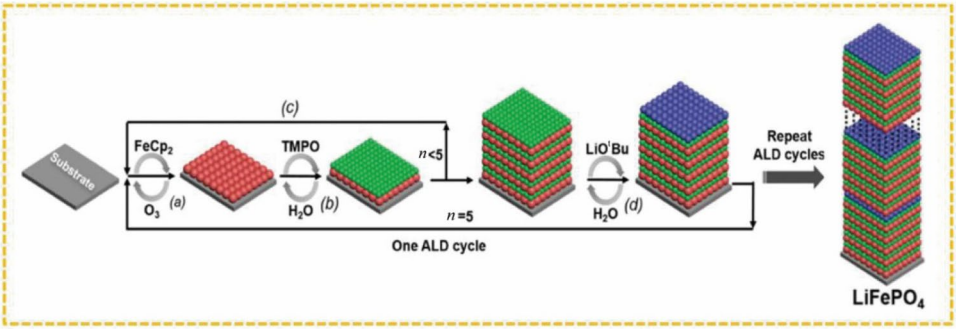

Fig. 13 ALD fabrication of amorphous $LiFePO_4$ at 300 °C. Reprinted with permission from Ref. [159]. Copyright © 2014, Wiley

subcycle deposition ratio. Therefore, the deposition of thin films via ALD on a carbon surface with high conductivity could result in the production of electrode materials with high cycling ability and excellent rate capability.

In another work, Chen et al. [171] successfully designed and analyzed a new concept of a V_2O_5 ALD process employing VTOP precursor and O_3 coreactant in the temperature range between 170 and 185 °C. The achieved V_2O_5 film thickness was 30 nm with a constant GPC of ~0.27 Å per cycle. On Si substrates, nucleation-controlled growth kinetics was observed for up to 250 cycles. The as-deposited V_2O_5 layers on the electrode surface in coin cell samples demonstrated a high theoretical specific capacity of 147 mAh g^{-1} versus (Li^+/Li) (Fig. 14a), an outstanding rate performance (Fig. 14b), a voltage range from 2.6 to 4.0 V (Fig. 14c), high coulombic efficiency, and a cycling stability of 105 cycles at ~1 C (Fig. 14d). These advantageous characteristics are mostly related to the material crystallinity and the usage of thin films for electricity storage to facilitate quick charge transfer. Moreover, the scanning electron microscopy (SEM) images of the AAO sample before and after 1 000 cycles of ALD V_2O_5-O_3 layer growth are presented in Fig. 14e, f, respectively.

Furthermore, Table 3 lists some of the cathode materials recently developed with ALD. Generally, the ALD technique can be concluded to be a promising method for the fabrication and development of active electrodes in next-generation LIBs and miniaturized batteries.

3.1.2 Modification of LIB Cathode Materials via ALD

In this section, surface modification of the cathode with two common methods of film coating and doping is discussed.

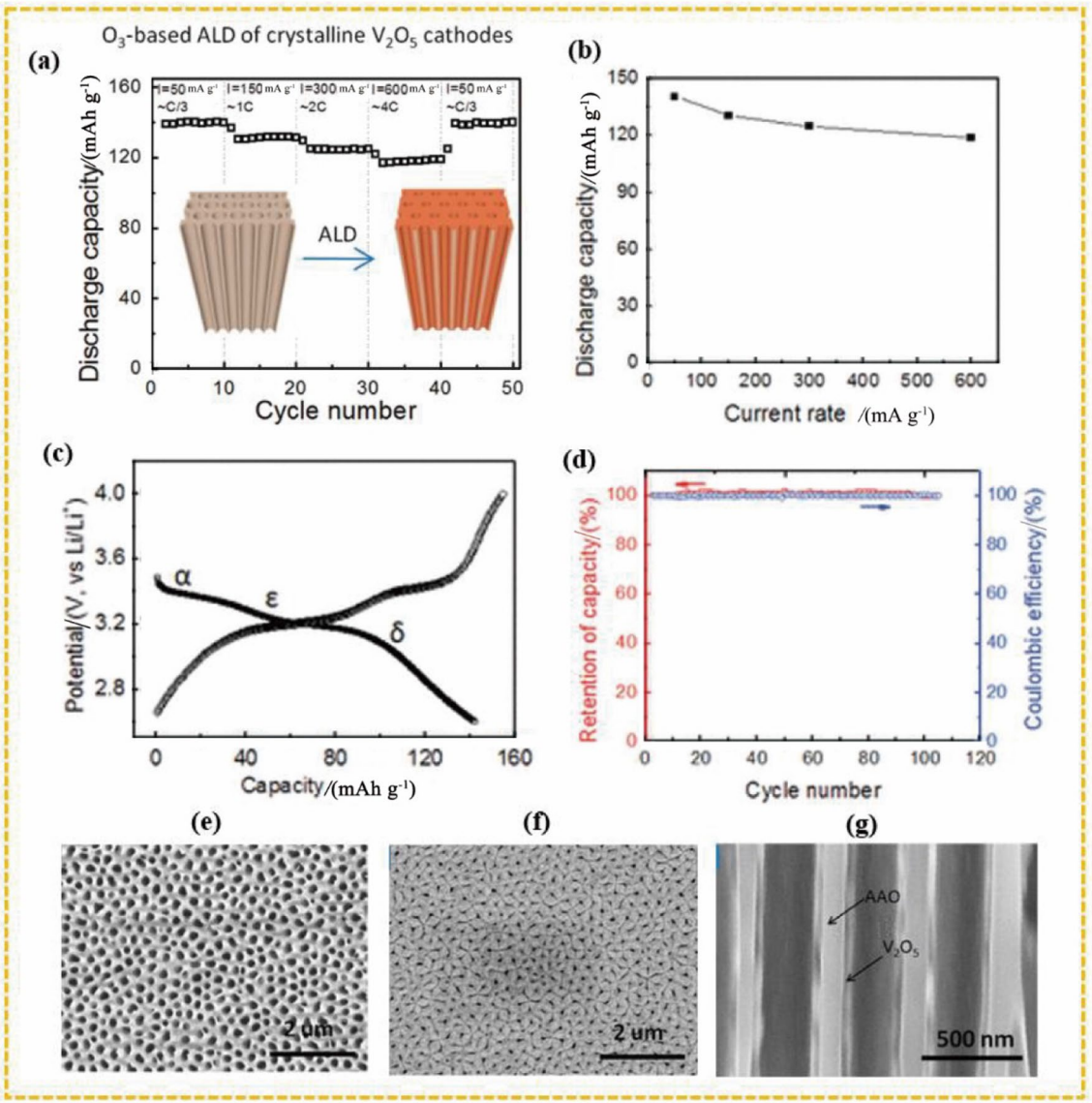

Fig. 14 Electrochemical performance of a V_2O_5-coated samples with a ~30 nm thick V_2O_5 film in the coin cell configuration: **a** rate performance at various current densities indicated by the discharge capacity plotted versus the cycle number; **b** current rate; **c** charge/discharge plots for the second cycle (the phase change is indicated on the discharge curve; the current density is 50 mA g^{-1}); and **d** cycle retention and coulombic performance for 105 cycles at ~1 C. SEM images of the AAO sample **e** before and **f** after 1 000-cycle ALD V_2O_5 layer growth; **g** SEM image of V_2O_5 nanotubes in AAO pores. Reprinted with permission from Ref. [171]. Copyright © 2012, American Chemical Society

Film coating and doping are promising ideas for enhancing the electrochemical performance of electrodes [173].

Surface coating is a suitable technique for the prevention of unwanted reactions and those that damage the electrode–electrolyte interface, such as transition metal dissolution, irreversible phase degradation, oxygen loss, electrolyte deposition and phase transformation. Coating materials should have the properties of electrochemical stability, permeability to Li ions, and compatibility with the electrolyte and solid electrode materials. Therefore, to produce an ideal coating with the fewest unwanted reactions, the characteristics of the coated surface should also be taken into account. To date, several coating materials, including metal oxides (TiO_2, Al_2O_3, ZnO, ZrO_2, etc.) [174-178], metal fluorides (LiF, AlF_3, etc.) [59, 179], phosphates (Li_3PO_4, $AlPO_4$, etc.) [180-182], metal nitrides (TiN, ZrN, AlN, etc.) [183, 184] and metal sulfides (ZnS, MoS_2) [60, 185], have been investigated. The selection of coating materials should be made such that the stability of the structure against heat and the ionic conductivity are not decreased. The deposited film can also be functionalized for isolation, which could provide more suitable rate capability and cycling stability.

Table 3 List of some of the cathode materials developed with ALD

Material	Substrate	Precursor	Temperature/℃	Specific capacity/ (mAh g^{-1})	References
$LiCoO_2$	$Si/TiO_2/Pt$, Si/SiO_2	$(LiO^tBu\text{-plasma } O_2)+(CoCp_2\text{-plasma } O_2)$	325	–	[157]
$LiMn_2O_4$	Si, SS	$(Li(thd)\text{-}O_3)+(Mn(thd)_3\text{-}O_3)$	225	134	[163]
$LiFePO_4$	CNTs, Si	$(LiO^tBu\text{-}H_2O)+(FeCp_2\text{-}O_3\text{-TMP-}H_2O)$	300	71	[159]
$FePO_4$	N-doped CNT	$(Fe(thd)_3\text{-}O_3)+(TMP\text{-}H_2O/O_3)$	200–350	177	[167]
$LiNiSiO_4$	SS, Si	$LiN[(CH_3)_3Si]_2+Ni(Cp)_2+\text{plasma } O_2$	110–160	-	[170]
$V_2O_5\text{-}TiO_2$	CNTs	$VOTP+TiCl_4+H_2O$	120–150	400	[168]
V_2O_5	SS, Si, glass	$VO(thd)_2+O_3$	215	104	[169]
V_2O_5	SS, Si, MWCNTs	$VTOP+H_2O$	120		[172]
V_2O_5	SS, AAO	$VTOP+O_3$	170–185	142	[171]

The application of the ALD method to achieve this goal has attracted more attention than conventional sol–gel and mechanical mixing methods due to its unique properties of film growth in a uniform manner and controllable nanometer sublayer thickness. In the following, a review is provided on the research works performed on ALD for engineering LIB cathode surfaces.

Doping is among the simplest and most efficient methods of improving the electrochemical properties of electrodes applied in LIBs. Doping, by changing the crystalline structure at the atomic scale, can improve the chemical and physical properties of materials, such as the bandgap, conductivity, defect concentration and charge distribution. In the doping process, small amounts of metals such as Al, Ti, Zn, V, Nb, and Ni are introduced onto the layer of the electrode surface in the form of islands to adjust the electrochemical properties of the electrode according to its application and requirements. For example, adding atoms with a high conductivity feature can enhance this property of the electrode [33]. Additionally, researchers have reported that the addition of Co atoms to electrode layers improved the performance of batteries at higher voltages [32]. Yang et al. [183] deposited a thin TiN film on a $LiNi_{0.8}Co_{0.1}Mn_{0.1}O_2$ (NCM811) surface via ALD. The TiN coating layer blocked side reactions and inhibited structural damage during cycling, decreased the contact resistance among NCM811 particles and improved the particle surface electronic conductivity during cycling. As shown in Fig. 15, samples with 20 coating cycles displayed great electrochemical performance. Once discharged and charged at a current density of 100 mAh g^{-1}, in the potential range from 2.8 to 4.3 V, the initial discharge specific capacity of the battery was 199.2 mAh g^{-1}, its capacity retention rate was 76.3%, and its reversible capacity up to 200 cycles was 152 mAh g^{-1}.

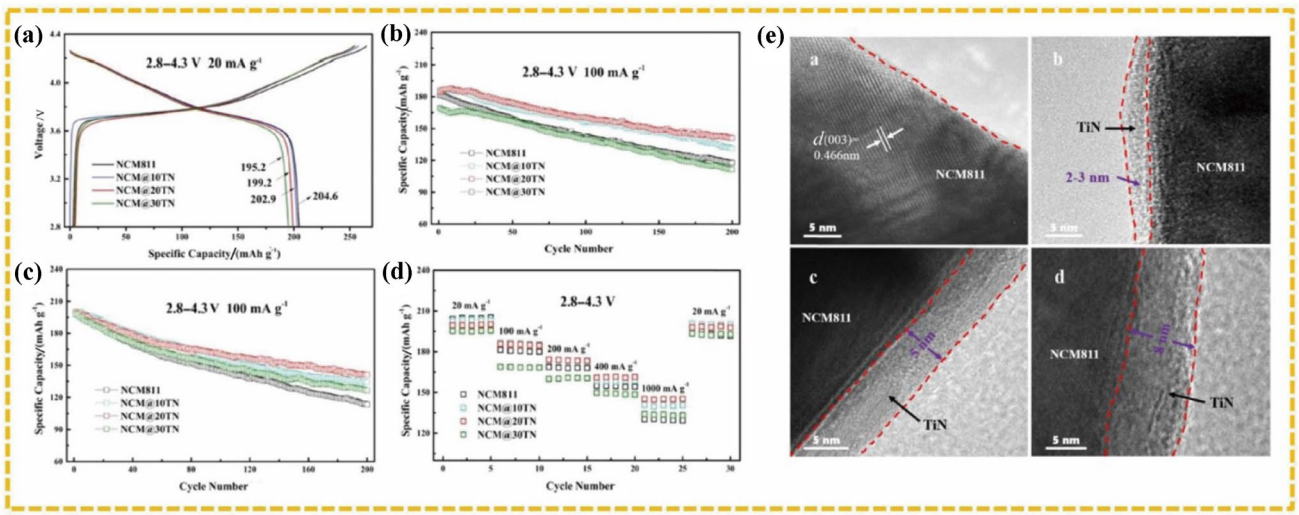

Fig. 15 **a** Initial charge−discharge plots at 20 mA g^{-1}; **b** cycling efficiency at 100 mA g^{-1} in the 2.8–4.3 V voltage range; **c** cycling efficiency at 100 mA g^{-1} in the 2.8–4.5 V range; **d** rate capability; and **e** TEM micrographs of pristine NCM811, NCM@10TN, NCM@20TN, and NCM@30TN. Reprinted with permission from Ref. [183]. Copyright © 2021, Elsevier B.V. All rights reserved

Christophe et al. [186] utilized Ti phosphate as a functional coating to improve the LiNiMnCo oxide (NMC) cathode via plasma ALD. A trimethyl phosphate plasma–oxygen plasma–titaniumisopropoxide exposure sequence was employed for investigation of a modified process with N_2 plasma (TMP-N_2-TTIP). This allowed nitrogen-doped (6 at.%; at.% means the atomic percentage) Ti phosphate deposition with a 0.4 nm cycle^{-1} GPC. A 2 nm coating on undoped Ti phosphate extensively enhanced the NMC electrode rate capability. Additionally, with the improved stability, 84% of the initial capacity was maintained after 100 cycles at 1 C, compared to 79% for the bare electrode. Then, the two-source precursor diethyl phosphoramidate (DEPA) plasma was replaced with TMP, enabling increments in the nitrogen level (8.6 at.%) and GPC (0.6 nm cycle^{-1}). However, a slight decrease was observed in the phosphate ion transparency due to the incorporation of N, but after N doping, the effective transversal electronic conductivity was three times higher. Kuk et al. [187] synthesized an ultrathin ZrO_2 coating on the developed NMC532 electrode surface through ALD to improve the electrochemical performance of a high-voltage NMC532/graphite system. They reported that the ZrO_2 coating enhanced the rate capability and capacity retention of the NMC532 electrode at a high voltage (4.6 V). Analysis of the ZrO_2-coated NMC532 electrode using cyclic voltammetry, X-ray diffraction, and X-ray photoelectron spectroscopy revealed that the enhanced electrochemical performance of the electrode was caused by decreased polarization, disorganized structure, and side reactions on the cathode surface. Therefore, ALD ZrO_2 coating on the developed electrode was a promising method for maintaining high LIB electrochemical efficiency during high-voltage operations. The SEM images of ZrO_2-coated and uncoated NMC532 electrodes (Fig. 16a) showed neither cathode deformation nor a difference from the pristine NMC532 electrode, proving that the ultrathin ZrO_2 film was noninvasively deposited on the as-prepared electrode. Figure 16b shows a transmission electron microscopy (TEM) image of the ALD-fabricated ZrO_2 film on a Si wafer. Because of the high porosity of the fabricated NMC532 electrode, the ZrO_2 film thickness per cycle was approximated by employing a Si wafer. A thickness of 20 nm was achieved through 400 ALD cycles. The composition of the ZrO_2 ALD coating was confirmed by using elemental mapping scanning of the film on the Si wafer. (Fig. 16c). Additionally, X-ray photoelectron spectroscopy (XPS) was performed to characterize the formation of the ZrO_2 film on the cathode surface (Fig. 16f). Moreover, electrochemical impedance spectroscopy (EIS) was adopted to reveal the improved cycling performance of ZrO_2-deposited NMC532 electrodes in high-voltage operations. Figure 16g presents the Nyquist plots of the NMC532/graphite cell up to 100 cycles at a 0.5 C rate, which consisted of a straight line (Z_w, Warburg impedance) at low frequencies and two partially overlapping semicircles in the high (R_s, surface resistance) to middle (R_{ct}, charge transfer resistance) frequency regions. The 20 nm ZiO_2-coated NMC532 showed the best specific capacity (Fig. 16d, e).

In another study, LLO cathode ($Li_{1.2}Mn_{0.6}Ni_{0.2}O_2$) surfaces were engineered by using thin films of a ZnO-TiO_2 nanolaminate with a thickness of (1.7 ± 0.4) nm produced through ALD with different coating rates. First, the coating formed by four ZnO cycles followed by six TiO_2 cycles on LLO was called P@Z@T. Then, the coating obtained by depositing six cycles of TiO_2 followed by four cycles of ZnO on LLO was given the name P@T@Z. Finally, P@T@Z@T was the name given to the coating on LLO that consisted of three TiO_2 cycles, four ZnO cycles, and three TiO_2 cycles. Figure 17(d(a–d)) show SEM images of the samples [177]. Interestingly, when ZnO-TiO_2 nanolamination was employed for bare samples, the discharge capacity was enhanced. In contrast to the bare sample with a discharge specific capacity of 228 mAh g^{-1}, the P@T@Z, P@Z@T, and P@T@Z@T configurations all had greater discharge specific capacities of 236 mAh g^{-1}, 240 mAh g^{-1}, and 232 mAh g^{-1}, respectively. Figure 17c shows the cycling performance of the configurations after 80 charge/discharge cycles at a 1 C rate. All nanolaminate-deposited LLO samples showed better capacity retention and higher specific discharge capacities than the pristine sample. Interestingly, the P@Z@T models exhibited better specific discharge capacity and capacity retention, 118 mAh g^{-1} and 97%, compared to the bare electrode with values of 71 mAh g^{-1} and 68%, P@T@Z with values of 98 mAh g^{-1} and 83%, and P@T@Z@T with values of 110 mAh g^{-1} and 97%. The P@Z@T models also exhibited initial capacity retention and specific discharge capacity comparable to those of LLO after one ALD TiO_2 deposition cycle (242 mAh g^{-1}, 94%) but better than those of ALD ZnO (220 mAh g^{-1}, 78%). At different C rates in 80 charge/discharge cycles, higher stability and specific discharge capacity of the P@Z@T models were also observed, as presented in Fig. 17e. Among the different coating sequences, ALD ZnO deposition followed by TiO_2 on the LLO cathode resulted in more uniform surfaces. After 80 charge−discharge cycles, the samples maintained a larger specific discharge capacity of 123 mAh g^{-1} at a 1 C rate. In addition, when the current density was increased to a 10 C rate, an excellent specific discharge capacity of 103 mAh g^{-1} was maintained. This was associated with lower charge transfer resistance and Li-ion migration because of the uniform surface and pre-electrochemical activation of the nanolaminate coating.

In another work, $Li_{1.2}Mn_{0.6}Ni_{0.2}O_2$ (LMR) was tailored with P doping to enhance the conductivity of Li^+ in the bare material. This was obtained by increasing the Li interlayer spacing, structural stability and electron transport, thus improving the safety and rate performance. Doping with

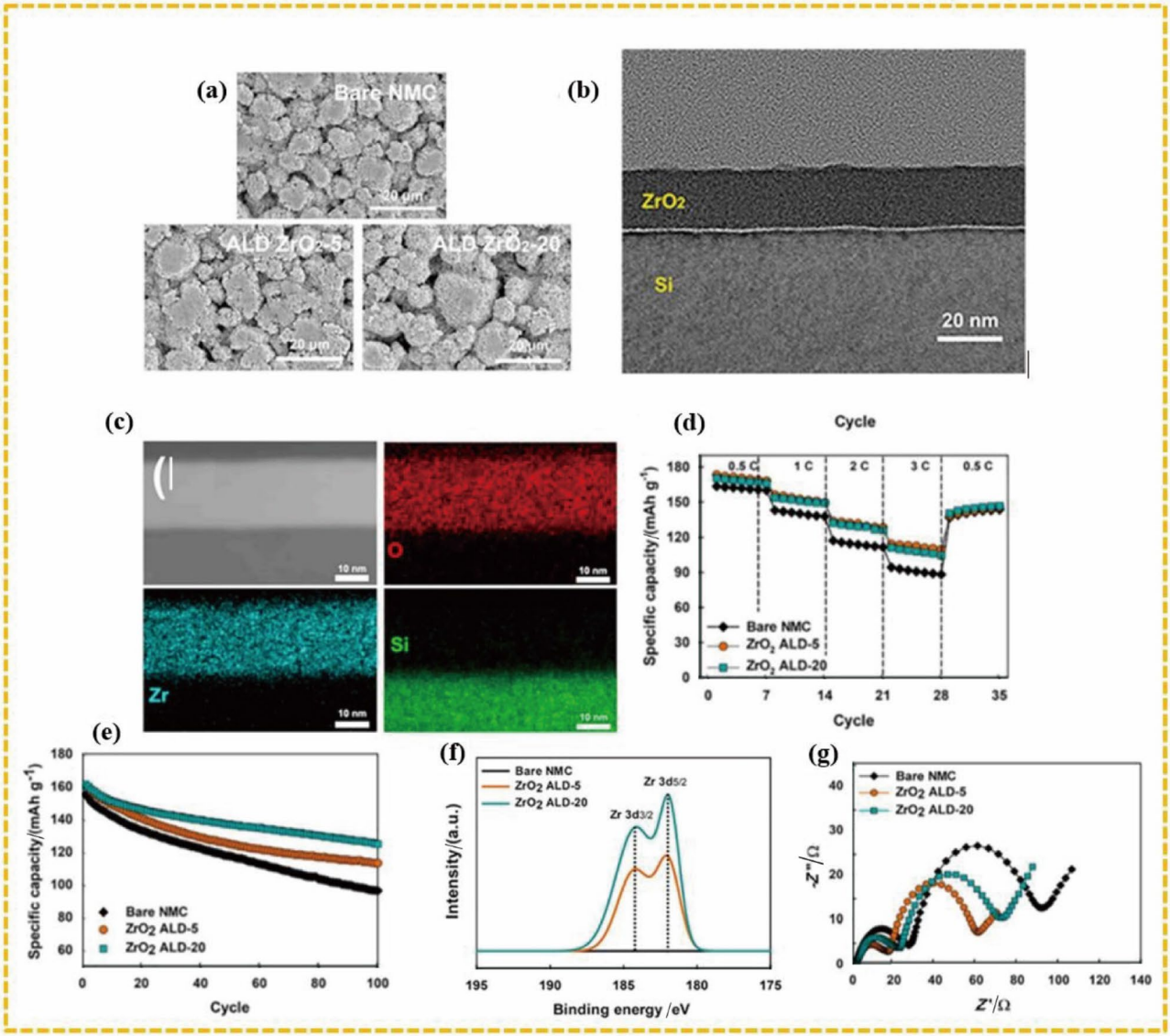

Fig. 16 **a** SEM images, **b** TEM image and **c** elemental mapping scan of the ZrO_2 film on a Si wafer. **d** Rate capability at different current densities of bare and ZrO_2-coated NMC532/graphite electrodes in the 2.7–4.6 V voltage range. **e** Cycling efficiency at a 1 C rate. **f** XPS spectra of the pristine and ALD ZrO_2-coated NMC electrodes. **g** Nyquist plots of the pristine and ZrO_2-coated NMC electrodes with different deposition cycles after the 100th cycle under high-voltage operation. Reprinted with permission from Ref. [187] Copyright © 2019, Elsevier B.V. All rights reserved

P^{5+} enhanced the distance between the (003) crystal planes in the range from ~ 0.474–0.488 nm and increased the stability of the structure through the formation of strong covalent bonds with oxygen atoms, leading to improved thermal stability (50% heat generation compared to the bare material) and capacity retention (rate performance from 38 to 50% at 0.05 C to 5 C) [188]. Oxygen release during the initial charge is a major issue pertaining to this material, which results in thermal instability, intense electrolyte oxidation, and low initial coulombic efficiency. Here, $AlPO_4$ coating via ALD was performed to protect the cathode surface. During the ALD process, some part of the *C*2/*m* Li_2MnO_3 structure was transformed into the spinel form. When $AlPO_4$ was coated on an electrode using only 5 ALD cycles, the initial coulombic efficiency was enhanced from 75.2% for the untreated electrode to 86.2%. The transformation successfully prevented oxygen release. In addition, $AlPO_4$ was concluded to more effectively improve the cathode material thermal stability compared to Al_2O_3-coated or uncoated samples [189].

As one of the most popular coating materials, Al_2O_3 was coated onto cathode material surfaces via different methods to delay surface side reactions and structural degradation because of HF attack. For example, Mohanty et al. applied

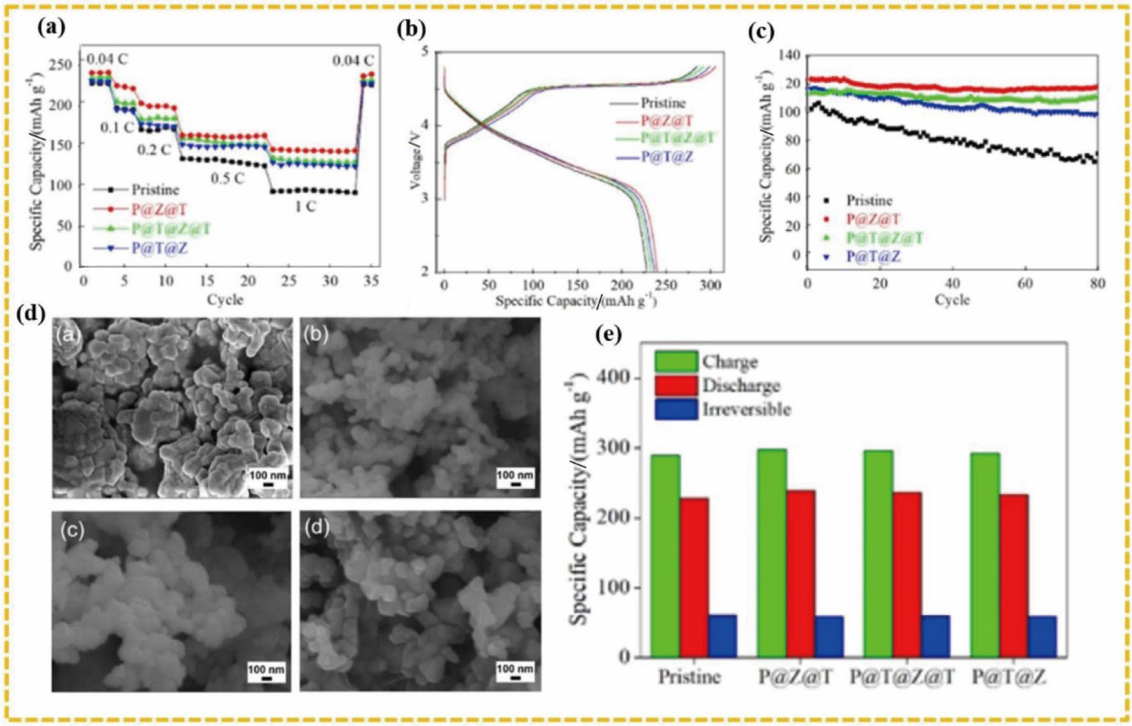

Fig. 17 **a** Electrode rate capabilities at different rates (0.04 to 1 C) in the voltage range from 2.0 to 4.8 V, **b** initial charge/discharge curves, **c** cycling efficiency for the models with and without a nanolaminate coating at a 1 C current density, **d** SEM images of the (a) bare, (b) P@Z@T, (c) P@T@Z@T and (d) P@T@Z configurations, and **e** associated histograms of the initial specific charge, discharge, and irreversible capacity retention under a 0.25 C rate. Reprinted with permission from Ref. [177]. Copyright © 2020 Elsevier B.V. All rights reserved

ALD to coat an NMC811 particle surface with Al_2O_3, greatly enhancing the structural stability of the NCM phase at the surface of particles, increasing the capacity retention and decreasing the growth rate of charge transfer impedance in cathode electrodes during high-rate cycling. The obtained great performance was mainly because the surface Al_2O_3 coating preserved the morphology of particles during Li intercalation/deintercalation processes and inhibited side reactions [90]. A novel $FePO_4$ coating obtained by ALD was proposed for high-voltage LNMO cathode materials. ALD cycles of 5, 10, 20, and 40 were used to deposit different $FePO_4$ thickness ranges onto LNMO powder. LNMO with 10-cycle ALD $FePO_4$ had the largest capacity and stable capacity retention at all current density rates. When LNMO was deposited with 40-cycle $FePO_4$ layers, the capacity retention was enhanced up to 100%. Their studies revealed that thin $FePO_4$ prevented severe reduction of surface Mn^{4+} to Mn^{2+} resulting from electrolyte distortion and the Jahn–Teller effect, and low amounts of Mn^{2+} assisted in maintaining the surface consistency with no severe dissolution into the electrolyte. Amorphous $FePO_4$ offered significant benefits in surface electron/ion transport compared to the most widely used insulating Al_2O_3 [190]. Wang et al. [110] studied surface doping with heavy ions and Nb in a Li-rich Mn-based layered oxide, $Li_{1.2}Mn_{0.54}Ni_{0.13}Co_{0.13}O_2$. The doped ions were verified to be situated on the surface of the Li layer oxide. They bound the slabs through "inactivated" surface oxygen and strong Nb–O bonds, improving the structure stability. In the initial cycle, the specific capacity of the tailored sample reached 320 mAh g^{-1}, and after 100 cycles, 94.5% remained. Lee et al. [191] found that atomic layer coating with Al_2O_3 materials improved the LCO capacity retention. ALD oxide coatings enhanced the electrochemical performance of different cathode materials, such as layered LCO and spinel $LiMn_2O_4$. Table 4 summarizes the recent LIB cathode materials modified by ALD.

3.2 Anode Materials

Anode materials in the negative electrode of LIBs also play essential roles in the LIB performance. Despite the availability of a variety of anode materials, they still suffer from problems and limitations. The development of future generation batteries depends heavily on advancements in anode materials, which are just as significant as cathode material enhancement. Anode materials have a simpler structure than cathode materials. Li metal has a low electrochemical redox potential and an extremely high theoretical specific capacity

Table 4 Summary of cathode materials modified via ALD for LIBs

Cathode material	Coating	Precursor	Temperature/℃	Deposition cycle/thickness	References
NMC811	TiN	TDMAT + NH_3	200	2–9 nm	[183]
LCO	Al_2O_3/TiO_2	TMA + H_2O + TTIP	150	10–500 cycles	[174]
LCO	NbO_x	$NbOEt_5$ + H_2O	175	30 nm	[165]
LCO	AlW_xF_y	TMA + WF_6	200	1 nm	[192]
LCO	AlF_3	TMA + HF	150	2 cycles	[179]
LNMO	Al_2O_3	TMA + H_2O	180	20 nm, 10 cycles	[176]
LNMO	LiF	LiO^tBu + Hfac + TiF_4	220	4 × 10 cycles	[59]
NMC811	$LiAlF_4$	Li(thd) + TiF_4 + $AlCl_3$	250	15 nm, 300 cycles	[193]
$LiMn_2O_4$	ZrO_2	ZTB + H_2O	120	10 nm, 50 cycles	[178]
$Li_{1.2}Mn_{0.54}Co_{0.13}Ni_{0.13}O_2$	$AlPO_4$	TMA + TMP + H_2O	150	20 cycles	[189]
$Li_{1.2}Mn_{0.6}Ni_{0.2}O_2$	ZnO–TiO_2	DEZ + TiCl4 + H_2O	150	4-cycle Zn/6-cycle Ti 1.2–1.7 nm	[177]
$Li_{1.2}Ni_{0.13}Mn_{0.54}Co_{0.13}O_2$	Al_2O_3/TiO_2	TMA + TTIP + H_2O	150	10-cycle TMA/20-cycle TTI	[194]
NMC622	N-doped Ti phosphate	TMP + Plasma O_2 + N_2 + TTIP + DEPA	300	0.4–0.6 nm $cycle^{-1}$	[186]
NMC333	Al_2O_3	TMA + H_2O	180	4 cycles	[195]
NMC532	ZrO_2	Tris(dimethylamino)zirconium + H_2O	120	0.25–1 nm, 5–20 cycles	[187]
NMC532	MgO	Mg[EtCp]$_2$ + H_2O	200	0.7 nm, 5 cycles	[161]
$LiNi_{0.5}Mn_{1.5}O_4$ (LNMO)	$FePO_4$	ferrocene ($FeCp_2$) + TMP + H_2O	300	40 cycles	[190]
$LiNi_{0.5}Mn_{1.5}O_4$ (LNMO)	$AlPO_4$	TMP + TMA + H_2O	250	1 nm, 10 cycles	[196]
$LiNi_{0.5}Mn_{1.5}O_4$ (LNMO)	TiO_2/Al_2O_3	TTIP + TMA + H_2O	250	0.389–0.816 Å	[197]
$LiNi_{0.5}Mn_{1.5}O_4$ (LNMO)	$LiAlO_2$	TMA + LiO^tBu + H_2O	200	2 nm, 10 cycles	[161]
(NMC333)	$LiTaO_3$	LiO^tBu + H_2O + tantalum ethoxide	225	20 cycles	[85]
(NMC442)	Al_2O_3	TMA + H_2O	120	0.6 nm	[198]

(3 861 mAh g^{-1}), making it one of the most often used materials to create anodes for LIBs [199, 200]. However, due to the formation of severe dendrites on the surface, reaction with the electrolyte at the interface occurs that leads to instability of the LIB function [201]. The destructive manner of dendrite formation limits the application of Li metal in the anode. Other promising anode materials with layered structures include carbonaceous materials such as graphite and CNTs [202, 203] and Si in which Li ions are dissolved [204]. Furthermore, lithium titanates ($Li_4Ti_5O_{12}$) were developed with better performance [205]. Notably, each of the above materials has its drawbacks; for example, $Li_4Ti_5O_{12}$ has weak electrical conductivity and a low diffusion coefficient of Li ions [206]. Compared to carbon, Si-based anodes can promote higher energy density and specific energy in LIBs, but in the lithiation process, they undergo high volume expansion of approximately 300%–400%, which imposes high stress, resulting in failure and crack formation in the structure [207]. Consequently, the high volume change in anode materials results in decreased contact with the electrolyte in cycling, leading to performance degradation [208].

Anode materials such as Li, Si, lithium titanate ($Li_4Ti_5O_{12}$) and SnO_2 have high capacity [209-211]. However, extensive research is required to decrease the common problem of a high volume change due to the high specific capacity, which results in low efficiency, capacity loss, mechanical degradation, and short longevity. In the last decade, to address these problems, different methods and strategies have been tested, among which ALD was superior to others due to its ability to fabricate and modify anode nanomaterials at the atomic scale. Li metal was first used in the negative electrodes of LIBs [212]. The theoretical specific capacity of Li is approximately 3 860 mA [213]; however, due to the formation of Li dendrites, which decreases the coulombic efficiency (CE) in the cycling process and finally results in failure and even explosion of the battery, it cannot be widely commercialized [199].

Graphite has been the most commonly and extensively applied LIB anode material developed in the last two decades. Graphite has unique advantages, such as high stability, a constant plateau voltage of approximately 0.1–0.2 V during discharge, reasonable cost, environmental friendliness, safety, and good capacity retention during cycling

[214]. However, it suffers from some disadvantages, such as low capacity, poor CE, low rate performance and sensitivity to some electrolytes, which limit its application in new generation LIBs [215]. Generally, the ethylene carbonate electrolyte is applied in LIBs with graphite anodes [216]. Additionally, due to the low capacity of graphite, it is not a suitable option for large systems such as EVs [217]. Therefore, researchers were forced to develop anode materials with higher capacity and lower potential. For example, new generation batteries require anode materials with a minimum capacity of 1 000 mAh g^{-1} [218].

Graphite and $Li_4Ti_5O_{12}$ have excellent cycling stability but limited theoretical capacity. The capacity of graphite is 372 mAh g^{-1}, and that of $Li_4Ti_5O_{12}$ is 175 mAh g^{-1}, which are not sufficient for today's batteries that require high energy density [219]. Thus, extensive efforts have been made to obtain anode materials with higher capacity for new generation LIBs. Generally, with the improvement of one property, other properties deteriorate, which is the greatest challenge in the science of batteries. Therefore, the aim of research on this topic is to develop an LIB component with optimum properties. Based on the Li-ion storage mechanism, anode materials are categorized into three groups: those undergoing conversion reactions, such as transition metal oxides, which are more popular because of their porous structure and high surface area; insertion reactions, including carbonaceous materials; and alloy reactions, based on alloys containing Si, Sn, Ge, etc.

Transition metal oxide electrodes (SnO_2, TiO_2, Fe_2O_3, ZnO, Mn_2O_3, etc.) have a theoretical capacity of 500–1 000 mAh g^{-1} [220]. Among their advantages are excellent cycling performance and adjustable operation voltage [221]. Compared to graphite anode materials, these materials have the advantages of higher safety, lower production cost, high specific capacity, and lack of formation of Li dendrites. However, they suffer from disadvantages such as inherent weak conductivity, electrode and electrolyte decomposition, rearrangement during lithiation and delithiation processes, and internal heat generation, which decrease the energy density and efficiency [222, 223]. Extensive research is being conducted to mitigate the problems of such anode materials. Si is a suitable material to substitute graphite anodes. Si has a low potential and a high gravimetric capacity of 4 200 mAh g^{-1}, which is 10 times larger than the value of 372 mAh g^{-1} for graphite [224]. To date, Si has been known as an excellent high-capacity anode material due to its high theoretical capacity. In terms of chemical capacity, each Si atom can form bonds with four Li ions, while in graphite, six C atoms can form bonds with one Li ion to give LiC_6. The Si anode has a delithiation voltage of approximately 0.4 V [225]. Overall, owing to its high capacity to store Li ions during lithiation/delithiation processes, Si undergoes very high volume expansion of approximately 400%, which, during cycling, can result in crack formation and, in turn, under high stress, fracture of Si particles [226]. The volume changes for SnO_2 and ZnO are 300% and 228%, respectively [227, 228]. The process of Si decomposition is called pulverization. These factors can cause problems such as particle dissociation, which is the reason for the lack of electrical contact at the interface and decreases in the performance and capacity. With the increment in the number of cracks, Si reacts with the electrolyte, resulting in decomposition and the creation of an SEI [229]. The SEI is obtained from decomposition of the salts in the electrolyte solution, and over time, its thickness is increased, Li ions are depleted, and a decrease in the electrical conductivity occurs.

Typically, capacity loss during the initial discharge process is mainly caused by SEI creation on the surface of the anode, leading to permanent Li^+ ion consumption. Batteries experience rapid capacity degradation and safety loss as the cycle number rises [230]. To improve the performance of anode materials in batteries, passivation layers can be applied through various methods. To date, several methods and approaches have been employed to address the limitations of anode materials with high capacity, such as nanoengineering [231], mixing of carbonaceous materials [232], surface modification [233, 234], and use of additives [235]. Among these methods, ALD has been found to be promising for surface modification and even design and fabrication of new electrode materials. A protective layer can be applied through the ALD technique as an adjustable coating to decrease crack formation and significantly increase the effective lifespan of batteries.

3.2.1 Fabrication of LIB Anode Materials via ALD

ALD can be used to fabricate anode materials in the following forms: 2D structures such as nanolaminates (composite films consisting of alternating layers of different materials) [236] and 3D architectures such as graphene foam (GF) [237], copper foam [238], nickel foam [239], and multiwalled CNT (MWCNT) sponges [172]. Since the structure of the anode is simpler than that of the cathode, the ALD technique is more commonly applied for the fabrication of anode materials, especially transition metal oxides (TMOs). ALD is also applied to improve the cycling stability of high-capacity anode materials through the formation of electrode nanostructures with uniform and controlled composite sizes. TMOs include TiO_2, ZnO, SnO_2, Fe_2O_3, MoO_3, MnO_2, CoO_3, Nb_2O_5, and RuO_2 [240, 241]. These anode materials have much better theoretical capacity than graphite. The capacities of these compounds are summarized in Table 5. The conversion reaction of a TMO and Li can be written as:

$$M_xO_y + 2yLi^+ + 2ye^- \leftrightarrow xM_0 + yLi_2O \quad (4)$$

Table 5 Summary of the LIB anodes fabricated by ALD

Material	Substrate	Precursor	Temperature/°C	Growth rate/thickness	References
SnO_2	CNT/Si	TDMASn + H_2O	150–200	0.06 nm cycle^{-1}, 150 cycles	[250]
Nb_2O_5	CNT	$Nb(OEt)_5$ + H_2O	235–350	100 cycles	[251]
V_2O_5	N-Graphene	VTIP + H_2O	150	1 Å cycle^{-1}, 50 cycles	[252]
ZnO/SnO_2	Si	DEZ + TDMASn + H_2O	200	0.6–0.9 Å cycle^{-1} 100 × (2 ZnO + 3 SnO_2)	[247]
Al_2O_3/SnO_2	CNT	TMA + TDMASn + H_2O	175	0.2 nm cycle^{-1}, 75 SnO_2/10 Al_2O_3	[253]
TiO_2	CNT/CFP	TiCl4 + H_2O	120	10 cycles	[254]
ZnO/TiO_2	Cu foil	DEZ + $TiCl_4$ + H_2O	130	26 ZnO/26 TiO_2 1.75 Å for ZnO, 0.36 Å for TiO_2	[236]
ZnO	Graphene	DEZ + H_2O	150	50–800 cycles	[255]
RuO_2	MWCNT	$RuCp_2$ + O_2	210–240	0.4 Å cycle^{-1}	[256]
MoO	CNT	$Mo(CO)_6$ + O_3	170	12–150 nm, 100–1 000 cycles	[257]
$Li_4Ti_5O_{12}$	N-CNT	TTIP + Li(O^tBu) + H_2O	250	5.5 Å cycle^{-1}	[258]
$Li_4Ti_5O_{12}$	Si	($TiCl_4$) + Li(O^tBu) + O_2	225	97 nm	[259]
SnO_2/HfO_2	Cu foil/MXene	TDMASn + H_2O + $Hf(NMe_2)_4$)	150–200	5–50 nm	[260]
Lithium terephthalate ($Li_2C_8H_4O_4$ or LiTP)	Si	Li(thd) + terephthalic acid (Benzene-TPA)	300	400 cycles 3.0 Å cycle^{-1}	[261]
SnO_2	Ni foam	TDMASn-H_2O	150	-	[262]
TiO_2	Au	$TiCl_4$-H_2O	100–110	2–20 nm	[263]

where M denotes the TMO.

Despite their advantages, some of these materials also have limitations. For example, TiO_2 anodes have inherently low ionic and electronic conductivity [242], and SnO_2 undergoes large volume expansion during charge/discharge processes [243]. Carbonaceous materials such as graphite, CNTs, and MXenes are suitable candidates for composite formation with TMOs due to their favorable electrical conductivity and high specific surface area (SSA) and can address the need for high rate capability [244-246]. ALD, with its capability to create thin coatings, can deposit TMO materials as 2D films on carbonaceous substrates. Thin oxide films deposited through ALD can tolerate stress due to their nanoscale compared to bulk micron-sized electrodes and facilitate ion and electron transfer [247, 248]. In addition, the crystallinity, thickness, and composition of the film can significantly affect the performance of anode materials, all of which can be adjusted by controlling the number of precursors, types of precursors, dose ratios, and deposition temperature [249].

Sun et al. [250] investigated the growth of SnO_2 films on CNTs through ALD. They evaluated the temperature effect on SnO_2 film growth and the effect of the deposited film thickness on the crystallographic structure and finally studied the electrochemical performance of the fabricated SnO_2/CNT composite as an LIB anode. They applied tetrakis(dimethylamido)tin and water for the fabrication of this composite material. A tetragonal crystal phase was observed for SnO_2 films deposited on the CNT surface at 150–200 °C, and SnO_2 of various thicknesses could be accurately fabricated by adjusting the ALD cycle number. They concluded that SnO_2 had high deposition rates at low deposition temperatures of less than 165 °C. Figure 18a–e present SEM images of the SnO_2@CNT complexes obtained with different ALD cycle numbers (0, 50, 100, and 150). The external nanotube diameter was clearly increased with an increasing ALD cycle number. Figure 18f presents a linear relationship between the ALD cycle number and SnO_2 layer average thickness, which reveals that the thickness of SnO_2 deposited on CNT surfaces can be accurately regulated by controlling the ALD cycle number. As indicated in Fig. 18i, l, the SnO_2/CNT-50 composites with 50 SnO_2 deposition cycles delivered a high specific capacity of 1 346.6 mAh g^{-1}, and after 100 cycles, a high capacity retention of 58.8% was achieved compared to the 2nd cycle. SnO_2@CNT-50 showed great cycling stability and rate capability due to lower crystal growth and low SnO_2 thickness in ultrathin films, which can address the degradation of the electrode and increase the electron kinetics of the electrode and the diffusion coefficient of Li ions. Additionally, after 100 cycles, SnO_2@CNT-50 showed a 99.27% CE, as presented in Fig. 18m.

In another work, Liu et al. [251] deposited amorphous Nb_2O_5 thin films on CNTs at 235–350 °C via controlled ALD. They explored the influences of the annealing and deposition temperatures on the surface morphology and crystal structure of Nb_2O_5@CNTs. Figure 19a presents a schematic diagram of Nb_2O_5 deposited on CNTs through ALD at 235 and 350 °C as well as the influence of the coating temperature on ALD-Nb_2O_5. The differences in the morphology and structure of Nb_2O_5 coated at 235

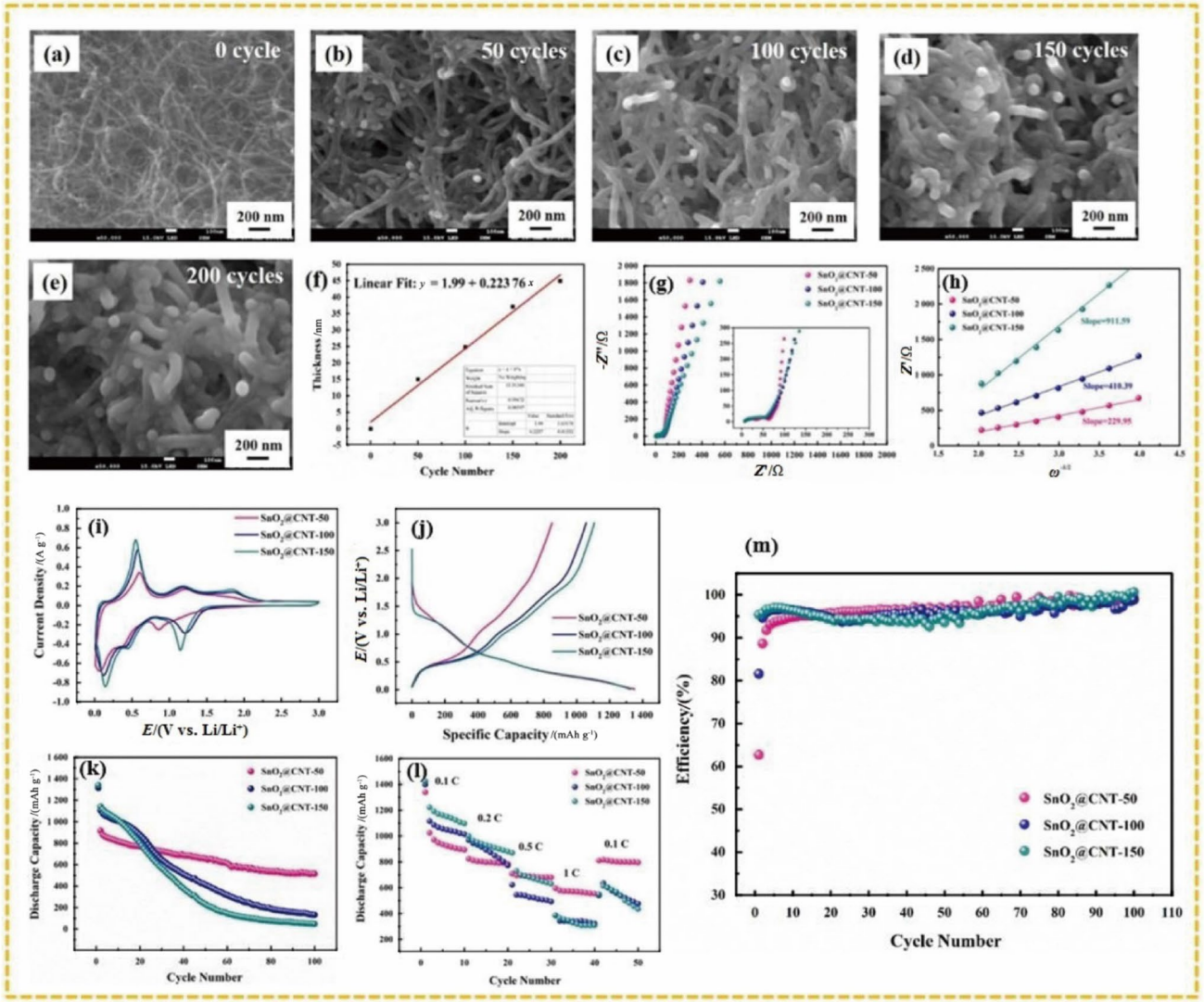

Fig. 18 **a**–**e** SEM photographs of SnO_2@CNT complexes obtained with different ALD cycle numbers. **f** Relationship between the SnO_2 film thickness and ALD cycle number under a 165 °C deposition temperature. **g** EIS spectra. **h** Dependence between the inverse square root of the angular frequency ($\omega^{-1/2}$) and real part of the impedance (Z') in the low-frequency region after the 3rd cycle for SnO_2@CNT complexes generated at 175 °C. **i** Cyclic voltammetry plots of ALD-SnO_2@CNT composites in the first cycle. **j** Discharge−charge curves of the SnO_2@CNT-50 sample in different cycles. **k** Cycling performance of SnO_2@CNT complexes at 0.1 C. **l** Rate capability of SnO_2@CNT complexes at different current densities. **m** CE plots for ALD-SnO_2@CNT composites at 0.1 C. Reprinted with permission from Ref. [250]. Copyright © 2019 Elsevier B.V. All rights reserved

and 350 °C could be attributed to various numbers of Nb_2O_5 nuclei in the ALD reaction. At high temperatures (such as 350 °C), oxygen-containing groups can have trouble in capturing $Nb(OEt)_5$, leading to a tiny amount of Nb_2O_5 nuclei on the CNT surface. These nuclei, which are far from each other, have a tendency to grow independently to form Nb_2O_5 nanoparticles with island-like shapes. For verification of this theory, first, 10-ALD-cycle Al_2O_3 interface films were grown on the CNT surface, and then, 100 ALD cycles of Nb_2O_5 films were performed at 350 °C. As presented in Fig. 19b, the Nb_2O_5@Al_2O_3@CNT surface was almost smooth, and no obviously visible nanoparticles existed on the CNT surface. Their findings revealed that Nb_2O_5 could be directly grown on Al_2O_3 interface layers without difficult nucleation stages or delays during the ALD-Nb_2O_5 process.

Interestingly, uniform and ultrathin Nb_2O_5 nanocrystal films with a hexagonal (TT) phase on CNTs resulted in a 325.1 mAh g^{-1} capacity at 0.2 A g^{-1} (Fig. 19d). Nb_2O_5@CNTs deposited at 235 and 350 °C revealed 44.7% and 49.8% capacity retention, respectively, with increasing current density from 0.2 to 3 A g^{-1}. Nb_2O_5@CNTs annealed

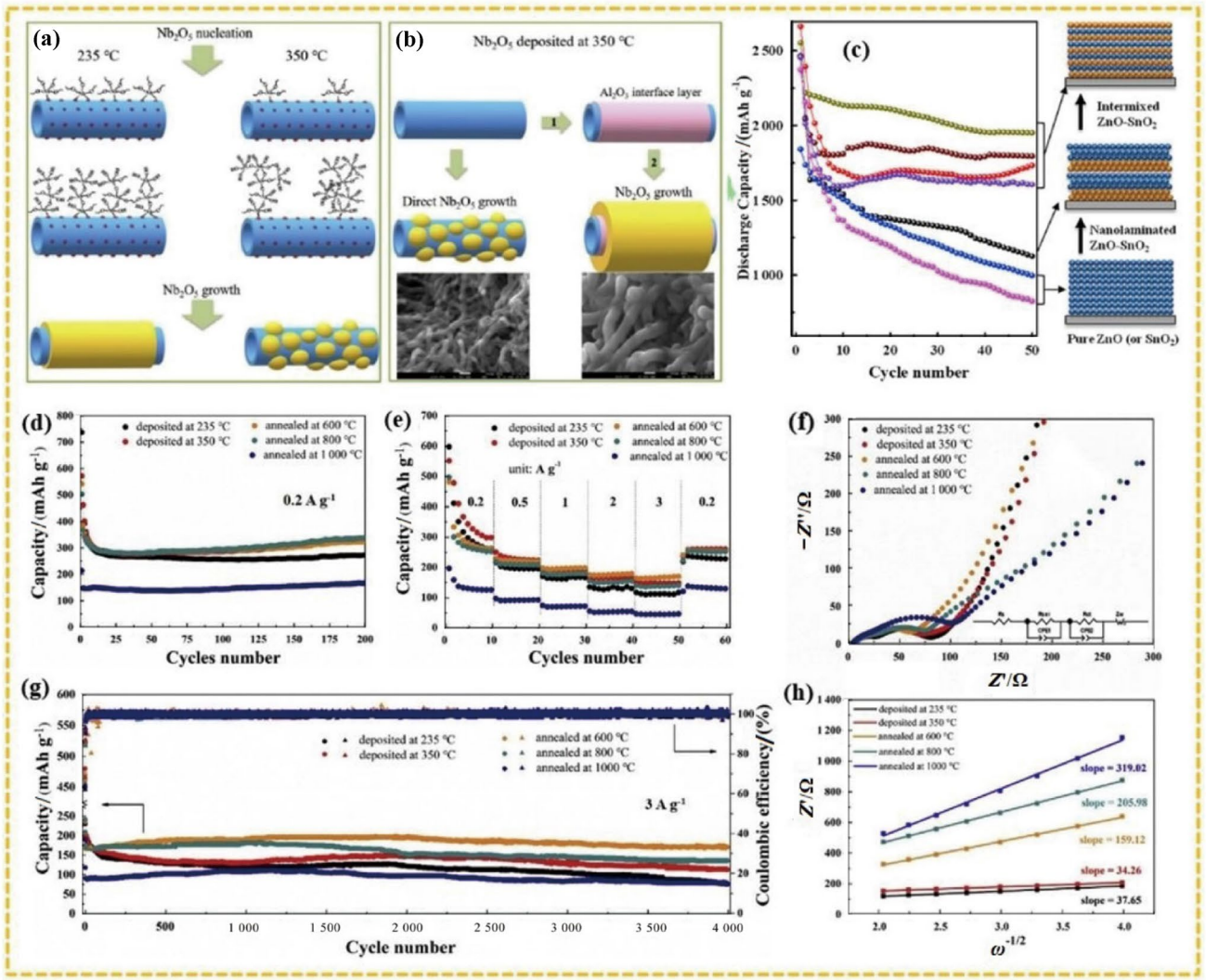

Fig. 19 **a** Schematic view of ALD-Nb_2O_5 on the CNT surface at temperatures of 235 °C and 350 °C **b** schematic view of artificial reaction sites, and SEM images of the Nb_2O_5@CNT complexes deposited at 350 °C with 100 ALD Nb_2O_5 cycles and Nb_2O_5@Al_2O_3@CNTs deposited at 350 °C with 10 ALD Al_2O_3 cycles and 100 ALD Nb_2O_5 cycles. Reprinted with permission from Ref. [251]. Copyright © 2020, Elsevier B.V. All rights reserved. **c** Comparison of the cycling stability for intermixed ZnO-SnO_2, nanolaminated ZnO-SnO_2, and bare ZnO or SnO_2 anodes. Reprinted with permission from Ref. [247]. Copyright © 2019 Elsevier B.V. All rights reserved. **d** Cycling performance of the samples achieved in the 0.01 to 3 V voltage range at a 0.2 A g^{-1} current density; **e** rate capability of samples achieved in the 0.01 to 3 V voltage range at different current densities; **f** Nyquist plots of Nb_2O_5@CNT electrodes after 200 cycles at 0.2 A g^{-1}, and equivalent circuit applied to fit experimental data in the inset. **g** Extended cycling efficiency of models at a 3 A g^{-1} current density. **h** Linear fitting of Z' versus $\omega^{-1/2}$ in the low-frequency region. Reprinted with permission from Ref. [251]. Copyright © 2020 Elsevier B.V. All rights reserved

at 600, 800 and 1 000 °C presented 65.3%, 55.7% and 37.1% capacity retention from 0.2 to 3 A g^{-1}, respectively (Fig. 19e). In addition, initial discharge capacities of 737 and 571.6 mAh g^{-1} as well as capacities of 272.7 and 333.4 mAh g^{-1} over 200 charge/discharge cycles, respectively, were obtained. The Nb_2O_5@CNT composites annealed at 600, 800 and 1 000 °C gave initial discharge capacities of 541.5, 503.8 and 214.3 mAh g^{-1}, respectively, and capacities of 325.1, 338 and 166.9 mAh g^{-1} were maintained over 200 cycles, respectively. Even at a current density as high as 3 A g^{-1}, a 170 mAh g^{-1} stable capacity was still obtained over 4 000 cycles (Fig. 19g). The resistance due to SEI films (R_{sei}) of the Nb_2O_5@CNT composites annealed at 800 and 1000 °C was remarkably higher than that of the other samples, which could be due to more SEI layer formation on the Nb_2O_5 nanoparticle surface and exposed CNTs. The charge transfer resistance (R_{ct}) of Nb_2O_5@CNTs annealed at 600 °C was lower than that of the materials annealed at 800 and 1 000 °C, which was generally due to greater contact areas between CNTs and uniform Nb_2O_5 thin films.

The correlation between Z' and $\omega^{-1/2}$ in the low-frequency region for Nb_2O_5@CNTs annealed at 600 °C was certainly lower than that of the materials annealed at 800 and 1 000 °C (Fig. 19f, h), proving that Nb_2O_5@CNTs annealed at 600 °C had a larger diffusion coefficient than the other annealed samples.

Detavernier et al. [247] applied ALD to explore the effects of the mixing degree, crystallinity, and composition of ZnO–SnO_2 ternary materials as anode materials on the LIB performance. First, they concluded that the deposited film was amorphous and could be crystallized after annealing. Spinel Zn_2SnO_4 films provided first and second discharge capacities of 2 363 and 1 915 mAh g^{-1} and a first CE of 81%; the capacity of Zn_2SnO_4 after 5 cycles remained stable, and a 1 515 mAh g^{-1} capacity was maintained even after 50 cycles at a 0.5 A g^{-1} current density. They also found that atomically intermixed ZnO-SnO_2 films showed higher performance than ZnO-SnO_2 nanolaminates. Figure 19c compares the cycling stability for intermixed ZnO-SnO_2 and nanolaminated ZnO-SnO_2 as well as pristine ZnO and SnO_2 anodes. Lie et al. [252] applied the ALD method for the deposition of V_2O_5 on porous nitrogen-doped graphene (NG) nanosheets to prepare NG-V composite electrodes with great electrochemical characteristics due to the synergistic effect between NG and V_2O_5, in which V_2O_5 was uniformly diffused on the porous graphene nanosheet surfaces because of strong chemical interactions. Graphene could mitigate the volume change of V_2O_5 within the discharge and charge process to guarantee structure stability. After 500 cycles at 1 000 mA g^{-1}, a 365 mAh g^{-1} discharge capacity for the whole electrode (675 mAh g^{-1} for V_2O_5) was obtained, the CE was approximately 100%, and great cycle retention of the capacity rate was sustained. Al_2O_3/SnO_2/CNT complexes were fabricated through a simple two-step ALD process. Ultrathin SnO_2 and Al_2O_3 layers played significant roles in improving the cycling stability, CE, and rate capability of Al_2O_3/SnO_2/CNT composites. In particular, the 10-Al_2O_3/SnO_2/CNT composite (with 10 Al_2O_3 and 75 SnO_2 cycles) obtained a 581.6 mAh g^{-1} discharge capacity after 200 charge/discharge cycles with 90.85% capacity retention and a 100 mA g^{-1} current density compared to the 2nd cycle. Although the Al_2O_3 layer increased the charge transfer resistance, as an artificial layer of the SEI, it provided good structural integrity and surface stability to suppress SEI layer growth and SnO_2 detachment [253]. A common TMO-based anode that combined carbonaceous materials was amorphous TiO_2 grown on CNT network/carbon fiber paper (CFP) substrates through ALD at 120 °C, where water and $TiCl_4$ were applied as oxygen and titanium sources, respectively [254].

Cao et al. [236] prepared novel ZnO/TiO_2 nanolaminates through ALD as anode materials by repeatedly depositing 26-cycle ZnO and 26-cycle TiO_2 units on Cu foil. The ZnO/TiO_2 nanolaminates were revealed to be significantly stabler than bare ZnO layers within charge/discharge operations. Therefore, the ZnO/TiO_2 nanolaminates revealed higher electrochemical performance than bare ZnO films in terms of higher CE, enhanced cycling performance, and higher rate capability. Because of their limited surface area, 2D anode materials suffer from low energy density. However, 3D materials, with their higher surface area, have higher mass loading capability and therefore higher capacity than 2D materials. Additionally, as current collectors, these materials can decrease the stress due to volume changes in charge/discharge processes. Li et al. [255] applied various ALD cycles for the deposition of ZnO on expanded graphene (EG) to form ZnO-EG composites. The 300-cycle ZnO-EG anode presented the highest rate capability with a capacity as high as 417 mAh g^{-1} at 800 mA g^{-1}. Additionally, it had a stable capacity of approximately 438 mAh g^{-1} at 200 mA g^{-1} after 500 cycles. Gregorczyk et al. [256] developed a 3D core–shell MWCNT@RuO_2 electrode via ALD of RuO_2 layers on MWCNT sponges. The obtained 3D core–shell MWCNT@RuO_2 electrode exhibited a 1.6 mAh cm^{-2} areal capacity, which was 50 times higher than that of the planar RuO_2 film. A ~ 0.6 mAh cm^{-2} areal capacity remained after 100 charge/discharge cycles, while the planar RuO_2 film only retained an ~ 0.02 mAh cm^{-2} areal capacity. Dhara et al. [257] synthesized 3D CNT@MoO_x composites, providing a much better areal capacity, ~ 27 times greater than that of planar MoO_x. They also concluded that thinner MoO_x represents higher cycling stability, and optimized MoO_x (~ 25 nm, 300 cycles)/CNTs displayed a stable reversible specific capacity of 915 mAh g^{-1} (645 μAh cm^{-2} areal capacity) with high capacity retention after 50 cycles (97.5% compared to the 2nd cycle).

Similar to the fabrication of lithiated ternary cathodes, ALD is employed for growing lithiated ternary anode materials. The $Li_4Ti_5O_{12}$ ALD process consists of two Ti–O and Li–O subcycles utilizing precursors of titanium isopropoxide, LiO^tBu and H_2O [258]. By adjusting the deposition cycle ratio of Li–O and Ti–O, amorphous Li-Ti–O thin films with desired composition were deposited on nitrogen-doped CNTs. Then, the amorphous Li-Ti–O films were transformed into crystalline $Li_4Ti_5O_{12}$ by annealing at 850–950 °C in air. Studies have also revealed that Ti precursors play a key role in adjusting the properties of $Li_xTi_yO_z$ films [259]. When $TiCl_4$ precursors were employed, the deposited $Li_xTi_yO_z$ layers were extremely air-sensitive, and the concentration of Li was low, while $Ti(OiPr)_4$ layers were stabler in air, and the content of Li could be simply tuned over a broad range. The reason for the difference was that the substrate surface was less reactive to LiO^tBu after $TiCl_4$-H_2O treatment than $Ti(OiPr)_4$-H_2O. Currently, SnO_2 has also been coated on novel 2D titanium carbide sheets (MXenes) through ALD to prepare anode materials for LIBs. Fluorine, oxygen, and

hydroxyl functional groups on the MXene surface were essential for preventing degradation of the MXene in the ALD process [260]. The SnO_2-MXene composites exploited the high Li-ion capacity introduced by SnO_2 while retaining the mechanical and structural integrity of the conductive MXene configuration.

3.2.2 Modification of LIB Anode Materials via ALD

The main aim of surface modification of anode materials is the creation of a protective film to prevent contact between the electrolyte and anode material at the interface. In high-capacity anode materials such as Sn and Si, due to the high volume change, cracks are formed on the surface, and fresh anode materials are exposed to the electrolyte, resulting in degradation of anode materials and depletion of the electrolyte and in a subsequent decrease in the capacity of the battery [264]. Therefore, engineering and designing the anode-electrolyte interface, which acts as an artificial SEI, is of great importance. The properties of the SEI layer should be such that it can, on the one hand, prevent unwanted reactions between the anode and electrolyte and, on the other hand, improve the ionic and electronic conductivity. Generally, modification of anode materials such as metal oxides and creation of protective surfaces are performed by common methods such as wet chemistry and the sol–gel method [265]. These methods include several complicated steps and require the application of large amounts of solution. Additionally, they are only applied for powder electrode materials and before the fabrication of electrodes [266]. In recent years, the ALD coating method has become popular as a promising method for film formation with controlled thickness at the Å-level on the powder and surface materials of electrodes. ALD coatings can be applied to protect original anode surface materials and improve the cycling stability and LIB safety.

As mentioned before, anode materials containing Li metal form dendrites during charge/discharge processes, which finally grow to pierce the separator and contact the cathode material, resulting in short circuit and explosion of the battery. To solve this problem, Jiang et al. applied ALD for the deposition of uniform and conformal ZnO coatings on carbon fibers to improve the wettability of Li and provide nucleation sites for Li metal. Figure 20a, b present schematic views of Li growth on Li/C-ALD and Li/C-Sol composite structures and SEM images, respectively [267]. They found that the ALD method promoted homogeneous distribution and conformal coating of ZnO on carbon fiber scaffolds compared to deposition from solution. ALD-ZnO-tailored carbon fiber/Li (Li/C-ALD) exhibited much higher rate and cycling performance than liquid coating ZnO-deposited carbon fiber/Li complex anodes. The electrodes displayed a very long lifespan of up to 400 cycles at 3.0 mA cm^{-2} and a high rate performance (338 mV deposition overpotential at 25.0 mA cm^{-2}) at a high Li deposition areal capacity of 5.0 mAh cm^{-2}. Zhang et al. [268] applied ALD to deposit ultrathin TiO_2 protective layers on a Li metal anode. They reported that a 5 nm TiO_2 layer was the optimum thickness with regard to cycling stability, rate capability and capacity in both full-cell and symmetric battery systems. The TiO_2 layer improved uniform Li^+ deposition and efficiently inhibited Li dendrite growth. As seen in Fig. 20c, d, symmetric Li/50TiO_2||Li/50TiO_2 batteries could cycle in a stable manner for more than 500 h at a 3 mA cm^{-2} current density and for more than 1 600 h at 1 mA cm^{-2} and 10 mA cm^{-2} current densities. Li/50TiO_2||NCM622 full cells presented higher rate and long-cycle performance and increased capacity retention by 23.3% compared to the pristine electrode after 100 cycles at a charge/discharge current density of 0.5 C.

In another study, Sung et al. [269] studied zirconia (ZrO_2) deposition on Li metal through subcycle plasma ALD (Fig. 20e). Li encapsulated with a ZrO_2 ALD nanolayer presented great resistance to atmospheric exposure for at least 1–5 h, high heat resistance up to 170–180 °C (near the Li melting point) and high rate capability because of the high ionic conductivity and great thermal resistance properties of the ZrO_2 ceramic. Schematics of the surface resistance of pristine Li metal and the metal after ZrO_2 deposition with 20, 50, and 100 ALD cycles under air exposure and thermal conditions for comparison are presented in Fig. 20g, h.

Huang et al. [270] deposited an alumina film on a Si anode. Al_2O_3 ALD was conducted at 250 °C utilizing precursors of TMA and H_2O. They found cracks on Si anodes after 40 cycles at 0.005–2 V (Fig. 20(f(a))). The effects of cracking were decreased by confining the discharge state to 0.23 V, but minor cracks were still observed after 100 cycles (Fig. 20b, f). No obvious cracks were observed in the electrodes with the alumina coating (Fig. 20(f(c)) and (f(d))). In terms of the mechanics of crack growth, nanoscale cracks and tiny pinholes are the major reasons for fracture. They proved that tiny cracks and pinholes were decreased by the fully conformal coating of Al_2O_3, which meant that beyond inhibiting side reactions, ALD coatings stabilized the silicon material structure by boosting their fracture resistance. Rubloff et al. [271] demonstrated as a proof-of-concept that an ALD-Al_2O_3 film with a 14 nm thickness can passivate the Li surface against corrosion caused by electrolyte, sulfur, and atmosphere exposure. They studied Li-S battery cells and demonstrated enhanced capacity retention for up to 100 cycles by implementing ALD-passivated anodes in cells assembled with pristine Li metal anodes. Li et al. [63] applied ALD to deposit MgO on nanosized porous Si dendrites achieved by etching an Al-Si alloy for LIBs. They used H_2O as an oxidizer and bis-encyclopedic

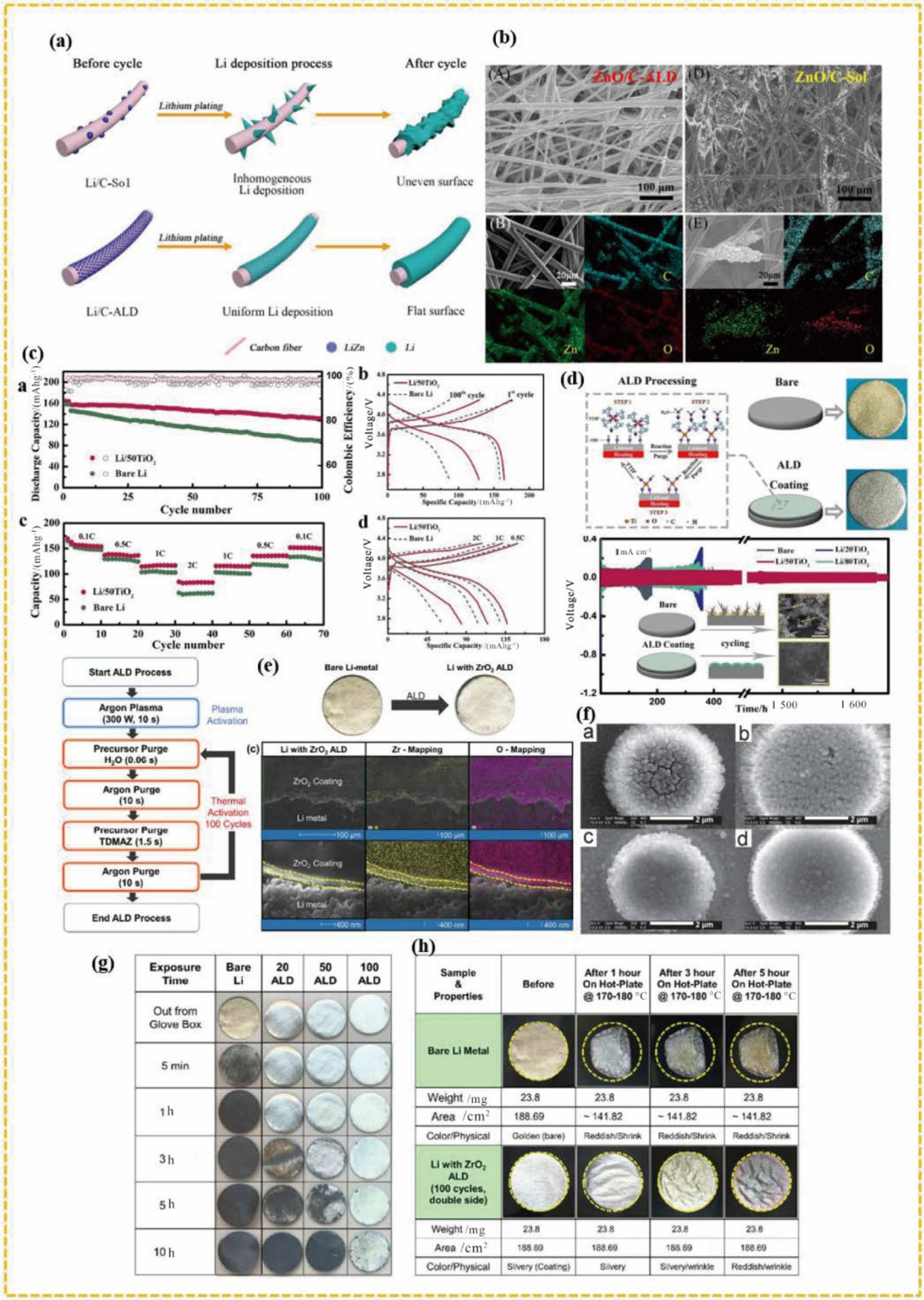
(a)
Before cycle
Li deposition process
After cycle
Lithium plating
Li/C-Sol
Inhomogeneous Li deposition
Uneven surface
Lithium plating
Li/C-ALD
Uniform Li deposition
Flat surface
(b)
ZnO/C-ALD
ZnO/C-Sol
100 μm
20μm
C
Zn
O
(c)
Carbon fiber
LiZn
Li
Discharge Capacity/(mAhg⁻¹)
Coulombic Efficiency/(%)
Li/50TiO2
Bare Li
Cycle number
Voltage/V
Specific Capacity/(mAhg⁻¹)
100th cycle
1st cycle
Capacity/(mAhg⁻¹)
0.1C
0.5C
1C
2C
(d)
ALD Processing
Bare
ALD Coating
Li/20TiO2
Li/80TiO2
cycling
Time/h
(e)
Bare Li-metal
Li with ZrO2 ALD
ALD
Start ALD Process
Argon Plasma (300 W, 10 s)
Plasma Activation
Precursor Purge H2O (0.06 s)
Argon Purge (10 s)
Precursor Purge TDMAZ (1.5 s)
Argon Purge (10 s)
Thermal Activation 100 Cycles
End ALD Process
Zr - Mapping
O - Mapping
ZrO2 Coating
Li metal
(f)
2 μm
(g)
Exposure Time
Bare Li
20 ALD
50 ALD
100 ALD
Out from Glove Box
5 min
1 h
3 h
5 h
10 h
(h)
Sample & Properties
Before
After 1 hour On Hot-Plate @ 170-180 °C
After 3 hour On Hot-Plate @ 170-180 °C
After 5 hour On Hot-Plate @ 170-180 °C
Bare Li Metal
Weight /mg
Area /cm²
Color/Physical
Golden (bare)
Reddish/Shrink
Li with ZrO2 ALD (100 cycles, double side)
Silvery (Coating)
Silvery
Silvery/wrinkle
Reddish/wrinkle

◂**Fig. 20** **a** Schematic of ALD Li coating on Li/C-Sol and Li/C-ALD composites. **b** SEM images of (A) ZnO/C-ALD and (D) ZnO/C-Sol. Elemental mapping of (B) ZnO/C-ALD and (E) ZnO/C-Sol. Reprinted with permission from Ref. [267]. Copyright © 2020, American Chemical Society. **c** and **d** Electrochemical and schematic views of an ultrathin TiO_2 film produced by ALD, and physical demonstrations of pristine Li and Li/50TiO_2 electrodes. Reprinted with permission from Ref. [268]. Copyright © 2021, Elsevier B.V. All rights reserved. **e** (a) Process flow chart of PEALD of ZrO_2 on Li metal. (b) Snapshots of the pristine Li metal (the diameter 19 mm) and post-coating by ZrO_2 ALD. (c) SEM−EDS images of a ZrO_2 coating on a Li metal cross-section represented by O and Zr mapping at various magnification scales of 100 μm and 400 nm. Reprinted with permission from Ref. [269]. Copyright © 2018, American Chemical Society. **f** SEM images of (a) a bare Si electrode and (b) an ALD-20 Si electrode in their 100% charged state after 40 charge/discharge cycles in the 0.005–2 V range. (c) Pristine Si electrode and (d) ALD-20 Si electrode in the 100% charged condition after 100 charge/discharge cycles in the 0.23–2 V voltage range. Reprinted with permission from Ref. [270]. Copyright © 2011, Wiley. **g** Photograph comparison of pristine Li metal and the metal after ZrO_2 deposition with different ALD cycles under ambient conditions. **h** Comparison of pristine and 100-cycle ALD-ZrO_2 Li metal under thermal exposure (170–180 °C). Reprinted with permission from Ref. [269]. Copyright © 2018, American Chemical Society

magnesium as a Mg precursor. The reactor temperature was adjusted to 250 °C. The engineered electrode presented excellent rate capability and cycling performance due to its special structure, such as porous MgO and Si films. The pSi@MgO (5C) electrode provided a reversible capacity of 969.4 mAh g^{-1} and a high CE of 98.57% up to 100 cycles. Furthermore, it presented a value of 765.1 mAh g^{-1} at 500 mA g^{-1} for up to 200 cycles. Moreover, a uniform MgO film coated via ALD could mitigate the very large volume expansion throughout the charge and discharge process.

Xiao et al. [272] conducted research to compare the morphology of pristine Si and an ALD-Al_2O_3-deposited Si ultrathin film electrode after 11 charge/discharge cycles. Obviously, the bare Si film had many cracks. However, the 5 nm Al_2O_3-deposited Si layer showed fewer cracks, proving that ALD inhibited the mechanical degradation of the Si anode. Wei et al. [273] coated an ALD-TiO_2 layer on the surface of SnO_2/nitrogen-doped carbon (NC) complexes, in which 5 nm SnO_2 nanoparticles (NPs) were uniformly diffused in interconnected NC. They reported that the SnO_2/NC composites could provide better performance than SnO_2. The ALD-TiO_2 coating could enhance the rate capability and cycling stability of the SnO_2/NC complexes. SnO_2/NC complexes with a 10 nm thick ALD-TiO_2 protective film demonstrated excellent electrochemical performance, providing 871 mAh g^{-1} after 200 cycles at 100 mA g^{-1}. Wang et al. [274] prepared germanium@graphene@TiO_2 (Ge@G@TiO_2) nanofibers (NFs) as anodes. Their results showed that the Ge@G electrode could provide a higher performance than pristine Ge, implying a capacity of 804 mAh g^{-1} after 100 cycles. Moreover, ALD-TiO_2 deposition could further enhance the remaining capacity of 1 050 mAh g^{-1} and cycling stability after 100 cycles. Table 6 lists some of the anode materials of LIBs whose surface was modified with ALD.

3.3 ALD of SSEs

Recently, researchers have increasingly tried to practically and scientifically apply inorganic SSEs instead of traditional organic liquid electrolytes (OLEs) in the new generation of LIBs. Typically, OLEs contain $LiPF_6$ dispersed in a mixture of liquid organic solvents containing low-viscosity components such as ethyl methyl carbonate (EMC), diethyl carbonate (DEC), and dimethyl carbonate (DMC) and high-dielectric components such as ethylene carbonate (EC). Due to their flammable nature and the possibility of leakage, OLEs are not very popular. SSEs have higher energy and power densities, longer lifespan, better ionic conductivity, higher reliability, and lower cost than liquid and polymeric electrolytes [283]. An ideal SSE needs to be a Li-ion conductor, an electron insulator, highly uniform, and mechanically robust and have a low activation energy for Li-ion diffusion [284]. Therefore, the ALD technique is ideal for achieving the above properties. To date, a variety of compounds, including oxides, nitrides, hydrides, fluorides, sulfides, and halides, have been introduced for SSEs in the literature [79, 285, 286]. Among them, due to their crystallinity, oxides and sulfides are classified as crystalline materials such as glasses and ceramics. Additionally, the most extensive research has been conducted on this topic. To date, traditional methods such as CVD, PVD, solid-state reactions, wet chemical processes and melt quenching have been applied for the fabrication and development of SSEs [287, 288]. Most of these methods have errors and limitations in adjusting the components of SSEs to achieve acceptable ionic conductivity, which limits the development of research on this topic. Therefore, a method is required to be able to precisely adjust the components of the deposited layer and accelerate research on the development of SSEs. Among the developed methods, ALD is a novel method with extraordinary features in the practical design and growth of compounds at the atomistic scale with uniform structure and precise thickness, freedom in employing different compounds, low in situ temperature, and high flexibility in the fabrication and modification of SSEs. ALD is used in the development of SSEs for two reasons: (i) synthesis of thin electrolyte films for solid-state 3D microbatteries with high energy and (ii) tailoring of the interface to improve the stability and ionic conductivity of both solid- and liquid-state batteries.

Table 6 Summary of ALD surface modifications of LIB anodes

Anode material	Coating	Precursor	Temperature/°C	Deposition cycle/thickness	References
Carbon fiber/Li	ZnO	DEZ + H_2O	100	0.2 Å $cycle^{-1}$, 30–50 nm, 150–250 cycles	[267]
Li	TiO_2	(TTIP) + H_2O	150	0.1 nm $cycle^{-1}$, 20–80 cycles	[268]
Li	ZrO_2	TDMAZ + H_2O	140–145	100 cycles	[269]
Si	Al_2O_3	TMA + H_2O	250	1 Å $cycle^{-1}$, 20–40 cycles	[270]
Li	Al_2O_3	TMA + Plasma O_2	150	1.2 Å $cycle^{-1}$, 14 nm, 100 cycles	[271]
Si	MgO		250	…	[63]
Si	Al_2O_3	TMA + H_2O	…	5 nm	[272]
SnO_2/NC	TiO_2	…	200	10 nm, 100–400 cycles	[273]
Li	LixAlyS	Li(O^tBu) + H_2S + (TDMA-Al)	150	50 nm	[275]
MoO_3	HfO_2	Hf(NMe_2)$_4$-H_2O	180	3 nm, 10 cycles	[276]
SnO_2/GO	Al_2O_3	TMA + H_2O	200	3 nm, 30 cycles	[277]
Carbon black	Al_2O_3	TMA + H_2O	180	2 nm, 20 cycles	[278]
CNTs	SiO_2	APTES + BDEAS + H_2O	150	10 nm, 300 cycles	[62]
SnS_2	Al_2O_3	TMA + H_2O	120	4.2 nm, 40 cycles	[279]
SnS_2	TiO_2	TDMAT + H_2O	150	4 nm, 80 cycles	[280]
Ge	TiO_2	TTIP + H_2O	180	5 nm	[274]
Fe_2O_3	TiO_2	$FeCp_{2+}$ H_2O	130	10 nm	[281]
CuO	Al_2O_3	TMA + H_2O	120	10–15 nm	[282]

Notably, in all-solid-state microbatteries, the overall fabrication of SSEs along with electrodes through ALD is highly popular. In the following, a summary of recent progress in the application of ALD to SSEs is provided. Li-containing thin films formed through ALD are applied for SSEs and LIB electrodes. SSE materials are generally ternary or even more complicated; therefore, subcycle ALD of these complexes combined with subcycle ALD of Li-containing films requires multiple precursors. As mentioned before, LiO^tBu, Li(thd), $LiOSiMe_3$ and Li($N(SiMe_3)_2$) are effective precursors in ALD. The application of these precursors is very efficient for the synthesis and development of SSEs. Notably, in addition to the above Li-containing precursors, hundreds of Li-free precursors have been introduced; however, little research has been conducted on their combination with Li-containing films. Therefore, the growth of SSE compounds via ALD has great potential for future research. Fabrication of a high-performance electrolyte–electrode interface is the main challenge for SSEs [283]. For example, the application of an ALD-Al_2O_3 interlayer on an SSE film surface provided a good Li metal anode-electrolyte interface. Such well-contacting interfaces could effectively decrease the specific resistance of the interfacial area from 1 710 to 1 Ω cm^2 [289]. Figure 21a illustrates a schematic view of the interface between Li metal and garnet. Pristine garnet has poor physical contact with Li metal. By means of ALD coating, the ultrathin Al_2O_3 film promotes the molten Li metal to uniformly deposit on the surface of garnet without interfacial vacancies. The SEM images in Fig. 21b evidently illustrate the improvement of interfacial contact by employing the ultrathin ALD-Al_2O_3 film on the garnet surface.

Recent studies have revealed that the modification of grain boundaries (primary particles) inside materials is critical. For instance, Zhang et al. [290] reported that the infusion of a solid electrolyte (i.e., Li_3PO_4) into $LiNi_{0.76}Mn_{0.14}Co_{0.10}O_2$ grain boundaries dramatically enhanced the voltage stability and capacity retention of cathodes fabricated via ALD and heating processes. The solid electrolyte Li_3PO_4 coated on the secondary particle surface and infused inside the boundaries facilitated Li diffusion and prevented the infiltration of the liquid electrolyte into the boundaries, enhancing the cycling performance of Ni-rich layered oxides. The effects of LPO application on the electrochemical performance are presented in Fig. 21(c(a-d)).

The challenges of interface impedance are not limited to the preparation of pristine batteries. The lack of contact due to inconsistent variations in volume among the electrolyte, anode and cathode materials during cycling is another problem (Fig. 21f, g) [291]. Hence, electrolyte–electrode engineering is another critical factor in the fabrication of SSEs. Figure 21f presents thick horizontal slices of one voxel derived from the inside of an SSE pellet throughout an experiment at different times. The formation of dark lines represents fracture of the high-contrast LAGP. The images below show that a crack network was formed by filtering all 2D slices of the pellet with an adjustable binary partition approach and then reassembling them into a 3D volume. Figure 21g presents the tensile peripheral stress that causes

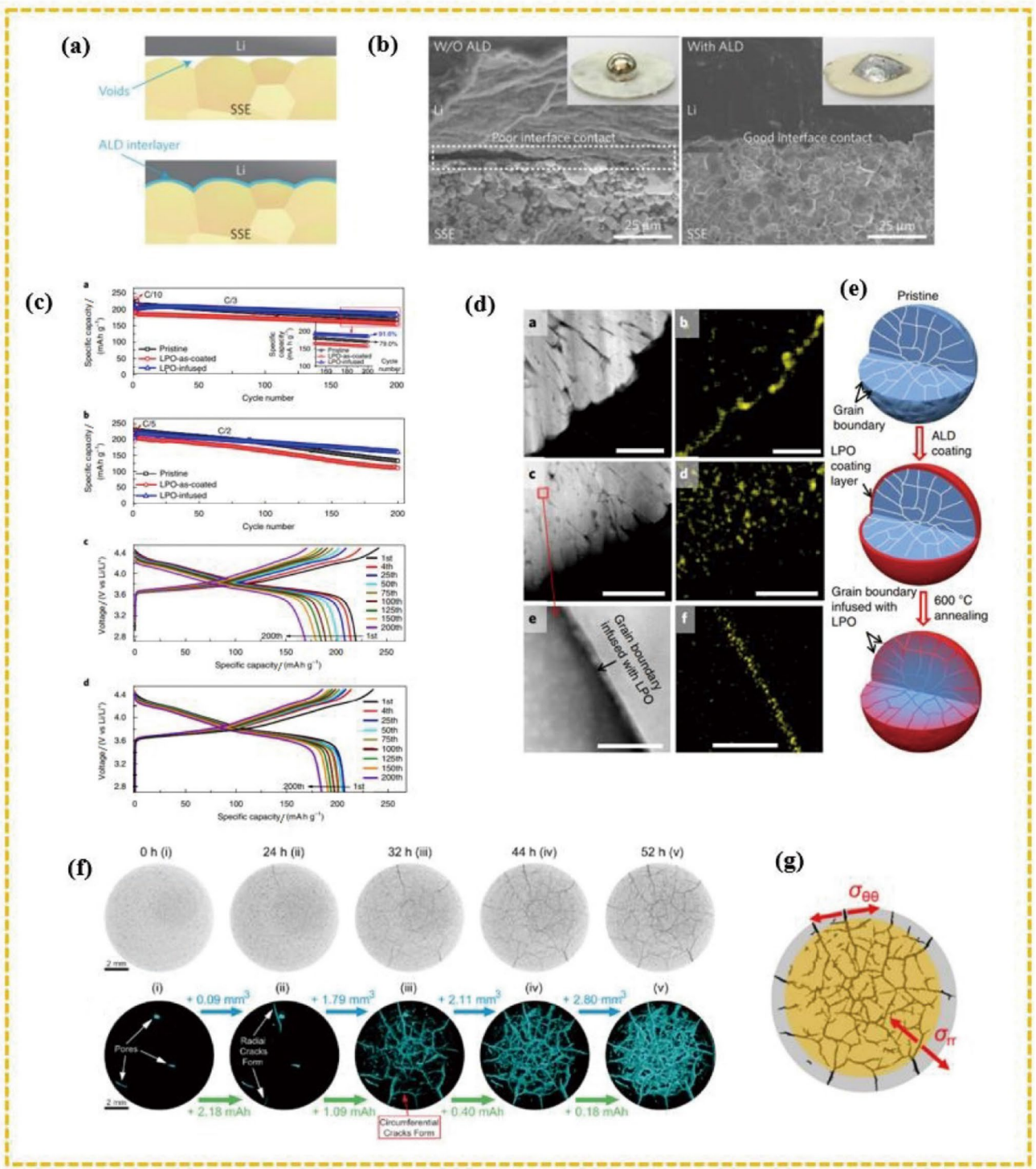

Fig. 21 **a** Schematics of an SSE with and without an ALD interlayer coating, and **b** SEM images for interface engineering of SSEs. Reprinted with permission from Ref. [289]. Copyright © 2016, Nature Publishing Group. **c**(a-d) Effects of LPO incorporation on the electrochemical efficiency. **d** Scan of the spatial distribution of LPO before battery cycling. **e** Schematic illustration of the LPO deposition film evolution on the secondary particle induced by coating and annealing. Reprinted with permission from Ref. [290]. Copyright © 2018, Pengfei Yan et al. **f** 2D slices derived from the 3D imaging of NASICON and the 3D crack network of the pellet. **g** Fragmented LAGP pellet in a segmented 2D picture slice. Reprinted with permission from Ref. [291]. Copyright © 2019, American Chemical Society

radial crack formation, and the tensile radial stress can cause peripheral crack creation.

Sun et al. [292] applied ALD for growing Li_3PO_4 SSEs at four temperatures of 250, 275, 300, and 325 °C, employing lithium trimethyl phosphate and tert-butoxide precursors. A linear relationship was observed between the ALD cycle number and film thickness, and uniform growth occurred at all the above temperatures. At deposition temperatures of 250, 275, 300, and 325 °C, growth rates of 0.57, 0.66, 0.69, and 0.72 cycle^{-1}, respectively, were achieved. In addition, an activation energy of ~0.51 eV and a maximum ionic conductivity of 1.73×10^{-8} S cm^{-1} at 323 K were obtained for ultrathin LPO layers coated at 300 °C, which were measured with electrochemical impedance spectroscopy. As a promising alternative solid-state thin film, lithium silicates can be deposited in the temperature range from 225 to 300 °C by incorporating ALD SiO_2 and Li_2O subcycles employing H_2O, tetraethylorthosilane (TEOS), and LiO^{t}Bu precursors [293]. Research has shown that due to their lower activation energy and higher lithium concentration, lithium silicate thin films provide a 1.45×10^{-6} S cm^{-1} ionic conductivity at 373 K.

Elam et al. [275] reported the successful synthesis of Li_xAl_yS SSE thin films via ALD. These films showed an ionic conductivity equal to 2.5×10^{-7} S cm^{-1} at room temperature and were found to effectively stabilize the liquid organic electrolyte-Li metal interface and decrease the interfacial impedance (by up to five times). Additionally, they found that Li_xAl_yS effectively suppressed the formation of Li dendrites during deposition and stripping cycles. These SSE coatings produced by ALD were found to be promising candidates for enhancing the performance of Li-O_2 and Li-S batteries. With the right selection of the film composition and precisely controlled thickness, lithium tantalate ($LiTaO_3$) SSEs were formed at 225 °C through ALD by applying a subcycle combination of $1\times Li_2O + n\times Ta_2O_5$ ($1\leqslant n\leqslant 10$). The $LiTaO_3$ thin layers presented great conformity and uniformity in 3D anodic Al_2O_3 templates. In addition, the $LiTaO_3$ thin films grown through subcycles of $1\times Li_2O$ and $6\times Ta_2O_5$ showed a 2×10^{-8} S cm^{-1} Li-ion conductivity at 25 °C [294]. The interaction mechanism of SSE materials and ALD-coated electrodes requires more research. To date, most reported works have focused on battery performance rather than the interactions of ALD materials and other battery components during charge/discharge cycles. ALD was successfully applied for the deposition of Li niobium oxide (LNO) ultrathin layers with precisely controlled composition and thickness of the film at 235 °C using niobium ethoxide and lithium tert-butoxide as Nb and Li sources, respectively. In addition, LNO thin films grown with a Nb:Li subcycle ratio of 4:1 provided a 6×10^{-8} S cm^{-1} Li-ion conductivity with a 0.62 eV activation energy at room temperature [295].

In another study, an artificial SEI of ALD-deposited graphite was examined. The obtained results showed that the TiO_2 coating enhanced the capacity of graphite by 5% and decreased the electrochemical generation of SEIs. Furthermore, an ALD-TiO_2 film on graphite improved the cycling ability and thermal stability over the long term at 55 °C [296]. Notably, some SSEs have been found to have an

Table 7 SSEs deposited by using the ALD process

SSEs	Substrate	Precursors	Temperature/°C	Deposition cycle/thickness	References
LLCZN/Al_2O_3	LLCZN	TMA + H_2O	150	5–6 nm 40 cycles	[289]
Li_3PO_4	$LiNi_{0.76}Mn_{0.14}Co_{0.10}O_2$	LiO^{t}Bu + TMP + H_2O	300	10 nm 0.07 nm cycle^{-1}	[290]
Li_3PO_4	Si	LiO^{t}Bu + TMP + H_2O	250–325	0.57–0.72 nm	[292]
Lithium Silicates	CNTs	LiO^{t}Bu + TEOS + H_2O	225–300	2.57 Å cycle^{-1}	[293]
Li_xAl_yS	Li/Cu foil	LiO^{t}Bu + H_2S + (TDMA-Al)	150	0.66 Å cycle^{-1}	[275]
$LiTaO_3$	Al_2O_3	LiO^{t}Bu + tantalum(V) ethoxide (Ta(OEt)) + H_2O	225	400 cycles ($1\times Li_2O + 6\times Ta_2O_5$)	[294]
Graphite/Al_2O_3/TiO_2	Graphite	TMA + TiI_4	150	100 cycles 20–30 nm	[296]
LiPON	Si	LiO^{t}Bu + TMP + H_2O + Plasma N_2	205	20–40 nm	[299]
$Li_xAl_ySi_zO$	Si	LiOH + Al_2O_3 + SiO_2 + H_2O	290	1–1.25 nm cycle^{-1}	[300]
$LiNbO_3$	Si/CNTs	LiO^{t}Bu + Nb(OEt)$_5$ + H_2O	235	1.82–2.87 Å cycle^{-1}	[295]
Li_4Si_2O	CNTs	LiO^{t}Bu + TEOS	225–300	2.57 Å cycle^{-1}	[293]
Li_2CO_3	Si	LiO^{t}Bu + O_2	50–300	0.82 Å cycle^{-1}	[301]
Li_3BO_3-Li_2CO_3	Si	LiO^{t}Bu + TIB + Plasma O_3	200–260	0.6 Å cycle^{-1}	[302]
Li_2PO_2N	Si	LiO^{t}Bu + DEPA	250	1 Å cycle^{-1}	[303]
LiPON	MWCNT	LiO^{t}Bu + TMP + H_2O + Plasma N_2	250	1 Å cycle^{-1}	[299]

extraordinary ionic conductivity magnitude of 10^{-2} S cm^{-1} at room temperature; examples are $Li_{10}GeP_2S_{12}$ (1.2×10^{-2} S cm^{-1}), $Li_{9.54}Si_{1.74}P_{1.44}S_{11.7}Cl_{0.3}$ (2.5×10^{-2} S cm^{-1}), $Li_{3.25}Ge_{0.25}P_{0.75}S_4$ (2.2×10^{-3} S cm^{-1}) [297] and $Li_7P_3S_{11}$ (1.7×10^{-2} S cm^{-1}) [298]. Meanwhile, the solid–solid interfaces between the electrode and SSE are still crucial factors in solid-state batteries. In recent years, several research studies have been performed on the incorporation of ALD for coating ion-conducting films on pellet SSEs to improve the cell performance and interfacial compatibility. Table 7 summarizes the current SSEs deposited by using the ALD process.

3.4 ALD of Separators

The separator is a critical component in LIBs that hinders physical contact between the positive and negative electrodes in batteries and prevents internal short circuits while acting as an electrolyte reservoir to allow ionic movement. An ideal separator not only needs large electrolyte uptake to decrease the cell internal resistance but also requires high mechanical strength with extremely low thickness, electrochemical and structural stability, and a porous matrix with high tortuosity to inhibit the growth of Li dendrites. Additionally, for the safety of the battery, the separator has to be able to shut down the battery in the case of overheating along with having a cost-effective manufacturing process. However, simultaneously achieving all these ideal characteristics for practical separators is difficult; therefore, balancing various characteristics of separators to fabricate high-performance batteries is essential. Furthermore, safety issues limit the application of separators in LIBs. Separator properties directly affect LIB performance factors such as the power and energy density, cycle life and safety by affecting the cell kinetics [304]. Therefore, separators play a critical role in the safety of batteries. The separator is a crucial safety component in LIBs, and its melting point, mechanical strength, and dimensional stability significantly affect the safety of batteries. Whereas polyethylene (PE) [305], polypropylene (PP) [306], and the combination of PP/PE/PP [307] are commercial microporous polyolefin separators that have been extensively employed due to their superior mechanical strength and chemical stability, they have drawbacks such as poor wettability and severe thermal wrinkling at high temperatures along with high cost in high-quality products, which limits their extensive utilization in EVs and large-scale energy storage systems. To address these limitations, extensive research has been performed to make sustained improvements in better and new separators.

Porous structures and chemically and thermally robust dielectric membranes are applied as separators to deliver the two functions of isolating the cathode and anode for prevention of short circuits and facilitating transport of ionic charge [308]. The separator characteristics affect LIB interface structures, the internal resistance of the battery, the electrolyte stability, etc., which directly affect the critical performance factors of LIBs, including the safety, cycle life, capacity, and charge–discharge current density. However, ceramic coatings on nonwoven separators effectively improve the heat tolerance and wettability of the separator, enhancing the battery safety [309]. Nevertheless, coating layers with thicknesses of several microns could obviously enhance the mass and thickness of separators and then reduce the energy density of the battery [271, 310]. Hence, reducing the mass and thickness of the ceramic coating layer is a critical demand for nonwoven separators to fabricate batteries with high safety and density. Previous research works have employed classic ALD for polyolefin separators and found it to be effective in functionalizing membranes with high thermal stability and wettability with no clear increase in mass or thickness [311]. Plasma enhancement before the ALD process can generate highly reactive ions and radicals and decrease the growth temperature [312]. Table 8 shows the general requirements for favorable LIB separators.

Wang et al. [314] applied ALD for the deposition of TiO_2 on porous PP membranes as separators in LIBs with Li cathodes and $Li_4Ti_5O_{12}$ (LTO) anodes. They concluded that a 20-cycle TiO_2 ALD thin film greatly prevented thermal wrinkling of separators, which improved LIB safety. In addition, the wetting of the separator with the electrolyte was simultaneously solved because of the configuration of a uniform hydrophilic TiO_2 layer. Using plasma activation, a great enhancement was achieved in the hydrophilicity of membranes coated by ALD with no pore shrinkage loss, which provided net passage of the electrolyte ions through the channels of the separator. Hence, an increase in the specific discharge capacity at different discharge rates was obtained while reasonably maintaining the cycling stability. Zhao et al. [315] developed a new core–shell composite

Table 8 General properties of separators implemented in LIBs [313]

Properties	Description
Porosity	40%–60%
Pore size	⩽1 μm
Thickness	20–25 μm
Permeability	⩽0.025 S μm^{-1}
Mechanical property	⩾1 000 kg cm^{-1} (98 060 kPa)
Wettability	Wets rapidly and completely
Dimensional stability	No crimping or flatting
Thermal stability	Shrinking after 60 min of less than 5% at 90 °C
Electrochemical stability	Stable for a long time
Shut down	At high temperatures

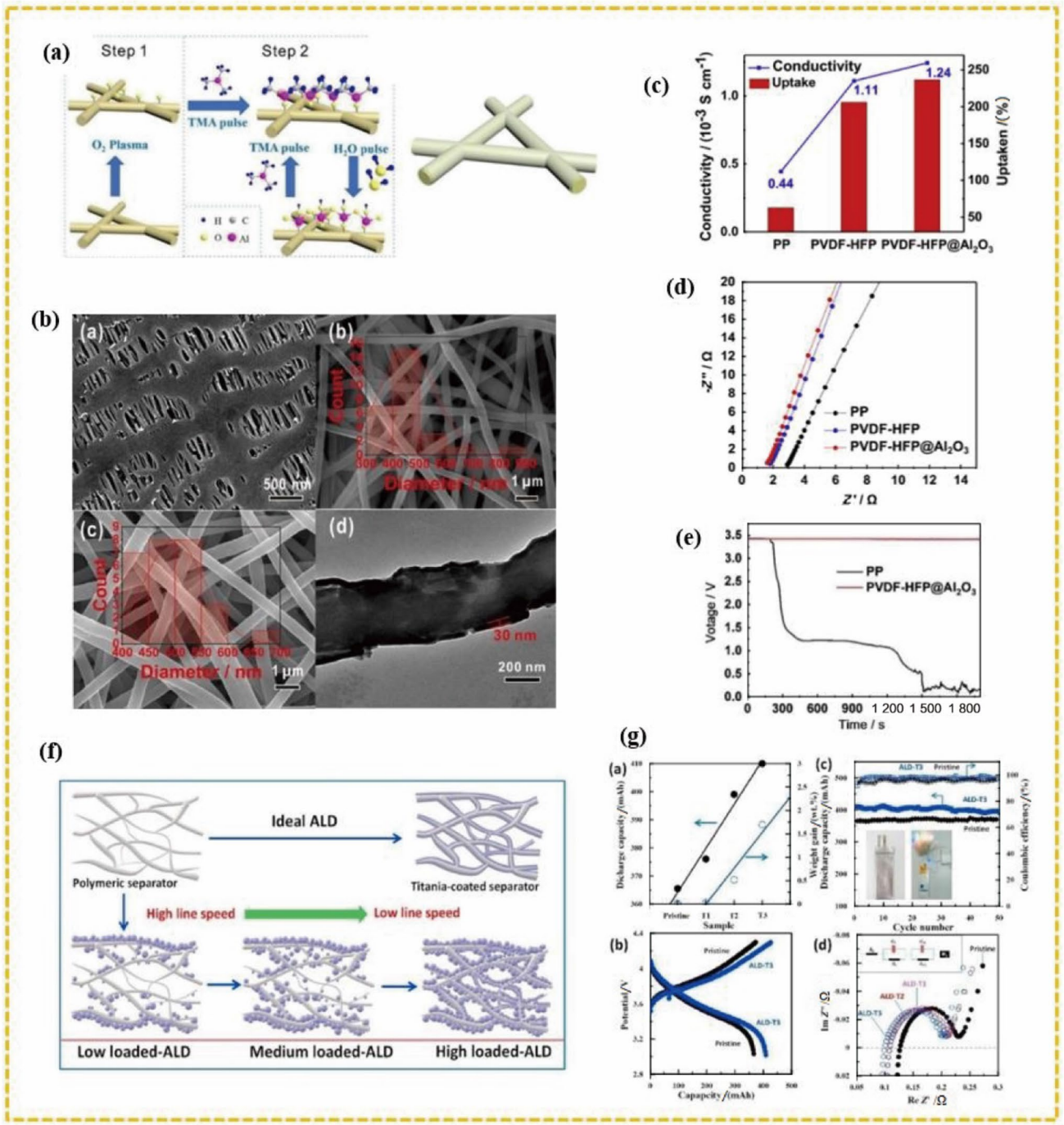

Fig. 22 Schematic image of **a** the fundamental production procedures and, on the right, the obtained core–shell configuration of ALD-Al_2O_3-modified separators. **b** SEM images of (a) PP, (b) PVDF-HFP and (c) PVDF-HFP@Al_2O_3, and (d) TEM image of the PVDF-HFP@Al_2O_3 fibers. **c** Electrolyte permeation diagram and ionic conductivity of separators. **d** AC impedance Nyquist curves. **e** Open-circuit voltage (OCV) plots of LFP/G full cells at 160 °C with various separators. Reprinted with permission from Ref. [315]. Copyright © 2018, Elsevier. **f** Cross-sectional images of TiO_2-modified separators. **g**(a) Discharge capacity and rise of the TiO_2 weight versus various separators. **g**(b) Charge/discharge plots of NCM/graphite electrodes utilizing bare and ALD-treated separators. **g**(c) Variety of CEs and discharge capacities at 0.2 C. **g**(d) Nyquist curves of the battery with various separators. Reprinted with permission from Ref. [316]. Copyright © 2018, Elsevier B.V. All rights reserved

nonwoven separator, polyvinylidene fluoride-hexafluoropropylene (PVDF-HFP)@Al_2O_3, by electrospinning a polymer followed by deposition of 30 nm Al_2O_3 onto a fiber mat through ALD. The fabricated separator had remarkable heat and fire resistance up to 200 °C and great thermal stability without any shrinkage, which significantly improved the safety of LIBs. In addition, the developed separator presented excellent electrochemical stability. Simultaneously, an excellent rate capability and a stable cycling performance were observed, which were consistent with the high ionic conductivity and electrolyte uptake ratio. The Nyquist plots in Fig. 22d from EIS tests showed bulk resistance values of 1.8, 1.6, and 2.8 Ω for PVDF-HFP, PVDF-HFP@Al_2O_3 and PP separators and corresponding conductivities of 1.11, 1.24, and 0.44 mS cm^{-1}, respectively, which slightly increased after ALD application. These findings were in accordance with the electrolyte penetration increase owing to the good affinity of Al_2O_3 to the electrolyte.

As indicated in Fig. 22e, the voltage of the cell containing the PP separator was strongly decreased after 300 s and tended to reach 0 V after 1 500 s. However, the PVDF-HFP@Al_2O_3 separator potential remained stable at the initial level, which showed the great thermal stability of the developed core–shell construction separator in practical battery devices. In another work, a plasma source was used by Chao et al. for ALD coating of TiO_2 on PE separators [316]. They developed a roll-to-roll (R2R) ALD method to coat a uniform TiO_2 film on porous PE separators for LIBs. Cross-sectional images of TiO_2-deposited separators obtained via ALD with different ALD cycles of TiO_2 on polymeric separators are presented in Fig. 22f. The R2R ALD approach utilizing the TTIP precursor and water as a coreactant provided accurate control over the formation of TiO_2 films on PE separators. A significant improvement in the LIB performance with TiO_2-modified separators was observed compared to the LIBs using bare polymeric separators. The TiO_2 coating also improved the structural and thermal stability by creating a steady and strong skeleton among the polymeric compounds. Consequently, the TiO_2 film played an important role in enhancing the performance of LIBs by enhancing the electrolyte wettability, improving the ionic conductivity, and reducing the high-frequency impedance. As seen in Fig. 22(g(a) and (b)), the discharge capacity of the battery was remarkably improved by up to 12.2% by implementing the TiO_2-coated separators. According to Fig. 22(g(c)), the LIBs sustained a stable charge/discharge capacity with an extremely high CE.

In a different paper, R2R ALD was suggested for a multilayer separator with the aim of easy mass manufacturing and high throughput [317]. In the study, an ultrathin layer of Al_2O_3 (approximately 5 nm) was deposited on both sides of a Celgard separator. The R2R ALD effectively deposited a uniform film at 90 °C, ensuring that the physical appearance remained constant. Then, the TMA precursor and water vapor were utilized for the growth of the Al_2O_3 layer. Later, the ALD-treated Celgard separator was examined by field emission SEM (FESEM) and XPS. The obtained results indicated that the separator porosity was maintained at 48%, without an appreciable impact on the pore size or total thickness of the synthesized separator. The ALD-treated Celgard separator demonstrated superior conformance, high flexibility, enhanced tensile strength, reduced thermal shrinkage, and great electrolyte wettability. The separator without the ALD layer rapidly shrunk soon after 120 °C thermal treatment, as shown in Fig. 23a. In contrast, the ALD-treated Celgard separator demonstrated remarkable thermal stability during a 1 h annealing process at 175 °C. Furthermore, TGA was used to determine the weight fractions of the ALD-treated separator, as illustrated in Fig. 23b. Figure 23c illustrates that the contact angle of the ALD-Celgard separator is smaller (34.5°) than that of the pristine separator (42.65°). Figure 23d presents the electrolyte uptake measured versus the soaking time. Compared to commercially existing separators, the proposed separator exhibited improved electrolyte wettability. Additionally, coated separator and Celgard tensile strength studies were carried out, as illustrated in Fig. 23e. Compared to the Celgard separator, the proposed multilayer separator demonstrated great tensile strength. When used in a polar electrolyte, the cycling performance of LCO/graphite cells with the ALD-treated Celgard separator demonstrated improved capacity retention of approximately 85% and stability compared to the pristine Celgard separator, which provided a considerably low retention of 70%. In addition, the generated separator demonstrated exceptional stability at temperatures as high as 80 °C while maintaining a capacity of 140 mAh g^{-1} and comparably improved efficiency when examined at different C rates (0.2, 0.5, and 1 C).

Accordingly, the ALD technique has helped advance LIBs, such as improving their specific capacity, cycle life, rate performance, and forward and backward efficiency. Since ALD can be adopted on an industrial scale, it can play an important role in research on these batteries. All of the above issues clearly revealed efforts to use ALD to improve batteries. With this review, ALD is expected to provide great progress in advanced battery technology in future decades.

3.5 ALD of 3D TSSBs

The greatest solutions for powering autonomous microsystems that can run remotely for long periods of time are energy harvesting systems and all-solid-state rechargeable batteries. These systems could be used in implantable medical devices such as pacemakers, distributed sensor networks, and smart cards. TSSBs offer higher power and energy while guaranteeing safety. Despite tremendous progress in

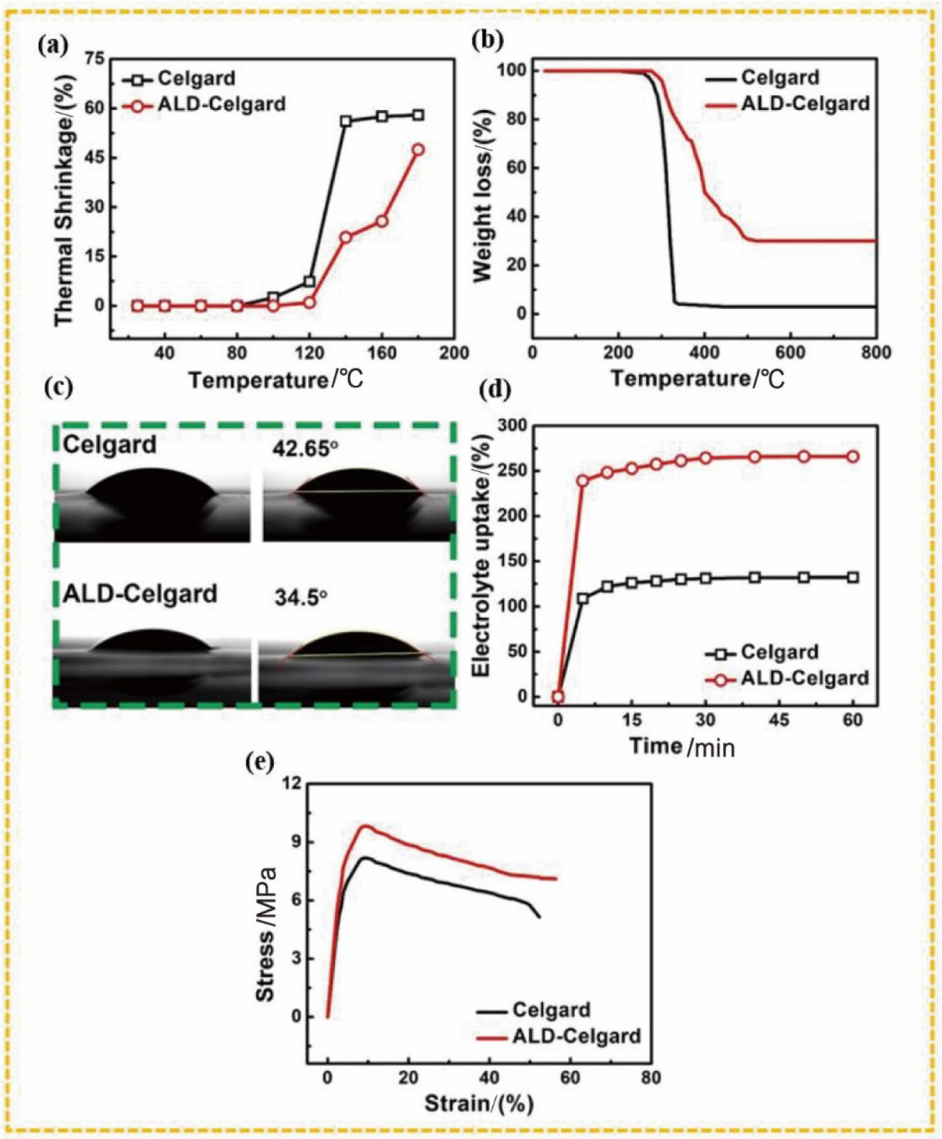

Fig. 23 **a** Shrinkage under thermal treatment (%) of bare Celgard and ALD-treated Celgard separators as a function of temperature between 20 °C and 180 °C. **b** TGA plots of bare Celgard and ALD-treated Celgard at 800 °C and 0 °C. **c** Images of the contact angle. **d** Profiles of electrolyte permeation. **e** Curves of the tensile strength of Celgard separators. Reprinted with permission from Ref. [317]. Copyright © 2020, Wiley

enhancing the performance of traditional LIBs, the use of liquid electrolytes hampers downsizing and combination with other standard Si-based microsystems. All-solid-state LIBs offer better safety due to their high temperature stability and low flammability, and they are compatible with Si-based on-chip integrated circuit (IC) production, have a very long lifespan, and self-discharge at very low rates.

Commercial TSSBs typically have a low areal energy density, which is generally less than 0.1 mAh cm^{-2} and restricts the performance and downsizing of standalone microsystems [318]. To store more energy, thickening the battery electrodes is one of the solutions, but this diminishes the energy capacity since the ions need to diffuse over longer distances, resulting in an inevitable tradeoff. Moreover, the fracture toughness of electrodes, such as cracking and delamination [319], limits the thickness. Therefore, TSSB synthesis on a 3D substrate has been suggested to enhance the surface area of electrodes per footprint area and the energy and power densities simultaneously. Moreover, a TSSB must be highly uniform, pinhole free, and electrically insulating to be a suitable conductor for Li ions. In this context, incorporating an ideal nanocoating method such as ALD capable of satisfying all requirements is essential.

Long et al. [320] developed the first successful TSSB in 2004 and highlighted the advantages of a 3D architecture as a structure-based strategy to concurrently increase the power and energy densities. Letiche et al. [321] claimed the first practical TSSB produced through ALD, in which Li_3PO_4 was deposited as an SSE by ALD (using LiO^tBu/TMP), and ionic conductivities on the order of 107 S cm^{-1} were attained at room temperature. Experimentally, four different films were coated on silicon single and double microtube structures with a high aspect ratio of 80:1, including an insulating layer of Al_2O_3 with a 120 nm thickness, a conducting

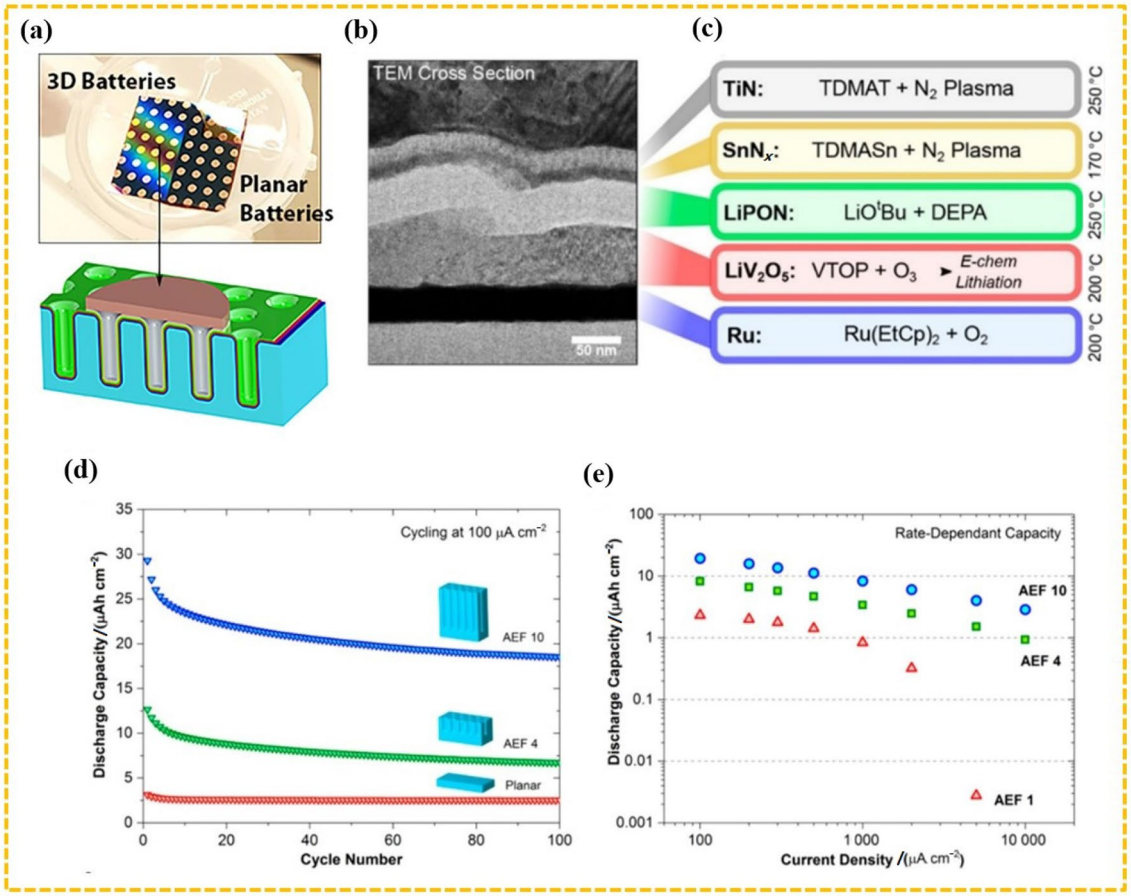

Fig. 24 **a** Optical image of the completed battery "chip". Each chip has two sides, one with 3D batteries and the other with planar batteries. **b** Cross-sectional TEM image of a fully ALD solid-state battery with 70 nm LiV_2O_5/40 nm Ru/25 nm TiN/10 nm SnN_x/50 nm Li_2PO_2N. **c** List of utilized precursors for the ALD process and temperature for each visible film in (b). **d** Cycling performance and electrochemical analysis of 3D solid-state batteries. **e** Discharge capacity as a function of the applied current density. Reprinted with permission from Ref. [288]. Copyright © 2018, American Chemical Society

layer of Pt with a 40 nm thickness, a 20–40 nm SSE layer of Li_3PO_4, and a 55–155 nm negative electrode layer of TiO_2. The obtained 3D solid-state microbatteries attained a great surface capacity of 0.37 mAh cm^{-2}, which is 105 times larger than that of their equivalents in thin film form of 3.5 Ah cm^{-2}. Pearse et al. [288] developed a completely conformal TSSB. The ALD method was used to deposit every component of an active battery, including electrodes, solid electrolytes, and current collectors, as demonstrated in Fig. 24a, b. LiO^tBu and DEPA precursors were used to create 40–100 nm Li_2PO_2N as an electrolyte. Three different substrate types, planar and Si trenches with aspect ratios of 4 and 10, were created and evaluated. The obtained electrochemical analysis results indicated a negligible capacity loss per cycle of approximately 0.02%. The Ru/LiV_2O_3/LiPON/SnN_x/TiN 3D TSSB showed an areal capacity of 37 Ah cm^{-2} (normalized to the cathode thickness). Figure 24e displays the evaluated rate performance of the three examined designs as a plot between 0.1 and 10 mA cm^{-2}, in which the applied current density was normalized by the wafer cell footprint area. By fabricating the cell in a conformal manner on 3D substrates, the whole cell areal discharge capacity was boosted by an order of magnitude, and its power performance was enhanced.

In a recent work published in 2017, Pearse et al. [303] developed the Li_2PO_2N SSE through ALD utilizing LiO^tBu/DEPA, which was utilized to create a solid-state flexible thin film battery. The ALD method was used to coat 90 nm Li_2PO_2N as the electrolyte of the battery. Then, as the cathode, 500 nm crystalline LCO was sputtered, and 80 nm Si was obtained as the anode through electron-beam vaporization. Additionally, the cathode and anode current collectors were made of thin films of Pt and Cu, respectively. The electrochemical performance of the resulting thin film battery cells was examined. The main electrochemical characteristics of the LCO/Si cells were visible in the initial three cycles of cyclic voltammetry (CV), which was performed in the voltage range from 2 to 4.4 V. The Li_2PO_2N thin films

were able to achieve a capacity of 20 Ah cm^{-2} at 50 Ah cm^{-2} and retained 65% of the capacity even while operating at 1 mAh cm^{-2} because of their lower resistance. This thin-film battery demonstrated high cyclability in addition to a constant CE of approximately 99.8% up to 150 cycles at a 300 A cm^{-2} current. Due to the irreversible nature of the Si anode, the reversible capacity in the steady state was only approximately 50% of the predicted LCO capacity after the first few cycles. ALD-V_2O_5 synthesized in the crystal form at 170 °C by utilizing a vanadium triisopropoxide precursor and ozone was used to replace the sputtered LCO, which required 700 °C annealing. A $LiClO_4$/propylene carbonate electrolyte was used to lithiate the generated V_2O_5 to form LiV_2O_5. This substitution enabled the creation of flexible electronics using metallized polyimide as the flexible substrate (Fig. 25a). A set of flexible solid-state batteries was then created by using 1 500 cycles of Li_2PO_2N and 40 nm thick Si. Moreover, the tolerance of the resulting cells to mild bending was examined. Then, at a current of 50 µA cm^{-2}, they were cycled 11 times and paused. The cells were subjected to cycling again after being stretched 10 times at a bending radius of 1 cm, revealing that they were electrically insulating and had a stable capacity of 1.6 µAh cm^{-2} (Fig. 25b). Although the actual capacity of the devices was very low for practical use, this study is noteworthy for two reasons: (1) ALD cathode fabrication at a low temperature and (2) a flexible polymer substrate.

Recent research by Put et al. [86] used H_2O/TMP/LiO^tBu/plasma N_2 to create thin-film LiPON solid-state batteries by ALD. Depositions were carried out on Si substrates covered with 70 nm sputtered TiN. Then, RF sputtering was used to deposit a 200 nm thick $Li_4Ti_5O_{12}$ layer, which was accompanied by an ALD LiPON film with a 70 nm thickness. The metallic lithium was then thermally evaporated to a thickness of 1 µm. The obtained $Li_4Ti_5O_{12}$/LiPON/Li cells (Fig. 25c) were evaluated at a rate of 5 C and in the voltage range from 0.8 to 2.6 V, and their capacity was found to be 0.3 Ah cm^{-3}. This research established the stability of 70 nm thick LiPON. In conclusion, ALD has proven to have several benefits for both adjusting electrode interfaces between pellet SSEs and electrodes and safeguarding Li metal anodes. Accordingly, ALD enables the development of 3D solid-state batteries because of its particular ability to produce uniform films

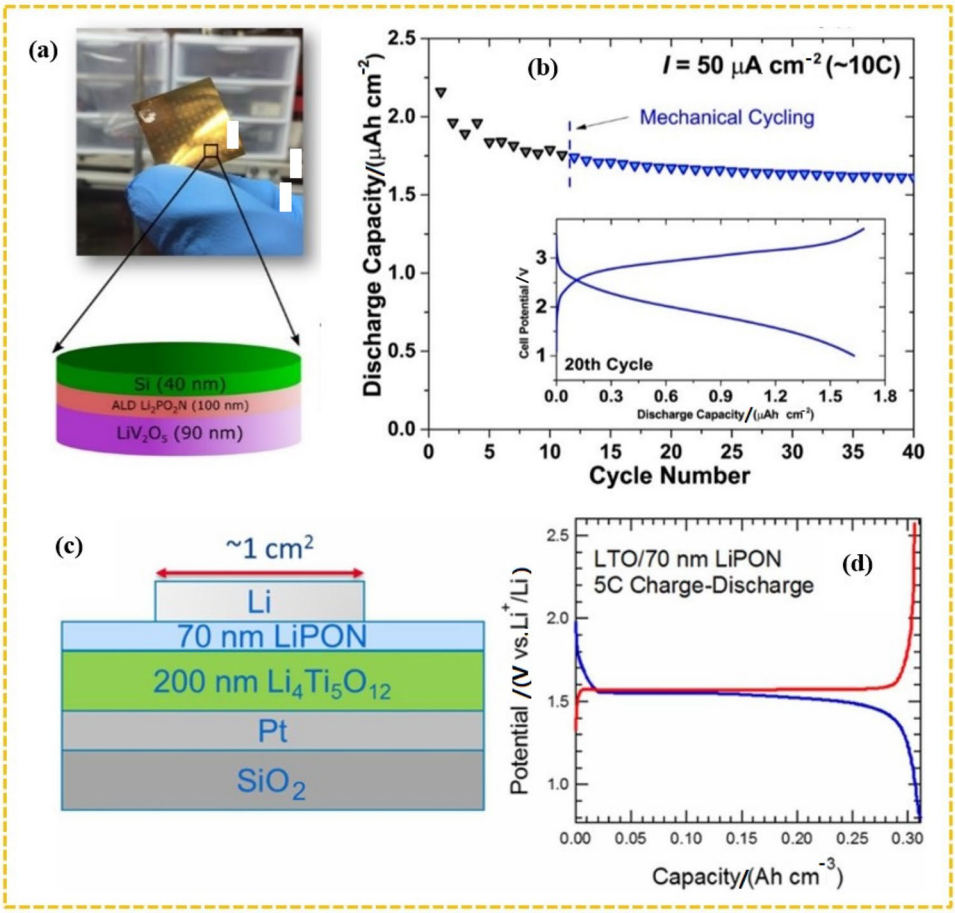

Fig. 25 A TSSB was used as a proof-of-concept to show how well ALD-lithium polyphosphazene (LPZ) works with polymer substrates. **a** Images of a sample with an array of solid-state cells that is both unbent and bent. **b** Demonstration of the battery electrochemical cycling stability; the charge/discharge plots are shown in the inset. Reprinted with permission from Ref. [303]. Copyright © 2017, American Chemical Society. **c** Solid-state cell shown schematically, consisting of an LTO cathode, a LiPON electrolyte, and a Li metal anode. **d** Charge−discharge behavior of the solid-state battery at the constant current indicated in (c) at a rate of 5 C; a 0.3 Ah cm^{-3} capacity is observed. Reprinted with permission from Ref. [86]. Copyright © 2019, The Electrochemical Society

of SSEs on high-aspect-ratio substrates. All these factors have made ALD a desirable method for advancing battery technology. Consequently, in light of this, the extraordinary conformality of ALD in combination with traditional semiconductor manufacturing techniques provides a path to realizing long-awaited 3D TSSBs that offer efficient power scaling over a wider range than that of planar form factor cells.

4 Future Perspectives

The future of batteries provides exciting opportunities for material scientists to inspect new methods and materials to improve battery performance, thus linking technology, and new materials and methods for different unique products can be discovered over time. At present, there is a significant idea to achieve potential technical progress through integrated material engineering to increase efficiency and reduce errors and research criteria, which has shown potential for rapid material exploration and incorporation of modern methods in commercial product development.

Future work on 3D TSSBs may employ a "mix-and-match" method for choosing materials and production techniques. Therefore, there is a great opportunity for ALD to build superionic SSEs in future research. Atomic-scale optimization of SSEs in terms of composition and crystallinity is anticipated by using the rational design capacity of ALD. Additionally, ALD is a perfect method for developing SSEs to advance the basics of solid-state ionics due to its atomic-scale precise development.

As the commonest and promising energy storage technologies, LIBs still need to overcome a number of obstacles in terms of cost, safety, energy density, and service life to maintain their leadership in the field of transportation applications. In tackling the problems related to LIBs, ALD shows extensive advantages over conventional approaches. Accordingly, we anticipate significant progress in this developing field because it places many new demands on conventional ALD technologies, including those related to the production capabilities, material diversity, and ALD coating characterization. In this setting, we carefully examined the most current ALD uses for LIBs in an effort to pique interest in them and encourage in-depth research in this developing field. As a result, new essential interests are predicted to inspire future research.

The ALD reactor in conventional ALD systems is an immovable, stationary, and small-sized flat chamber. ALD is a thin film technology that is especially well suited for growing nanoscale films on large substrates such as silicon wafers. Therefore, typical ALD reactors appear to be incapable of guaranteeing the bulk synthesis of powder-based nanomaterials, which is a crucial prerequisite for large-sized LIBs in upcoming HEVs, plug-in HEVs (PHEVs), and EVs. As a result, renovation of the ALD reactor design, such as in R2R ALD, should alter the current setups of ALD reactors. Consequently, more effort is needed to increase their manufacturing capability.

In this section, we present our views on future LIB production. We hope that such an article will help promote greater collaboration between industry and academia with the ultimate aim of addressing some of the key points of LIB production, which may ultimately increase its efficiency and reduce production costs and energy consumption.

5 Conclusion and Outlook

In this review, we give a broad overview of the principles and application of ALD technology in the development of LIBs. Currently, LIBs are the most widely utilized and competitive energy storage technology in devices and EVs. However, they still face critical challenges due to deviations in the manufacturing process of battery component materials. In recent decades, ALD has emerged as an advanced technology due to its atomic-scale precision and excellent conformal film deposition. In this way, electrode and SSE electrolyte material performance can be improved by adjusting the film thickness and optimizing the composition through a novel copulsing technique. In addition, ALD is a potential tool for the production and modification of high-performance electrode materials and SSEs of LIBs to accomplish tasks that are challenging or impossible to carry out with other conventional methods. Therefore, we have summarized the latest progress in research on LIBs using ALD nanotechnology with particular emphasis being placed on three areas: (i) synthesis of nanostructured LIB components; (ii) interface tailoring to optimize the surface and interfacial surroundings of LIB components; and (iii) modification of materials of LIB components, including the cathode, anode, electrolyte, and separator, and full-cell thin batteries, with the purpose of improving the electrochemical performance.

In terms of interface engineering, the properties of protective layers, such as the conductivity and thickness, affect Li-ion transport throughout the electrodes. In fact, ALD film materials may not be chemically inactive; for example, they can interact with electrode substrates during ALD processes and/or battery cycling. These phenomena could cause SEI layer formation, defect points on the cathode, etc. and consequently hamper the electrochemical performance of batteries. Hence, more research is required on the interaction mechanism to design better electrode structures. Further development of ALD technology significantly depends on the invention of new precursors and new reactor designs,

such as R2R ALD and PEALD, that facilitate the synthesis of different film composites, such as Li-containing layers, metal oxides, phosphates, and fluorides, that cannot be obtained by other methods. For example, PEALD enables a decrease in the processing temperature; therefore, films can be formed on electrode substrates with lower melting points, such as the S cathode and Li anode. Consequently, ALD is a promising technique for advancing the LIB performance parameters such as the specific capacity, cycle life, rate performance, and fast charge/discharge capability. Finally, we emphasize the importance of rational design of ALD systems for achieving large-scale manufacturing in the future. All of the above discussions clearly revealed efforts to use ALD to improve the LIB performance. Accordingly, with this review, ALD is expected to enable great progress in next-generation battery technology in future decades.

Acknowledgements The authors would like to acknowledge the financial support from the Global Excellence Statue (GES) Fellowship and National Research Foundation (NRF) of South Africa, which is gratefully acknowledged.

Funding Open access funding provided by University of Johannesburg.

Declarations

Conflict of interest The authors declare no conflict interest.

References

1. Ding, Y.L., Cano, Z.P., Yu, A.P., et al.: Automotive Li-ion batteries: current status and future perspectives. Electrochem. Energy Rev. **2**, 1–28 (2019). https://doi.org/10.1007/s41918-018-0022-z
2. Singh, K.V., Bansal, H.O., Singh, D.: A comprehensive review on hybrid electric vehicles: architectures and components. J. Mod. Transp. **27**, 77–107 (2019). https://doi.org/10.1007/s40534-019-0184-3
3. Laadjal, K., Cardoso, A.J.M.: Estimation of lithium-ion batteries state-condition in electric vehicle applications: issues and state of the art. Electronics **10**, 1588 (2021). https://doi.org/10.3390/electronics10131588
4. Solyali, D., Safaei, B., Zargar, O., et al.: A comprehensive state-of-the-art review of electrochemical battery storage systems for power grids. Int. J. Energy Res. **46**, 17786–17812 (2022). https://doi.org/10.1002/er.8451
5. Notter, D.A., Gauch, M., Widmer, R., et al.: Contribution of Li-ion batteries to the environmental impact of electric vehicles. Environ. Sci. Technol. **44**, 6550–6556 (2010). https://doi.org/10.1021/es903729a
6. Peters, J.F., Baumann, M., Zimmermann, B., et al.: The environmental impact of Li-ion batteries and the role of key parameters: a review. Renew. Sustain. Energy Rev. **67**, 491–506 (2017). https://doi.org/10.1016/j.rser.2016.08.039
7. Liu, M., Wang, C., Zhao, C.L., et al.: Quantification of the Li-ion diffusion over an interface coating in all-solid-state batteries via NMR measurements. Nat. Commun. **12**, 5943 (2021). https://doi.org/10.1038/s41467-021-26190-2
8. Duan, J., Tang, X., Dai, H., et al.: Building safe lithium-ion batteries for electric vehicles: a review. Electrochem. Energy Rev. **31**(3), 1–42 (2019). https://doi.org/10.1007/S41918-019-00060-4
9. Johnson, R.W., Hultqvist, A., Bent, S.F.: A brief review of atomic layer deposition: from fundamentals to applications. Mater. Today **17**, 236–246 (2014). https://doi.org/10.1016/j.mattod.2014.04.026
10. Suntola, T.: Atomic layer epitaxy. Mater. Sci. Rep. **4**, 261–312 (1989). https://doi.org/10.1016/S0920-2307(89)80006-4
11. Lin, S.X., Shi, X.Z., Zhang, X., et al.: Ternary semiconductor compounds $CuInS_2$ (CIS) thin films synthesized by electrochemical atomic layer deposition (EC-ALD). Appl. Surf. Sci. **256**, 4365–4369 (2010). https://doi.org/10.1016/j.apsusc.2010.02.032
12. Shin, J.W., Oh, S., Lee, S., et al.: ALD CeO_2-coated Pt anode for thin-film solid oxide fuel cells. Int. J. Hydrog. Energy **46**, 20087–20092 (2021). https://doi.org/10.1016/j.ijhydene.2021.03.133
13. Santasalo-Aarnio, A., Sairanen, E., Arán-Ais, R.M., et al.: The activity of ALD-prepared PtCo catalysts for ethanol oxidation in alkaline media. J. Catal. **309**, 38–48 (2014). https://doi.org/10.1016/j.jcat.2013.08.027
14. La Zara, D., Zhang, F.W., Sun, F.L., et al.: Drug powders with tunable wettability by atomic and molecular layer deposition: From highly hydrophilic to superhydrophobic. Appl. Mater. Today **22**, 100945 (2021). https://doi.org/10.1016/j.apmt.2021.100945
15. Wei, B., Chen, H.M., Hua, W.Q., et al.: Formation mechanism and photoelectric properties of Al_2O_3 film based on atomic layer deposition. Appl. Surf. Sci. **572**, 151419 (2022). https://doi.org/10.1016/j.apsusc.2021.151419
16. Lee, S.Y., Park, D., Yoon, B.S., et al.: Atomic layer deposition-based synthesis of TiO_2 and Al_2O_3 thin-film coatings on nanoparticle powders for sodium-ion batteries with enhanced cyclic stability. J. Alloys Compd. **897**, 163113 (2022). https://doi.org/10.1016/j.jallcom.2021.163113
17. Wan, X.K., Xu, Y.B., Wang, X.Y., et al.: Atomic layer deposition assisted surface passivation on bismuth vanadate photoanodes for enhanced solar water oxidation. Appl. Surf. Sci. **573**, 151492 (2022). https://doi.org/10.1016/j.apsusc.2021.151492
18. Urbanová, V., Plutnar, J., Pumera, M.: Atomic layer deposition of electrocatalytic layer of MoS_2 onto metal-based 3D-printed electrode toward tailoring hydrogen evolution efficiency. Appl. Mater. Today **24**, 101131 (2021). https://doi.org/10.1016/j.apmt.2021.101131
19. Sundberg, P., Karppinen, M.: Organic and inorganic–organic thin film structures by molecular layer deposition: a review. Beilstein J. Nanotechnol. **5**, 1104–1136 (2014). https://doi.org/10.3762/bjnano.5.123
20. Bazito, F.F.C., Torresi, R.M.: Cathodes for lithium ion batteries: the benefits of using nanostructured materials. J. Braz. Chem. Soc. **17**, 627–642 (2006). https://doi.org/10.1590/s0103-50532006000400002
21. Ren, Y., Yin, X.C., Xiao, R., et al.: Layered porous silicon encapsulated in carbon nanotube cage as ultra-stable anode for

lithium-ion batteries. Chem. Eng. J. **431**, 133982 (2022). https://doi.org/10.1016/j.cej.2021.133982
22. Zhao, Y., Zheng, K., Sun, X.L.: Addressing interfacial issues in liquid-based and solid-state batteries by atomic and molecular layer deposition. Joule **2**, 2583–2604 (2018). https://doi.org/10.1016/j.joule.2018.11.012
23. Imachi, N., Nakamura, H., Fujitani, S., et al.: Insertion of an insulating layer between cathode and separator for improving storage characteristics of Li-ion batteries. J. Electrochem. Soc. **159**, A269–A272 (2012). https://doi.org/10.1149/2.070203jes
24. Zhou, Q.B., Wang, L.L., Li, W.Y., et al.: Sodium superionic conductors (NASICONs) as cathode materials for sodium-ion batteries. Electrochem. Energy Rev. **4**, 793–823 (2021). https://doi.org/10.1007/s41918-021-00120-8
25. Deng, Z., Mo, Y.F., Ong, S.P.: Computational studies of solid-state alkali conduction in rechargeable alkali-ion batteries. NPG Asia Mater. **8**, e254 (2016). https://doi.org/10.1038/am.2016.7
26. Mishra, A., Mehta, A., Basu, S.M., et al.: Electrode materials for lithium-ion batteries. Mater. Sci. Energy Technol. **1**, 182–187 (2018). https://doi.org/10.1016/j.mset.2018.08.001
27. Mauger, A., Julien, C.: Surface modifications of electrode materials for lithium-ion batteries: status and trends. Ionics **20**, 751–787 (2014). https://doi.org/10.1007/s11581-014-1131-2
28. Stumpf, C.: Better batteries for a more sustainable world. Chemistry World, https://www.chemistryworld.com/sustainability/better-batteries-for-a-more-sustainable-world/4013747.article (2021). Accessed 4 April 2023
29. Reynolds, C.D., Slater, P.R., Hare, S.D., et al.: A review of metrology in lithium-ion electrode coating processes. Mater. Des. **209**, 109971 (2021). https://doi.org/10.1016/j.matdes.2021.109971
30. Neudeck, S., Mazilkin, A., Reitz, C., et al.: Effect of low-temperature Al_2O_3 ALD coating on Ni-rich layered oxide composite cathode on the long-term cycling performance of lithium-ion batteries. Sci. Rep. **9**, 5328 (2019). https://doi.org/10.1038/s41598-019-41767-0
31. Nisar, U., Muralidharan, N., Essehli, R., et al.: Valuation of surface coatings in high-energy density lithium-ion battery cathode materials. Energy Storage Mater. **38**, 309–328 (2021). https://doi.org/10.1016/j.ensm.2021.03.015
32. Mao, J., Ma, M.Z., Liu, P.P., et al.: The effect of cobalt doping on the morphology and electrochemical performance of high-voltage spinel $LiNi_{0.5}Mn_{1.5}O_4$ cathode material. Solid State Ion. **292**, 70–74 (2016). https://doi.org/10.1016/j.ssi.2016.05.008
33. Gao, Y., Xiong, K., Zhang, H.D., et al.: Effect of Ru doping on the properties of $LiFePO_4$/C cathode materials for lithium-ion batteries. ACS Omega **6**, 14122–14129 (2021). https://doi.org/10.1021/acsomega.1c00595
34. Kalaf, O., Solyali, D., Asmael, M., et al.: Experimental and simulation study of liquid coolant battery thermal management system for electric vehicles: a review. Int. J. Energy Res. **45**, 6495–6517 (2021). https://doi.org/10.1002/er.6268
35. Nisar, U., Petla, R., Ahmad Jassim Al-Hail, S., et al.: Impact of surface coating on electrochemical and thermal behaviors of a Li-rich $Li_{1.2}Ni_{0.16}Mn_{0.56}Co_{0.08}O_2$ cathode. RSC Adv. **10**, 15274–15281 (2020). https://doi.org/10.1039/d0ra02060e
36. Pender, J.P., Jha, G., Youn, D.H., et al.: Electrode degradation in lithium-ion batteries. ACS Nano **14**, 1243–1295 (2020). https://doi.org/10.1021/acsnano.9b04365
37. Qu, X.Y., Huang, H., Wan, T., et al.: An integrated surface coating strategy to enhance the electrochemical performance of nickel-rich layered cathodes. Nano Energy **91**, 106665 (2022). https://doi.org/10.1016/j.nanoen.2021.106665
38. Guan, P.Y., Zhou, L., Yu, Z.L., et al.: Recent progress of surface coating on cathode materials for high-performance lithium-ion batteries. J. Energy Chem. **43**, 220–235 (2020). https://doi.org/10.1016/j.jechem.2019.08.022
39. Luo, X.J., Ben, L.B.: Effect of MgO and Ta_2O_5 co-coatings on electrochemical performance of high-voltage spinel $LiNi_{0.5}Mn_{1.5}O_4$ cathode material. J. Alloys Compd. **810**, 151951 (2019). https://doi.org/10.1016/j.jallcom.2019.151951
40. Darjazi, H., Rezvani, S.J., Brutti, S., et al.: Improvement of structural and electrochemical properties of NMC layered cathode material by combined doping and coating. Electrochim. Acta **404**, 139577 (2022). https://doi.org/10.1016/j.electacta.2021.139577
41. Rajoba, S.J., Shirsat, A.N., Tyagi, D., et al.: Sol-gel assisted spinel $Li_4Ti_5O_{12}$ and its performance and stability as anode for long life Li-ion battery. Mater. Lett. **285**, 129134 (2021). https://doi.org/10.1016/j.matlet.2020.129134
42. Xu, H.M., Shen, H.J., Song, X.L., et al.: Hydrothermal synthesis of porous hydrangea-like $MnCo_2O_4$ as anode materials for high performance lithium ion batteries. J. Electroanal. Chem. **851**, 113455 (2019). https://doi.org/10.1016/j.jelechem.2019.113455
43. Liu, D., Chen, L.C., Liu, T.J., et al.: An effective mixing for lithium ion battery slurries. Adv. Chem. Eng. Sci. **4**, 515–528 (2014). https://doi.org/10.4236/aces.2014.44053
44. Hou, Q., Cao, G.Z., Wang, P., et al.: Carbon coating nanostructured-$LiNi_{1/3}Co_{1/3}Mn_{1/3}O_2$ cathode material synthesized by chemical vapor deposition method for high performance lithium-ion batteries. J. Alloys Compd. **747**, 796–802 (2018). https://doi.org/10.1016/j.jallcom.2018.03.115
45. Smaldone, A., Brutti, S., De Bonis, A., et al.: Iron doped $LiCoPO_4$ thin films for lithium-ion microbatteries obtained by ns pulsed laser deposition. Appl. Surf. Sci. **445**, 56–64 (2018). https://doi.org/10.1016/j.apsusc.2018.03.168
46. Liu, J.S., Bai, X.J., Hao, J., et al.: Efficient liberation of electrode materials in spent lithium-ion batteries using a cryogenic ball mill. J. Environ. Chem. Eng. **9**, 106017 (2021). https://doi.org/10.1016/j.jece.2021.106017
47. Wang, M.Y., Huang, Y., Wang, K., et al.: PVD synthesis of binder-free silicon and carbon coated 3D α-Fe_2O_3 nanorods hybrid films as high-capacity and long-life anode for flexible lithium-ion batteries. Energy **164**, 1021–1029 (2018). https://doi.org/10.1016/j.energy.2018.09.046
48. Li, J.J., Shen, J., Li, Z.Q., et al.: Wet chemical route to the synthesis of kesterite Cu_2ZnSnS_4 nanocrystals and their applications in lithium ion batteries. Mater. Lett. **92**, 330–333 (2013). https://doi.org/10.1016/j.matlet.2012.10.125
49. Tranquillo, E., Bollino, F.: Surface modifications for implants lifetime extension: an overview of sol-gel coatings. Coatings **10**, 589 (2020). https://doi.org/10.3390/coatings10060589
50. Dahmen, K.H.: Chemical vapor deposition. In: Encyclopedia of physical science and technology, pp. 787–808. Elsevier, Amsterdam (2003). https://doi.org/10.1016/b0-12-227410-5/00102-2
51. George, S.M.: Atomic layer deposition: an overview. Chem. Rev. **110**, 111–131 (2010). https://doi.org/10.1021/cr900056b
52. Meng, X.B.: Towards high-energy and durable lithium-ion batteries via atomic layer deposition: elegantly atomic-scale material design and surface modification. Nanotechnology **26**, 020501 (2015). https://doi.org/10.1088/0957-4484/26/2/020501
53. O'Neill, B.J., Jackson, D.H.K., Lee, J., et al.: Catalyst design with atomic layer deposition. ACS Catal. **5**, 1804–1825 (2015). https://doi.org/10.1021/cs501862h
54. Hossain, M.A., Khoo, K.T., Cui, X., et al.: Atomic layer deposition enabling higher efficiency solar cells: a review. Nano Mater. Sci. **2**, 204–226 (2020). https://doi.org/10.1016/j.nanoms.2019.10.001

55. Pakkala, A., Putkonen, M.: Atomic layer deposition. In: Handbook of Deposition Technologies for Films and Coatings, pp. 364–391. Elsevier, Amsterdam (2010). https://doi.org/10.1016/b978-0-8155-2031-3.00008-9
56. Weimer, A.W.: Particle atomic layer deposition. J. Nanopart. Res. **21**, 9 (2019). https://doi.org/10.1007/s11051-018-4442-9
57. Hirvikorpi, T., Vähä-Nissi, M., Nikkola, J., et al.: Thin Al_2O_3 barrier coatings onto temperature-sensitive packaging materials by atomic layer deposition. Surf. Coat. Technol. **205**, 5088–5092 (2011). https://doi.org/10.1016/j.surfcoat.2011.05.017
58. Sivagurunathan, A.T., Adhikari, S., Kim, D.H.: Strategies and implications of atomic layer deposition in photoelectrochemical water splitting: recent advances and prospects. Nano Energy **83**, 105802 (2021). https://doi.org/10.1016/j.nanoen.2021.105802
59. Tiurin, O., Solomatin, N., Auinat, M., et al.: Atomic layer deposition (ALD) of lithium fluoride (LiF) protective film on Li-ion battery $LiMn_{1.5}Ni_{0.5}O_4$ cathode powder material. J. Power Sources **448**, 227373 (2020). https://doi.org/10.1016/j.jpowsour.2019.227373
60. Dasgupta, N.P., Meng, X.B., Elam, J.W., et al.: Atomic layer deposition of metal sulfide materials. Acc. Chem. Res. **48**, 341–348 (2015). https://doi.org/10.1021/ar500360d
61. Zhang, H., Hagen, D.J., Li, X., et al.: Atomic layer deposition of cobalt phosphide for efficient water splitting. Angew. Chem. Int. Ed. **59**, 17172–17176 (2020). https://doi.org/10.1002/anie.202002280
62. Karg, M., Lokare, K.S., Limberg, C., et al.: Atomic layer deposition of silica on carbon nanotubes. Chem. Mater. **29**, 4920–4931 (2017). https://doi.org/10.1021/acs.chemmater.7b01165
63. Tai, X., Li, X.F., Kakimov, A., et al.: Optimized ALD-derived MgO coating layers enhancing silicon anode performance for lithium ion batteries. J. Mater. Res. **34**, 2425–2434 (2019)
64. Hwang, C.J.: ALD (atomic layer deposition) process technology in the semiconductor industry. Phys. High Technol. **21**, 37–41 (2012). https://doi.org/10.3938/PHIT.21.006
65. Johnson, A.L., Parish, J.D.: Recent developments in molecular precursors for atomic layer deposition. In: Organometallic chemistry, pp. 1–53. Royal Society of Chemistry, Cambridge (2018). https://doi.org/10.1039/9781788010672-00001
66. Tiurin, O., Ein-Eli, Y.: A critical review: the impact of the battery electrode material substrate on the composition and properties of atomic layer deposition (ALD) coatings. Adv. Mater. Interfaces **6**, 1901455 (2019). https://doi.org/10.1002/admi.201901455
67. Lee, Y., DuMont, J.W., George, S.M.: Trimethylaluminum as the metal precursor for the atomic layer etching of Al_2O_3 using sequential, self-limiting thermal reactions. Chem. Mater. **28**, 2994–3003 (2016). https://doi.org/10.1021/acs.chemmater.6b00111
68. Meng, X.B., Yang, X.Q., Sun, X.L.: Emerging applications of atomic layer deposition for lithium-ion battery studies. Adv. Mater. **24**, 1200397 (2012). https://doi.org/10.1002/adma.201200397
69. Tian, L., Bottala-Gambetta, I., Marchetto, V., et al.: Improved critical temperature of superconducting plasma-enhanced atomic layer deposition of niobium nitride thin films by thermal annealing. Thin Solid Films **709**, 138232 (2020). https://doi.org/10.1016/j.tsf.2020.138232
70. Cai, J.Y., Han, X.X., Wang, X., et al.: Atomic layer deposition of two-dimensional layered materials: processes, growth mechanisms, and characteristics. Matter **2**, 587–630 (2020). https://doi.org/10.1016/j.matt.2019.12.026
71. Charvot, J., Zazpe, R., Macak, J.M., et al.: Organoselenium precursors for atomic layer deposition. ACS Omega **6**, 6554–6558 (2021). https://doi.org/10.1021/acsomega.1c00223
72. Hornsveld, N., Kessels, W.M.M., Creatore, M.: Mass spectrometry study of Li_2CO_3 film growth by thermal and plasma-assisted atomic layer deposition. J. Phys. Chem. C **123**, 4109–4115 (2019). https://doi.org/10.1021/acs.jpcc.8b12216
73. Lee, J., Yoon, J., Kim, H.G., et al.: Highly conductive and flexible fiber for textile electronics obtained by extremely low-temperature atomic layer deposition of Pt. NPG Asia Mater. **8**, e331 (2016). https://doi.org/10.1038/am.2016.182
74. Putkonen, M., Aaltonen, T., Alnes, M., et al.: Atomic layer deposition of lithium containing thin films. J. Mater. Chem. **19**, 8767–8771 (2009). https://doi.org/10.1039/B913466B
75. Hämäläinen, J., Munnik, F., Hatanpää, T., et al.: Study of amorphous lithium silicate thin films grown by atomic layer deposition. J. Vac. Sci. Technol. A **30**, 01A106 (2012). https://doi.org/10.1116/1.3643349
76. Østreng, E., Vajeeston, P., Nilsen, O., et al.: Atomic layer deposition of lithium nitride and carbonate using lithium silylamide. RSC Adv. **2**, 6315–6322 (2012). https://doi.org/10.1039/C2RA20731A
77. Gregorczyk, K., Henn-Lecordier, L., Gatineau, J., et al.: Atomic layer deposition of ruthenium using the novel precursor bis(2, 6, 6-trimethyl-cyclohexadienyl)ruthenium. Chem. Mater. **23**, 2650–2656 (2011). https://doi.org/10.1021/cm2004825
78. Niskanen, A., Hatanpää, T., Ritala, M., et al.: Thermogravimetric study of volatile precursors for chemical thin film deposition. Estimation of vapor pressures and source temperatures. J. Therm. Anal. Calorim. **64**, 955–964 (2001)
79. Meng, X.B.: Atomic layer deposition of solid-state electrolytes for next-generation lithium-ion batteries and beyond: opportunities and challenges. Energy Storage Mater. **30**, 296–328 (2020). https://doi.org/10.1016/j.ensm.2020.05.001
80. Yahya, M.Z.A., Arof, A.K.: Conductivity and X-ray photoelectron studies on lithium acetate doped chitosan films. Carbohydr. Polym. **55**, 95–100 (2004). https://doi.org/10.1016/j.carbpol.2003.08.018
81. Huseynova, G., Shin, E.Y., Park, W.T., et al.: Lithium benzoate doped high performance n-type diketopyrrolopyrrole based organic thin-film transistors. Dyes Pigments **162**, 243–248 (2019). https://doi.org/10.1016/j.dyepig.2018.10.032
82. Merchant, K.J.: Potassium trimethylsilanolate mediated hydrolysis of nitriles to primary amides. Tetrahedron Lett. **41**, 3747–3749 (2000). https://doi.org/10.1016/S0040-4039(00)00482-2
83. Meng, X.B.: Atomic and molecular layer deposition in pursuing better batteries. J. Mater. Res. **36**, 2–25 (2021)
84. Ren, Q.Q., Yuan, Y.F., Wang, S.: Interfacial strategies for suppression of Mn dissolution in rechargeable battery cathode materials. ACS Appl. Mater. Interfaces (2021). https://doi.org/10.1021/acsami.1c20406
85. Li, X.F., Liu, J., Banis, M.N., et al.: Atomic layer deposition of solid-state electrolyte coated cathode materials with superior high-voltage cycling behavior for lithium ion battery application. Energy Environ. Sci. **7**, 768–778 (2014). https://doi.org/10.1039/C3EE42704H
86. Put, B., Mees, M.J., Hornsveld, N., et al.: Plasma-assisted ALD of LiPO(N) for solid state batteries. J. Electrochem. Soc. **166**, A1239–A1242 (2019). https://doi.org/10.1149/2.1191906jes
87. ForgeNano: ALD enabled batteries: making batteries better with particle atomic layer deposition with downloadable whitepaper. https://forgenano.com/ald-enabled-batteries-making-batteries-better-with-particle-atomic-layer-deposition-with-downloadable-whitepaper/
88. Song, J., Han, X.G., Gaskell, K.J., et al.: Enhanced electrochemical stability of high-voltage $LiNi_{0.5}Mn_{1.5}O_4$ cathode by surface modification using atomic layer deposition. J. Nanoparticle Res. **16**, 1–8 (2014). https://doi.org/10.1007/s11051-014-2745-z

89. Guan, C., Wang, J.: Recent development of advanced electrode materials by atomic layer deposition for electrochemical energy storage. Adv. Sci. **3**, 1500405 (2016). https://doi.org/10.1002/advs.201500405
90. Mohanty, D., Dahlberg, K., King, D.M., et al.: Modification of Ni-rich FCG NMC and NCA cathodes by atomic layer deposition: preventing surface phase transitions for high-voltage lithium-ion batteries. Sci. Rep. **6**, 26532 (2016). https://doi.org/10.1038/srep26532
91. Jung, Y.S., Lu, P., Cavanagh, A.S., et al.: Unexpected improved performance of ALD coated $LiCoO_2$/graphite Li-ion batteries. Adv. Energy Mater. **3**, 213–219 (2013). https://doi.org/10.1002/aenm.201200370
92. Gao, Y., Yu, H., Sandineni, P., et al.: Fe doping in $LiMn_{1.5}Ni_{0.5}O_4$ by atomic layer deposition followed by annealing: depths and occupation sites. J. Phys. Chem. C **125**, 7560–7567 (2021). https://doi.org/10.1021/acs.jpcc.1c00225
93. Dou, F., Shi, L.Y., Chen, G.R., et al.: Silicon/carbon composite anode materials for lithium-ion batteries. Electrochem. Energy Rev. **2**, 149–198 (2019)
94. Dahlberg, K., Trevey, J.E., Dameron, A., et al.: ALD-coated graphite anode materials for improved cycle life, calendar life, and safety of Li-ion cells. ECS Meet. Abstr. **MA2017–02**, 116 (2017). https://doi.org/10.1149/ma2017-02/1/116
95. Snyder, M.Q., Trebukhova, S.A., Ravdel, B., et al.: Synthesis and characterization of atomic layer deposited titanium nitride thin films on lithium titanate spinel powder as a lithium-ion battery anode. J. Power Sources **165**, 379–385 (2007). https://doi.org/10.1016/j.jpowsour.2006.12.015
96. Memarzadeh Lotfabad, E., Kalisvaart, P., Cui, K., et al.: ALD TiO_2 coated silicon nanowires for lithium ion battery anodes with enhanced cycling stability and coulombic efficiency. Phys. Chem. Chem. Phys. **15**, 13646–13657 (2013). https://doi.org/10.1039/c3cp52485j
97. Yesibolati, N., Shahid, M., Chen, W., et al.: SnO_2 anode surface passivation by atomic layer deposited HfO_2 improves Li-ion battery performance. Small **10**, 2849–2858 (2014). https://doi.org/10.1002/smll.201303898
98. Lu, Y., Zhang, Y.D., Zhang, Q., et al.: Recent advances in Ni-rich layered oxide particle materials for lithium-ion batteries. Particuology **53**, 1–11 (2020). https://doi.org/10.1016/j.partic.2020.09.004
99. Liu, T.C., Yu, L., Lu, J., et al.: Rational design of mechanically robust Ni-rich cathode materials via concentration gradient strategy. Nat. Commun. **12**, 6024 (2021). https://doi.org/10.1038/s41467-021-26290-z
100. Julien, C.M., Mauger, A.: NCA, NCM811, and the route to Ni-richer lithium-ion batteries. Energies **13**, 6363 (2020). https://doi.org/10.3390/en13236363
101. Lu, W., Liang, L.W., Sun, X., et al.: Recent progresses and development of advanced atomic layer deposition towards high-performance Li-ion batteries. Nanomaterials (Basel) **7**, 325 (2017). https://doi.org/10.3390/nano7100325
102. Eftekhari, A.: Aluminum oxide as a multi-function agent for improving battery performance of $LiMn_2O_4$ cathode. Solid State Ion. **167**, 237–242 (2004). https://doi.org/10.1016/j.ssi.2004.01.016
103. Welch, C., Mohammad, A.K., Hosmane, N.S., et al.: Effect of aluminum oxide on the performance of ionic liquid-based aluminum–air battery. Energies **13**, 2014 (2020). https://doi.org/10.3390/EN13082014
104. Luo, D., Fang, S.H., Tamiya, Y., et al.: Countering the segregation of transition-metal ions in $LiMn_{1/3}Co_{1/3}Ni_{1/3}O_2$ cathode for ultralong life and high-energy Li-ion batteries. Small **12**, 4421–4430 (2016). https://doi.org/10.1002/smll.201601923
105. Mohamed, N., Allam, N.K.: Recent advances in the design of cathode materials for Li-ion batteries. RSC Adv. **10**, 21662–21685 (2020). https://doi.org/10.1039/d0ra03314f
106. Piao, J.Y., Gu, L., Wei, Z.X., et al.: Phase control on surface for the stabilization of high energy cathode materials of lithium ion batteries. J. Am. Chem. Soc. **141**, 4900–4907 (2019). https://doi.org/10.1021/jacs.8b13438
107. Manthiram, A.: A reflection on lithium-ion battery cathode chemistry. Nat. Commun. **11**, 1550 (2020). https://doi.org/10.1038/s41467-020-15355-0
108. Mizushima, K., Jones, P.C., Wiseman, P.J., et al.: Li_xCoO_2 ($0<x<-1$): a new cathode material for batteries of high energy density. Mater. Res. Bull. **15**, 783–789 (1980). https://doi.org/10.1016/0025-5408(80)90012-4
109. Lyu, Y.C., Wu, X., Wang, K., et al.: An overview on the advances of $LiCoO_2$ cathodes for lithium-ion batteries. Adv. Energy Mater. **11**, 2000982 (2021). https://doi.org/10.1002/aenm.202000982
110. Liu, S., Liu, Z.P., Shen, X., et al.: Surface doping to enhance structural integrity and performance of Li-rich layered oxide. Adv. Energy Mater. **8**, 1802105 (2018). https://doi.org/10.1002/aenm.201802105
111. Kalluri, S., Yoon, M., Jo, M., et al.: Surface engineering strategies of layered $LiCoO_2$ cathode material to realize high-energy and high-voltage Li-ion cells. Adv. Energy Mater. **7**, 1601507 (2017). https://doi.org/10.1002/aenm.201601507
112. Jian, Z.L., Wang, W.T., Wang, M.Y., et al.: Al_2O_3 coated $LiCoO_2$ as cathode for high-capacity and long-cycling Li-ion batteries. Chin. Chem. Lett. **29**, 1768–1772 (2018). https://doi.org/10.1016/j.cclet.2018.11.002
113. Moon, S.H., Kim, M.C., Kim, E.S., et al.: TiO_2-coated $LiCoO_2$ electrodes fabricated by a sputtering deposition method for lithium-ion batteries with enhanced electrochemical performance. RSC Adv. **9**, 7903–7907 (2019). https://doi.org/10.1039/c8ra10451d
114. Wang, D., Astruc, D.: The recent development of efficient Earth-abundant transition-metal nanocatalysts. Chem. Soc. Rev. **46**, 816–854 (2017). https://doi.org/10.1039/c6cs00629a
115. Julien, C., Mauger, A., Zaghib, K., et al.: Comparative issues of cathode materials for Li-ion batteries. Inorganics **2**, 132–154 (2014). https://doi.org/10.3390/inorganics2010132
116. Jo, M.R., Kim, Y., Yang, J., et al.: Triggered reversible phase transformation between layered and spinel structure in Manganese-based layered compounds. Nat. Commun. **10**, 3385 (2019). https://doi.org/10.1038/s41467-019-11195-9
117. Sun, H., Zhao, K.J.: Electronic structure and comparative properties of $LiNi_xMn_yCo_zO_2$ cathode materials. J. Phys. Chem. C **121**, 6002–6010 (2017). https://doi.org/10.1021/acs.jpcc.7b00810
118. Noerochim, L., Suwarno, S., Idris, N.H., et al.: Recent development of nickel-rich and cobalt-free cathode materials for lithium-ion batteries. Batteries **7**, 84 (2021). https://doi.org/10.3390/batteries7040084
119. Xu, R., Sun, H., de Vasconcelos, L.S., et al.: Mechanical and structural degradation of $LiNi_xMn_yCo_zO_2$Cathode in Li-ion batteries: an experimental study. J. Electrochem. Soc. **164**, A3333–A3341 (2017). https://doi.org/10.1149/2.1751713jes
120. Li, T.Y., Yuan, X.Z., Zhang, L., et al.: Degradation mechanisms and mitigation strategies of nickel-rich NMC-based lithium-ion batteries. Electrochem. Energy Rev. **3**, 43–80 (2020)
121. Xie, Y., Saubanère, M., Doublet, M.L.: Requirements for reversible extra-capacity in Li-rich layered oxides for Li-ion batteries. Energy Environ. Sci. **10**, 266–274 (2017). https://doi.org/10.1039/C6EE02328B
122. Chen, Q., Pei, Y., Chen, H.W., et al.: Highly reversible oxygen redox in layered compounds enabled by surface polyanions.

Nat. Commun. **11**, 3411 (2020). https://doi.org/10.1038/s41467-020-17126-3
123. Li, X.F., Xu, Y.L., Wang, C.L.: Suppression of Jahn-Teller distortion of spinel $LiMn_2O_4$ cathode. J. Alloys Compd. **479**, 310–313 (2009). https://doi.org/10.1016/j.jallcom.2008.12.081
124. Xia, H., Luo, Z.T., Xie, J.P.: Nanostructured $LiMn_2O_4$ and their composites as high-performance cathodes for lithium-ion batteries. Prog. Nat. Sci. Mater. Int. **22**, 572–584 (2012). https://doi.org/10.1016/j.pnsc.2012.11.014
125. Massé, R.C., Liu, C.F., Li, Y.W., et al.: Energy storage through intercalation reactions: electrodes for rechargeable batteries. Natl Sci Rev **4**, 26–53 (2017). https://doi.org/10.1093/nsr/nww093
126. Rajapakse, M., Karki, B., Abu, U.O., et al.: Intercalation as a versatile tool for fabrication, property tuning, and phase transitions in 2D materials. NPJ 2D Mater. Appl. **5**, 1–21 (2021). https://doi.org/10.1038/s41699-021-00211-6
127. Allen, J.L., Xu, K., Zhang, S.S., et al.: $LiMBO_3$ (M=Fe, Mn): potential cathode for lithium ion batteries. MRS Online Proc. Libr. **730**, 18 (2002)
128. Kalantarian, M.M., Hafizi-Barjini, M., Momeni, M.: Ab initio study of $AMBO_3$ (A = Li, Na and M = Mn, Fe Co, Ni) as cathode materials for Li-ion and Na-ion batteries. ACS Omega **5**, 8952–8961 (2020). https://doi.org/10.1021/acsomega.0c00718
129. Bini, M., Ferrari, S., Ferrara, C., et al.: Polymorphism and magnetic properties of Li_2MSiO_4 (M = Fe, Mn) cathode materials. Sci. Rep. **3**, 3452 (2013). https://doi.org/10.1038/srep03452
130. Yang, F., Xia, Z.C., Huang, S., et al.: High field phase transition of cathode material Li_2MnSiO_4 for lithium-ion battery. Mater. Res. Express **7**, 026104 (2020). https://doi.org/10.1088/2053-1591/ab5c39
131. Thackeray, M.M., Amine, K.: $LiMn_2O_4$ spinel and substituted cathodes. Nat. Energy **6**, 566 (2021). https://doi.org/10.1038/s41560-021-00815-8
132. Haik, O., Leifer, N., Samuk-Fromovich, Z., et al.: On the surface chemistry of $LiMO_2$ cathode materials (M=[MnNi] and[MnNiCo]): electrochemical, spectroscopic, and calorimetric studies. J. Electrochem. Soc. **157**, A1099 (2010). https://doi.org/10.1149/1.3474222
133. Liu, L., Zhou, M., Wang, X.Y., et al.: Synthesis and electrochemical performance of spherical FeF_3/ACMB composite as cathode material for lithium-ion batteries. J. Mater. Sci. **47**, 1819–1824 (2012)
134. Karapidakis, E., Vernardou, D.: Progress on V_2O_5 cathodes for multivalent aqueous batteries. Materials (Basel) **14**, 2310 (2021). https://doi.org/10.3390/ma14092310
135. Liu, J., Liu, W., Wan, Y.L., et al.: Facile synthesis of layered LiV_3O_8 hollow nanospheres as superior cathode materials for high-rate Li-ion batteries. RSC Adv. **2**, 10470–10474 (2012). https://doi.org/10.1039/C2RA20969A
136. Zhang, Y.N., Liu, Y.P., Liu, Z.H., et al.: MnO_2 cathode materials with the improved stability via nitrogen doping for aqueous zinc-ion batteries. J. Energy Chem. **64**, 23–32 (2022). https://doi.org/10.1016/j.jechem.2021.04.046
137. Chen, R.J., Zhao, T.L., Zhang, X.X., et al.: Advanced cathode materials for lithium-ion batteries using nanoarchitectonics. Nanoscale Horiz. **1**, 423–444 (2016). https://doi.org/10.1039/c6nh00016a
138. Huang, K.J., Ceder, G., Olivetti, E.A.: Manufacturing scalability implications of materials choice in inorganic solid-state batteries. Joule **5**, 564–580 (2021). https://doi.org/10.1016/j.joule.2020.12.001
139. Wang, L., Wu, H.H., Hu, Y.C., et al.: Environmental sustainability assessment of typical cathode materials of lithium-ion battery based on three LCA approaches. Processes **7**, 83 (2019). https://doi.org/10.3390/pr7020083
140. Eshetu, G.G., Zhang, H., Judez, X., et al.: Production of high-energy Li-ion batteries comprising silicon-containing anodes and insertion-type cathodes. Nat. Commun. **12**, 5459 (2021). https://doi.org/10.1038/s41467-021-25334-8
141. Guo, S.H., Li, Q., Liu, P., et al.: Environmentally stable interface of layered oxide cathodes for sodium-ion batteries. Nat. Commun. **8**, 135 (2017). https://doi.org/10.1038/s41467-017-00157-8
142. Chen, M.Z., Liu, Q.N., Wang, S.W., et al.: High-abundance and low-cost metal-based cathode materials for sodium-ion batteries: problems, progress, and key technologies. Adv. Energy Mater. **9**, 1803609 (2019). https://doi.org/10.1002/aenm.201803609
143. Jiang, S.S., Wang, Y.S.: Synthesis and characterization of vanadium-doped $LiFePO_4$@C electrode with excellent rate capability for lithium-ion batteries. Solid State Ion. **335**, 97–102 (2019). https://doi.org/10.1016/j.ssi.2019.03.002
144. Breuer, O., Chakraborty, A., Liu, J., et al.: Understanding the role of minor molybdenum doping in $LiNi_{0.5}Co_{0.2}Mn_{0.3}O_2$ electrodes: from structural and surface analyses and theoretical modeling to practical electrochemical cells. ACS Appl. Mater. Interfaces **10**, 29608–29621 (2018). https://doi.org/10.1021/acsami.8b09795
145. Edström, K., Gustafsson, T., Thomas, J.O.: The cathode–electrolyte interface in the Li-ion battery. Electrochim. Acta **50**, 397–403 (2004). https://doi.org/10.1016/j.electacta.2004.03.049
146. Jo, C.H., Cho, D.H., Noh, H.J., et al.: An effective method to reduce residual lithium compounds on Ni-rich $Li[Ni_{0.6}Co_{0.2}Mn_{0.2}]O_2$ active material using a phosphoric acid derived Li_3PO_4 nanolayer. Nano Res.**8**, 1464–1479 (2015). https://doi.org/10.1007/s12274-014-0631-8
147. Qian, J.W., Liu, L., Yang, J.X., et al.: Electrochemical surface passivation of $LiCoO_2$ particles at ultrahigh voltage and its applications in lithium-based batteries. Nat. Commun. **9**, 4918 (2018). https://doi.org/10.1038/s41467-018-07296-6
148. Kubicka, M., Bakierska, M., Świętosławski, M., et al.: The temperature effect on the electrochemical performance of sulfur-doped $LiMn_2O_4$ in Li-ion cells. Nanomaterials (Basel) **9**, 1722 (2019). https://doi.org/10.3390/nano9121722
149. Jin, C., Zhang, X.D., He, W., et al.: Effect of ion doping on the electrochemical performances of $LiFePO_4$–$Li_3V_2(PO_4)_3$ composite cathode materials. RSC Adv. **4**, 15332–15339 (2014). https://doi.org/10.1039/c3ra47734g
150. Wolfenstine, J., Allen, J.: Ni^{3+}/Ni^{2+} redox potential in $LiNiPO_4$. J. Power Sources **142**, 389–390 (2005). https://doi.org/10.1016/j.jpowsour.2004.11.024
151. Liu, G.Q., Wen, L., Liu, Y.M.: Spinel $LiNi_{0.5}Mn_{1.5}O_4$ and its derivatives as cathodes for high-voltage Li-ion batteries. J. Solid State Electrochem. **14**, 2191–2202 (2010)
152. Zhu, M.J., Li, J.G., Liu, Z.B., et al.: Preparation and electrochemical properties of $LiNi_{2/3}Co_{1/6}Mn_{1/6}O_2$ cathode material for lithium-ion batteries. Materials (Basel) **14**, 1766 (2021). https://doi.org/10.3390/ma14071766
153. Song, C.H., Wang, W.G., Peng, H.L., et al.: Improving the electrochemical performance of $LiNi_{0.80}Co_{0.15}Al_{0.05}O_2$ in lithium ion batteries by $LiAlO_2$ surface modification. Appl. Sci. **8**, 378 (2018). https://doi.org/10.3390/app8030378
154. Aliahmad, N., Biswas, P.K., Dalir, H., et al.: Synthesis of V_2O_5/single-walled carbon nanotubes integrated into nanostructured composites as cathode materials in high performance lithium-ion batteries. Energies **15**, 552 (2022). https://doi.org/10.3390/en15020552
155. Pei, F., Lin, L.L., Ou, D.H., et al.: Self-supporting sulfur cathodes enabled by two-dimensional carbon yolk-shell nanosheets for high-energy-density lithium-sulfur batteries. Nat. Commun. **8**, 482 (2017). https://doi.org/10.1038/s41467-017-00575-8
156. Hautier, G., Jain, A., Ong, S.P., et al.: Phosphates as lithium-ion battery cathodes: an evaluation based on high-throughput

ab initio calculations. Chem. Mater. **23**, 3495–3508 (2011). https://doi.org/10.1021/cm200949v
157. Donders, M.E., Arnoldbik, W.M., Knoops, H.C.M., et al.: Atomic layer deposition of $LiCoO_2$Thin-film electrodes for all-solid-state Li-ion micro-batteries. J. Electrochem. Soc. **160**, A3066–A3071 (2013). https://doi.org/10.1149/2.011305jes
158. Srur-Lavi, O., Miikkulainen, V., Markovsky, B., et al.: Studies of the electrochemical behavior of $LiNi_{0.80}Co_{0.15}Al_{0.05}O_2$ electrodes coated with $LiAlO_2$. J. Electrochem. Soc. **164**, A3266–A3275 (2017). https://doi.org/10.1149/2.1631713jes
159. Liu, J., Banis, M.N., Sun, Q., et al.: Rational design of atomic-layer-deposited $LiFePO_4$ as a high-performance cathode for lithium-ion batteries. Adv. Mater. **26**, 1401805 (2014). https://doi.org/10.1002/adma.201401805
160. Mukhopadhyay, A., Sheldon, B.W.: Deformation and stress in electrode materials for Li-ion batteries. Prog. Mater. Sci. **63**, 58–116 (2014). https://doi.org/10.1016/j.pmatsci.2014.02.001
161. Laskar, M.R., Jackson, D.H.K., Xu, S.Z., et al.: Atomic layer deposited MgO: a lower overpotential coating for $Li[Ni_{0.5}Mn_{0.3}Co_{0.2}]O_2$ cathode. ACS Appl. Mater. Interfaces **9**, 11231–11239 (2017). https://doi.org/10.1021/acsami.6b16562
162. Mackus, A.J.M., Schneider, J.R., MacIsaac, C., et al.: Synthesis of doped, ternary, and quaternary materials by atomic layer deposition: a review. Chem. Mater. **31**, 1142–1183 (2019). https://doi.org/10.1021/acs.chemmater.8b02878
163. Miikkulainen, V., Ruud, A., Østreng, E., et al.: Atomic layer deposition of spinel lithium manganese oxide by film-body-controlled lithium incorporation for thin-film lithium-ion batteries. J. Phys. Chem. C **118**, 1258–1268 (2014). https://doi.org/10.1021/jp409399y
164. Ming, H., Yan, Y.R., Ming, J., et al.: Gradient V_2O_5 surface-coated $LiMn_2O_4$ cathode towards enhanced performance in Li-ion battery applications. Electrochim. Acta **120**, 390–397 (2014). https://doi.org/10.1016/j.electacta.2013.12.096
165. Aribia, A., Sastre, J., Chen, X.B., et al.: In situ lithiated ALD niobium oxide for improved long term cycling of layered oxide cathodes: a thin-film model study. J. Electrochem. Soc. **168**, 040513 (2021). https://doi.org/10.1149/1945-7111/abf215
166. Li, G., Yang, Z.X., Yang, W.S.: Effect of $FePO_4$ coating on electrochemical and safety performance of $LiCoO_2$ as cathode material for Li-ion batteries. J. Power Sources **183**, 741–748 (2008). https://doi.org/10.1016/j.jpowsour.2008.05.047
167. Liu, J., Xiao, B.W., Banis, M.N., et al.: Atomic layer deposition of amorphous iron phosphates on carbon nanotubes as cathode materials for lithium-ion batteries. Electrochim. Acta **162**, 275–281 (2015). https://doi.org/10.1016/j.electacta.2014.12.158
168. Xie, M., Sun, X., Sun, H.T., et al.: Stabilizing an amorphous V_2O_5/carbon nanotube paper electrode with conformal TiO_2 coating by atomic layer deposition for lithium ion batteries. J. Mater. Chem. A **4**, 537–544 (2016). https://doi.org/10.1039/C5TA01949D
169. Østreng, E., Gandrud, K.B., Hu, Y., et al.: High power nanostructured V_2O_5 thin film cathodes by atomic layer deposition. J. Mater. Chem. A **2**, 15044–15051 (2014). https://doi.org/10.1039/C4TA00694A
170. Maximov, M., Nazarov, D., Rumyantsev, A., et al.: Atomic layer deposition of lithium–nickel–silicon oxide cathode material for thin-film lithium-ion batteries. Energies **13**, 2345 (2020). https://doi.org/10.3390/en13092345
171. Chen, X.Y., Pomerantseva, E., Banerjee, P., et al.: Ozone-based atomic layer deposition of crystalline V_2O_5 films for high performance electrochemical energy storage. Chem. Mater. **24**, 1255–1261 (2012). https://doi.org/10.1021/cm202901z
172. Chen, X.Y., Zhu, H.L., Chen, Y.C., et al.: MWCNT/V_2O_5 core/shell sponge for high areal capacity and power density Li-ion cathodes. ACS Nano **6**, 7948–7955 (2012). https://doi.org/10.1021/nn302417x
173. Sattar, T., Lee, S.H., Jin, B.S., et al.: Influence of Mo addition on the structural and electrochemical performance of Ni-rich cathode material for lithium-ion batteries. Sci. Rep. **10**, 8562 (2020). https://doi.org/10.1038/s41598-020-64546-8
174. Cheng, H.M., Wang, F.M., Chu, J.P., et al.: Enhanced cycleabity in lithium ion batteries: resulting from atomic layer depostion of Al_2O_3 or TiO_2 on $LiCoO_2$ electrodes. J. Phys. Chem. C **116**, 7629–7637 (2012). https://doi.org/10.1021/jp210551r
175. Fan, Q.L., Lin, K.J., Yang, S.D., et al.: Constructing effective TiO_2 nano-coating for high-voltage Ni-rich cathode materials for lithium ion batteries by precise kinetic control. J. Power Sources **477**, 228745 (2020). https://doi.org/10.1016/j.jpowsour.2020.228745
176. Kim, J.W., Kim, D.H., Oh, D.Y., et al.: Surface chemistry of $LiNi_{0.5}Mn_{1.5}O_4$ particles coated by Al_2O_3 using atomic layer deposition for lithium-ion batteries. J. Power Sources **274**, 1254–1262 (2015). https://doi.org/10.1016/j.jpowsour.2014.10.207
177. Wang, C.C., Lin, J.W., Yu, Y.H., et al.: Nanolaminated ZnO–TiO_2 coated lithium-rich layered oxide cathodes by atomic layer deposition for enhanced electrochemical performances. J. Alloys Compd. **842**, 155845 (2020). https://doi.org/10.1016/j.jallcom.2020.155845
178. Zhao, J.Q., Wang, Y.: Atomic layer deposition of epitaxial ZrO_2 coating on $LiMn_2O_4$ nanoparticles for high-rate lithium ion batteries at elevated temperature. Nano Energy **2**, 882–889 (2013). https://doi.org/10.1016/j.nanoen.2013.03.005
179. Zhou, Y., Lee, Y., Sun, H.X., et al.: Coating solution for high-voltage cathode: AlF_3 atomic layer deposition for freestanding $LiCoO_2$ electrodes with high energy density and excellent flexibility. ACS Appl. Mater. Interfaces **9**, 9614–9619 (2017). https://doi.org/10.1021/acsami.6b15628
180. Hämäläinen, J., Holopainen, J., Munnik, F., et al.: Lithium phosphate thin films grown by atomic layer deposition. J. Electrochem. Soc. **159**, A259–A263 (2012). https://doi.org/10.1149/2.052203jes
181. Li, W., Yang, L.S., Li, Y.J., et al.: Ultra-thin $AlPO_4$ layer coated $LiNi_{0.7}Co_{0.15}Mn_{0.15}O_2$ cathodes with enhanced high-voltage and high-temperature performance for lithium-ion half/full batteries. Front. Chem. **8**, 597 (2020). https://doi.org/10.3389/fchem.2020.00597
182. Cho, J., Kim, T.G., Kim, C., et al.: Comparison of Al_2O_3- and $AlPO_4$-coated $LiCoO_2$ cathode materials for a Li-ion cell. J. Power Sources **146**, 58–64 (2005). https://doi.org/10.1016/j.jpowsour.2005.03.118
183. Liu, Y., Liu, W.B., Zhu, M.Y., et al.: Coating ultra-thin TiN layer onto $LiNi_{0.8}Co_{0.1}Mn_{0.1}O_2$ cathode material by atomic layer deposition for high-performance lithium-ion batteries. J. Alloys Compd. **888**, 161594 (2021). https://doi.org/10.1016/j.jallcom.2021.161594
184. Hu, Y.Y., Lu, J., Feng, H.: Surface modification and functionalization of powder materials by atomic layer deposition: a review. RSC Adv. **11**, 11918–11942 (2021). https://doi.org/10.1039/d1ra00326g
185. Nandi, D.K., Sen, U.K., Choudhury, D., et al.: Atomic layer deposited MoS_2 as a carbon and binder free anode in Li-ion battery. Electrochim. Acta **146**, 706–713 (2014). https://doi.org/10.1016/j.electacta.2014.09.077
186. Henderick, L., Hamed, H., Mattelaer, F., et al.: Plasma enhanced atomic layer deposition of a (nitrogen doped) Ti phosphate coating for improved energy storage in Li-ion batteries. J. Power Sources **497**, 229866 (2021). https://doi.org/10.1016/j.jpowsour.2021.229866
187. Ahn, J., Jang, E.K., Yoon, S., et al.: Ultrathin ZrO_2 on $LiNi_{0.5}Mn_{0.3}Co_{0.2}O_2$ electrode surface via atomic layer deposition

for high-voltage operation in lithium-ion batteries. Appl. Surf. Sci. **484**, 701–709 (2019). https://doi.org/10.1016/j.apsusc.2019.04.123
188. Kang, Y.Q., Guo, X.G., Guo, Z.W., et al.: Phosphorus-doped lithium- and manganese-rich layered oxide cathode material for fast charging lithium-ion batteries. J. Energy Chem. **62**, 538–545 (2021). https://doi.org/10.1016/j.jechem.2021.04.026
189. Xiao, B.W., Wang, B.Q., Liu, J., et al.: Highly stable $Li_{1.2}Mn_{0.54}Co_{0.13}Ni_{0.13}O_2$ enabled by novel atomic layer deposited $AlPO_4$ coating. Nano Energy **34**, 120–130 (2017). https://doi.org/10.1016/j.nanoen.2017.02.015
190. Xiao, B.W., Liu, J., Sun, Q., et al.: Unravelling the role of electrochemically active $FePO_4$ coating by atomic layer deposition for increased high-voltage stability of $LiNi_{0.5}Mn_{1.5}O_4$ cathode material. Adv. Sci. (Weinh) **2**, 1500022 (2015). https://doi.org/10.1002/advs.201500022
191. Jung, Y.S., Cavanagh, A.S., Dillon, A.C., et al.: Enhanced stability of $LiCoO_2$ cathodes in lithium-ion batteries using surface modification by atomic layer deposition. J. Electrochem. Soc. **157**, A75 (2010). https://doi.org/10.1149/1.3258274
192. Park, J.S., Mane, A.U., Elam, J.W., et al.: Amorphous metal fluoride passivation coatings prepared by atomic layer deposition on $LiCoO_2$ for Li-ion batteries. Chem. Mater. **27**, 1917–1920 (2015). https://doi.org/10.1021/acs.chemmater.5b00603
193. Xie, J., Sendek, A.D., Cubuk, E.D., et al.: Atomic layer deposition of stable $LiAlF_4$ lithium ion conductive interfacial layer for stable cathode cycling. ACS Nano **11**, 7019–7027 (2017). https://doi.org/10.1021/acsnano.7b02561
194. Zhang, X.F., Belharouak, I., Li, L., et al.: Structural and electrochemical study of Al_2O_3 and TiO_2 coated $Li_{1.2}Ni_{0.13}Mn_{0.54}Co_{0.13}O_2$ cathode material using ALD. Adv. Energy Mater. **3**, 1299–1307 (2013). https://doi.org/10.1002/aenm.201300269
195. Kim, J.W., Travis, J.J., Hu, E.Y., et al.: Unexpected high power performance of atomic layer deposition coated $Li[Ni_{1/3}Mn_{1/3}Co_{1/3}]O_2$ cathodes. J. Power Sources **254**, 190–197 (2014). https://doi.org/10.1016/j.jpowsour.2013.12.119
196. Deng, S.X., Xiao, B.W., Wang, B.Q., et al.: New insight into atomic-scale engineering of electrode surface for long-life and safe high voltage lithium ion cathodes. Nano Energy **38**, 19–27 (2017). https://doi.org/10.1016/j.nanoen.2017.05.007
197. Cho, H.M., Chen, M.V., MacRae, A.C., et al.: Effect of surface modification on nano-structured $LiNi_{0.5}Mn_{1.5}O_4$ spinel materials. ACS Appl. Mater. Interfaces **7**, 16231–16239 (2015). https://doi.org/10.1021/acsami.5b01392
198. Wise, A.M., Ban, C.M., Weker, J.N., et al.: Effect of Al_2O_3 coating on stabilizing $LiNi_{0.4}Mn_{0.4}Co_{0.2}O_2$ cathodes. Chem. Mater. **27**, 6146–6154 (2015). https://doi.org/10.1021/acs.chemmater.5b02952
199. Xu, W., Wang, J.L., Ding, F., et al.: Lithium metal anodes for rechargeable batteries. Energy Environ. Sci. **7**, 513–537 (2014). https://doi.org/10.1039/C3EE40795K
200. Lin, D.C., Liu, Y.Y., Cui, Y.: Reviving the lithium metal anode for high-energy batteries. Nat. Nanotechnol. **12**, 194–206 (2017). https://doi.org/10.1038/nnano.2017.16
201. Cao, D.X., Sun, X., Li, Q., et al.: Lithium dendrite in all-solid-state batteries: growth mechanisms, suppression strategies, and characterizations. Matter **3**, 57–94 (2020). https://doi.org/10.1016/j.matt.2020.03.015
202. Ikonen, T., Kalidas, N., Lahtinen, K., et al.: Conjugation with carbon nanotubes improves the performance of mesoporous silicon as Li-ion battery anode. Sci. Rep. **10**, 5589 (2020). https://doi.org/10.1038/s41598-020-62564-0
203. Zhang, J.X., Xie, Z.W., Li, W., et al.: High-capacity graphene oxide/graphite/carbon nanotube composites for use in Li-ion battery anodes. Carbon **74**, 153–162 (2014). https://doi.org/10.1016/j.carbon.2014.03.017
204. Ozanam, F., Rosso, M.: Silicon as anode material for Li-ion batteries. Mater. Sci. Eng. B **213**, 2–11 (2016). https://doi.org/10.1016/j.mseb.2016.04.016
205. Wu, C.B., Wang, Y.W., Ma, G.Q., et al.: Enhanced rate capability of $Li_4Ti_5O_{12}$ anode material by a photo-assisted sol–gel route for lithium-ion batteries. Electrochem. Commun. **131**, 107119 (2021). https://doi.org/10.1016/j.elecom.2021.107119
206. Shi, X.Y., Yu, S.S., Deng, T., et al.: Unlock the potential of $Li_4Ti_5O_{12}$ for high-voltage/long-cycling-life and high-safety batteries: dual-ion architecture superior to lithium-ion storage. J. Energy Chem. **44**, 13–18 (2020). https://doi.org/10.1016/j.jechem.2019.09.015
207. Maranchi, J.P., Hepp, A.F., Evans, A.G., et al.: Interfacial properties of the a-Si/Cu: active-inactive thin-film anode system for lithium-ion batteries. J. Electrochem. Soc. **153**, A1246 (2006). https://doi.org/10.1149/1.2184753
208. Ryu, J., Hong, D., Lee, H.W., et al.: Practical considerations of Si-based anodes for lithium-ion battery applications. Nano Res. **10**, 3970–4002 (2017)
209. Sivashanmugam, A., Gopukumar, S., Thirunakaran, R., et al.: Novel $Li_4Ti_5O_{12}$/Sn nano-composites as anode material for lithium ion batteries. Mater. Res. Bull. **46**, 492–500 (2011). https://doi.org/10.1016/j.materresbull.2011.01.007
210. Nitta, N., Yushin, G.: High-capacity anode materials for lithium-ion batteries: choice of elements and structures for active particles. Part. Part. Syst. Charact. **31**, 317–336 (2014). https://doi.org/10.1002/ppsc.201300231
211. Liang, B., Liu, Y.P., Xu, Y.H.: Silicon-based materials as high capacity anodes for next generation lithium ion batteries. J. Power Sources **267**, 469–490 (2014). https://doi.org/10.1016/j.jpowsour.2014.05.096
212. Wang, H.S., Liu, Y.Y., Li, Y.Z., et al.: Lithium metal anode materials design: interphase and host. Electrochem. Energy Rev. **2**, 509–517 (2019)
213. Liu, B., Zhang, J.G., Xu, W.: Advancing lithium metal batteries. Joule **2**, 833–845 (2018). https://doi.org/10.1016/j.joule.2018.03.008
214. Cheng, Q., Okamoto, Y., Tamura, N., et al.: Graphene-like-graphite as fast-chargeable and high-capacity anode materials for lithium ion batteries. Sci. Rep. **7**, 14782 (2017). https://doi.org/10.1038/s41598-017-14504-8
215. Cheng, H., Shapter, J.G., Li, Y.Y., et al.: Recent progress of advanced anode materials of lithium-ion batteries. J. Energy Chem. **57**, 451–468 (2021). https://doi.org/10.1016/j.jechem.2020.08.056
216. Asenbauer, J., Eisenmann, T., Kuenzel, M., et al.: The success story of graphite as a lithium-ion anode material: fundamentals, remaining challenges, and recent developments including silicon (oxide) composites. Sustain. Energy Fuels **4**, 5387–5416 (2020). https://doi.org/10.1039/D0SE00175A
217. Luo, P., Zheng, C., He, J.W., et al.: Structural engineering in graphite-based metal-ion batteries. Adv. Funct. Mater. **32**, 2107277 (2022). https://doi.org/10.1002/adfm.202107277
218. Shah, R., Mittal, V., Matsil, E., et al.: Magnesium-ion batteries for electric vehicles: current trends and future perspectives. Adv. Mech. Eng. **13**, 168781402110033 (2021). https://doi.org/10.1177/16878140211003398
219. Wang, G.J., Gao, J., Fu, L.J., et al.: Preparation and characteristic of carbon-coated $Li_4Ti_5O_{12}$ anode material. J. Power Sources **174**, 1109–1112 (2007). https://doi.org/10.1016/j.jpowsour.2007.06.107
220. Lai, S.Y., Cavallo, C., Abdelhamid, M.E., et al.: Advanced and emerging negative electrodes for Li-ion capacitors: pragmatism

vs. performance. Energies **14**, 3010 (2021). https://doi.org/10.3390/en14113010
221. Wei, W., Wang, Z.H., Liu, Z., et al.: Metal oxide hollow nanostructures: fabrication and Li storage performance. J. Power Sources **238**, 376–387 (2013). https://doi.org/10.1016/j.jpowsour.2013.03.173
222. Madian, M., Eychmüller, A., Giebeler, L.: Current advances in TiO_2-based nanostructure electrodes for high performance lithium ion batteries. Batteries **4**, 7 (2018). https://doi.org/10.3390/batteries4010007
223. Bui, V.K.H., Pham, T.N., Hur, J., et al.: Review of ZnO binary and ternary composite anodes for lithium-ion batteries. Nanomater. Basel Switz. **11**, 2001 (2021). https://doi.org/10.3390/nano11082001
224. Casimir, A., Zhang, H.G., Ogoke, O., et al.: Silicon-based anodes for lithium-ion batteries: effectiveness of materials synthesis and electrode preparation. Nano Energy **27**, 359–376 (2016). https://doi.org/10.1016/j.nanoen.2016.07.023
225. Andersen, H.F., Foss, C.E.L., Voje, J., et al.: Silicon-Carbon composite anodes from industrial battery grade silicon. Sci. Rep. **9**, 14814 (2019). https://doi.org/10.1038/s41598-019-51324-4
226. Kim, H., Kweon, K.E., Chou, C.Y., et al.: On the nature and behavior of Li atoms in Si: a first principles study. J. Phys. Chem. C **114**, 17942–17946 (2010). https://doi.org/10.1021/jp104289x
227. Dai, L., Zhong, X., Zou, J., et al.: Highly ordered SnO_2 nanopillar array as binder-free anodes for long-life and high-rate Li-ion batteries. Nanomater. Basel Switz. **11**, 1307 (2021). https://doi.org/10.3390/nano11051307
228. Ma, Y.N., Li, W.J., Ji, S.D., et al.: Fabrication of bristlegrass-like VO_2(B)-ZnO heteroarchitectures as anode materials for lithium-ion batteries. Mater. Res. Express **4**, 085033 (2017). https://doi.org/10.1088/2053-1591/aa84c3
229. An, S.J., Li, J.L., Daniel, C., et al.: The state of understanding of the lithium-ion-battery graphite solid electrolyte interphase (SEI) and its relationship to formation cycling. Carbon **105**, 52–76 (2016). https://doi.org/10.1016/j.carbon.2016.04.008
230. Xu, B.L., Oudalov, A., Ulbig, A., et al.: Modeling of lithium-ion battery degradation for cell life assessment. IEEE Trans. Smart Grid **9**, 1131–1140 (2018). https://doi.org/10.1109/TSG.2016.2578950
231. Qi, W., Shapter, J.G., Wu, Q., et al.: Nanostructured anode materials for lithium-ion batteries: principle, recent progress and future perspectives. J. Mater. Chem. A **5**, 19521–19540 (2017). https://doi.org/10.1039/C7TA05283A
232. Kim, H., Lee, E.J., Sun, Y.K.: Recent advances in the Si-based nanocomposite materials as high capacity anode materials for lithium ion batteries. Mater. Today **17**, 285–297 (2014). https://doi.org/10.1016/j.mattod.2014.05.003
233. Fu, L.J., Liu, H., Li, C., et al.: Surface modifications of electrode materials for lithium ion batteries. Solid State Sci. **8**, 113–128 (2006). https://doi.org/10.1016/j.solidstatesciences.2005.10.019
234. Son, S.B., Kappes, B., Ban, C.M.: Surface modification of silicon anodes for durable and high energy lithium-ion batteries. Isr. J. Chem. **55**, 558–569 (2015). https://doi.org/10.1002/ijch.201400173
235. Tornheim, A., He, M.N., Su, C.C., et al.: The role of additives in improving performance in high voltage lithium-ion batteries with potentiostatic holds. J. Electrochem. Soc. **164**, A6366–A6372 (2017). https://doi.org/10.1149/2.0471701jes
236. Cao, Y.Q., Wang, S.S., Liu, C., et al.: Atomic layer deposition of ZnO/TiO_2 nanolaminates as ultra-long life anode material for lithium-ion batteries. Sci. Rep. **9**, 11526 (2019). https://doi.org/10.1038/s41598-019-48088-2
237. Yang, J.H., Sagar, R.U.R., Anwar, T., et al.: Graphene foam as a stable anode material in lithium-ion batteries. Int. J. Energy Res. **46**, 5226–5234 (2022). https://doi.org/10.1002/er.7514
238. Qin, L.G., Xu, H., Wang, D., et al.: Fabrication of lithiophilic copper foam with interfacial modulation toward high-rate lithium metal anodes. ACS Appl. Mater. Interfaces **10**, 27764–27770 (2018). https://doi.org/10.1021/acsami.8b07362
239. Song, Y., Hwang, J., Lee, S., et al.: Synthesis of a high-capacity NiO/Ni foam anode for advanced lithium-ion batteries. Adv. Eng. Mater. **22**, 2000351 (2020). https://doi.org/10.1002/ADEM.202000351
240. Cho, J.S.: Large scale process for low crystalline MoO_3-carbon composite microspheres prepared by one-step spray pyrolysis for anodes in lithium-ion batteries. Nanomater. **9**, 539 (2019). https://doi.org/10.3390/NANO9040539
241. Sun, Y., Huang, F.Z., Li, S.K., et al.: Novel porous starfish-like Co_3O_4@nitrogen-doped carbon as an advanced anode for lithium-ion batteries. Nano Res. **10**, 3457–3467 (2017). https://doi.org/10.1007/s12274-017-1557-8
242. Liu, Y., Yang, Y.F.: Recent progress of TiO_2-based anodes for Li ion batteries. J. Nanomater. **2016**, 2 (2016). https://doi.org/10.1155/2016/8123652
243. Xin, F.X., Whittingham, M.S.: Challenges and development of tin-based anode with high volumetric capacity for Li-ion batteries. Electrochem. Energy Rev. **3**, 643–655 (2020). https://doi.org/10.1007/s41918-020-00082-3
244. Liu, A.M., Liang, X.Y., Ren, X.F., et al.: Recent progress in MXene-based materials for metal-sulfur and metal-air batteries: potential high-performance electrodes. Electrochem. Energy Rev. **5**, 112–144 (2022). https://doi.org/10.1007/s41918-021-00110-w
245. Abbasi, N.M., Xiao, Y., Zhang, L., et al.: Heterostructures of titanium-based MXenes in energy conversion and storage devices. J. Mater. Chem. C **9**, 8395–8465 (2021). https://doi.org/10.1039/D1TC00327E
246. Forouzandeh, P., Pillai, S.C.: MXenes-based nanocomposites for supercapacitor applications. Curr. Opin. Chem. Eng. **33**, 100710 (2021). https://doi.org/10.1016/j.coche.2021.100710
247. Zhao, B., Mattelaer, F., Kint, J., et al.: Atomic layer deposition of ZnO–SnO_2 composite thin film: the influence of structure, composition and crystallinity on lithium-ion battery performance. Electrochim. Acta **320**, 134604 (2019). https://doi.org/10.1016/j.electacta.2019.134604
248. Mitrofanov, I., Nazarov, D., Koshtyal, Y., et al.: Nickel-cobalt oxide thin-films anodes for lithium-ion batteries. In: NANOCON 2020 Conference Proeedings, TANGER Ltd., October 2021
249. Han, L., Hsieh, C.T., Chandra Mallick, B., et al.: Recent progress and future prospects of atomic layer deposition to prepare/modify solid-state electrolytes and interfaces between electrodes for next-generation lithium batteries. Nanoscale Adv. **3**, 2728–2740 (2021). https://doi.org/10.1039/d0na01072c
250. Zhu, S.Y., Liu, J.Q., Sun, J.M.: Growth of ultrathin SnO_2 on carbon nanotubes by atomic layer deposition and their application in lithium ion battery anodes. Appl. Surf. Sci. **484**, 600–609 (2019). https://doi.org/10.1016/j.apsusc.2019.04.163
251. Zhu, S.Y., Xu, P.H., Liu, J.Q., et al.: Atomic layer deposition and structure optimization of ultrathin Nb_2O_5 films on carbon nanotubes for high-rate and long-life lithium ion storage. Electrochim. Acta **331**, 135268 (2020). https://doi.org/10.1016/j.electacta.2019.135268
252. Zhao, H.L., Gao, H.X., Li, B.Q., et al.: Atomic layer deposition of V_2O_5 on nitrogen-doped graphene as an anode for lithium-ion batteries. Mater. Lett. **252**, 215–218 (2019). https://doi.org/10.1016/j.matlet.2019.05.059
253. Zhu, S.Y., Liu, J.Q., Sun, J.M.: Precise growth of Al_2O_3/SnO_2/CNTs composites by a two-step atomic layer deposition and their

application as an improved anode for lithium ion batteries. Electrochim. Acta **319**, 490–498 (2019). https://doi.org/10.1016/j.electacta.2019.07.027
254. Wang, H.W., Jia, G.C., Guo, Y.Y., et al.: Atomic layer deposition of amorphous TiO_2 on carbon nanotube networks and their superior Li and Na ion storage properties. Adv. Mater. Interfaces **3**, 1600375 (2016). https://doi.org/10.1002/admi.201600375
255. Li, Y.L., Zhao, Y.T., Huang, G.S., et al.: ZnO nanomembrane/expanded graphite composite synthesized by atomic layer deposition as binder-free anode for lithium ion batteries. ACS Appl. Mater. Interfaces **9**, 38522–38529 (2017). https://doi.org/10.1021/acsami.7b11735
256. Gregorczyk, K.E., Kozen, A.C., Chen, X.Y., et al.: Fabrication of 3D core-shell multiwalled carbon nanotube@RuO_2 lithium-ion battery electrodes through a RuO_2 atomic layer deposition process. ACS Nano **9**, 464–473 (2015). https://doi.org/10.1021/nn505644q
257. Dhara, A., Sarkar, S.K., Mitra, S.: Controlled 3D carbon nanotube architecture coated with MoO_x material by ALD technique: a high energy density lithium-ion battery electrode. Adv. Mater. Interfaces **4**, 1700332 (2017). https://doi.org/10.1002/admi.201700332
258. Meng, X.B., Liu, J., Li, X.F., et al.: Atomic layer deposited $Li_4Ti_5O_{12}$ on nitrogen-doped carbon nanotubes. RSC Adv. **3**, 7285–7288 (2013). https://doi.org/10.1039/C3RA00033H
259. Miikkulainen, V., Nilsen, O., Laitinen, M., et al.: Atomic layer deposition of $Li_xTi_yO_z$ thin films. RSC Adv. **3**, 7537–7542 (2013). https://doi.org/10.1039/C3RA40745D
260. Ahmed, B., Anjum, D.H., Gogotsi, Y., et al.: Atomic layer deposition of SnO_2 on MXene for Li-ion battery anodes. Nano Energy **34**, 249–256 (2017). https://doi.org/10.1016/j.nanoen.2017.02.043
261. Nisula, M., Karppinen, M.: Atomic/molecular layer deposition of lithium terephthalate thin films as high rate capability Li-ion battery anodes. Nano Lett. **16**, 1276–1281 (2016). https://doi.org/10.1021/acs.nanolett.5b04604
262. Haag, J.M., Pattanaik, G., Durstock, M.F.: Nanostructured 3D electrode architectures for high-rate Li-ion batteries. Adv. Mater. **25**, 1205079 (2013). https://doi.org/10.1002/adma.201205079
263. Ye, J.C., Baumgaertel, A.C., Wang, Y.M., et al.: Structural optimization of 3D porous electrodes for high-rate performance lithium ion batteries. ACS Nano **9**, 2194–2202 (2015). https://doi.org/10.1021/nn505490u
264. Xu, Y., Wood, K., Coyle, J., et al.: Chemistry of electrolyte reduction on lithium silicide. J. Phys. Chem. C **123**, 13219–13224 (2019). https://doi.org/10.1021/acs.jpcc.9b02611
265. Su, Y.F., Chen, G., Chen, L., et al.: Advances and prospects of surface modification on nickel-rich materials for lithium-ion batteries. Chin. J. Chem. **38**, 1817–1831 (2020). https://doi.org/10.1002/cjoc.202000385
266. Yang, C.C., Shih, J.Y., Wu, M.Y.: Preparation of silicon oxide coated KS-6 graphite composite anode materials by sol-gel method in lithium ion batteries. Energy Procedia **61**, 1428–1433 (2014). https://doi.org/10.1016/j.egypro.2014.12.140
267. Zhao, B., Li, B.B., Wang, Z.X., et al.: Uniform Li deposition sites provided by atomic layer deposition for the dendrite-free lithium metal anode. ACS Appl. Mater. Interfaces **12**, 19530–19538 (2020). https://doi.org/10.1021/acsami.0c02153
268. Wang, M.M., Cheng, X.P., Cao, T.C., et al.: Constructing ultrathin TiO_2 protection layers via atomic layer deposition for stable lithium metal anode cycling. J. Alloys Compd. **865**, 158748 (2021). https://doi.org/10.1016/j.jallcom.2021.158748
269. Alaboina, P.K., Rodrigues, S., Rottmayer, M., et al.: In situ dendrite suppression study of nanolayer encapsulated Li metal enabled by zirconia atomic layer deposition. ACS Appl. Mater. Interfaces **10**, 32801–32808 (2018). https://doi.org/10.1021/acsami.8b08585
270. He, Y., Yu, X.Q., Wang, Y.H., et al.: Alumina-coated patterned amorphous silicon as the anode for a lithium-ion battery with high coulombic efficiency. Adv. Mater. **23**, 1102568 (2011). https://doi.org/10.1002/adma.201102568
271. Kozen, A.C., Lin, C.F., Pearse, A.J., et al.: Next-generation lithium metal anode engineering via atomic layer deposition. ACS Nano **9**, 5884–5892 (2015). https://doi.org/10.1021/acsnano.5b02166
272. Xiao, X.C., Lu, P., Ahn, D.: Ultrathin multifunctional oxide coatings for lithium ion batteries. Adv. Mater. **23**, 1101915 (2011). https://doi.org/10.1002/adma.201101915
273. Wei, D.H., Zhong, S.Y., Zhang, H., et al.: In situ construction of interconnected SnO_2/nitrogen-doped carbon@TiO_2 networks for lithium-ion half/full cells. Electrochim. Acta **290**, 312–321 (2018). https://doi.org/10.1016/j.electacta.2018.08.094
274. Wang, X.Y., Fan, L., Gong, D.C., et al.: Battery anodes: core-shell Ge@graphene@TiO_2 nanofibers as a high-capacity and cycle-stable anode for lithium and sodium ion battery. Adv. Funct. Mater. **26**, 1143 (2016). https://doi.org/10.1002/adfm.201670045
275. Cao, Y.Q., Meng, X.B., Elam, J.W.: Atomic layer deposition of Li_xAl_yS solid-state electrolytes for stabilizing lithium-metal anodes. ChemElectroChem **3**, 858–863 (2016). https://doi.org/10.1002/celc.201600139
276. Ahmed, B., Shahid, M., Nagaraju, D.H., et al.: Surface passivation of MoO_3 nanorods by atomic layer deposition toward high rate durable Li ion battery anodes. ACS Appl. Mater. Interfaces **7**, 13154–13163 (2015). https://doi.org/10.1021/acsami.5b03395
277. Liu, X., Sun, Q., Ng, A.M.C., et al.: An alumina stabilized graphene oxide wrapped SnO_2 hollow sphere LIB anode with improved lithium storage. RSC Adv. **5**, 100783–100789 (2015). https://doi.org/10.1039/C5RA22482A
278. Molina Piper, D., Son, S.B., Travis, J.J., et al.: Mitigating irreversible capacity losses from carbon agents via surface modification. J. Power Sources **275**, 605–611 (2015). https://doi.org/10.1016/j.jpowsour.2014.11.032
279. Guan, D.S., Ma, L.L., Pan, D.Q., et al.: Atomic layer deposition of alumina coatings onto SnS_2 for lithium-ion battery applications. Electrochim. Acta **242**, 117–124 (2017). https://doi.org/10.1016/j.electacta.2017.05.023
280. Guan, D.S., Yuan, C.: Enhancing the cycling stability of tin sulfide anodes for lithium ion battery by titanium oxide atomic layer deposition. J. Electrochem. Energy Convers. Storage **13**, 021004 (2016). https://doi.org/10.1115/1.4034809
281. Lv, X.X., Deng, J.J., Sun, X.H.: Cumulative effect of Fe_2O_3 on TiO_2 nanotubes via atomic layer deposition with enhanced lithium ion storage performance. Appl. Surf. Sci. **369**, 314–319 (2016). https://doi.org/10.1016/j.apsusc.2016.02.075
282. Cao, F., Xia, X.H., Pan, G.X., et al.: Construction of carbon nanoflakes shell on CuO nanowires core as enhanced core/shell arrays anode of lithium ion batteries. Electrochim. Acta **178**, 574–579 (2015). https://doi.org/10.1016/j.electacta.2015.08.055
283. Chu, Y.L., Shen, Y.B., Guo, F., et al.: Advanced characterizations of solid electrolyte interphases in lithium-ion batteries. Electrochem. Energy Rev. **3**, 187–219 (2020)
284. Ding, Z.L., Li, J.L., Li, J., et al.: Review—interfaces: key issue to be solved for all solid-state lithium battery technologies. J. Electrochem. Soc. **167**, 070541 (2020). https://doi.org/10.1149/1945-7111/ab7f84
285. Liu, J., Wang, S., Qie, Y., et al.: Identifying lithium fluorides for promising solid-state electrolyte and coating material of high-voltage cathode. Mater. Today Energy **21**, 100719 (2021). https://doi.org/10.1016/j.mtener.2021.100719

286. Zhang, T.F., He, W.J., Zhang, W., et al.: Designing composite solid-state electrolytes for high performance lithium ion or lithium metal batteries. Chem. Sci. **11**, 8686–8707 (2020). https://doi.org/10.1039/d0sc03121f
287. Oh, D.Y., Kim, D.H., Jung, S.H., et al.: Single-step wet-chemical fabrication of sheet-type electrodes from solid-electrolyte precursors for all-solid-state lithium-ion batteries. J. Mater. Chem. A **5**, 20771–20779 (2017). https://doi.org/10.1039/C7TA06873E
288. Pearse, A., Schmitt, T., Sahadeo, E., et al.: Three-dimensional solid-state lithium-ion batteries fabricated by conformal vapor-phase chemistry. ACS Nano **12**, 4286–4294 (2018). https://doi.org/10.1021/acsnano.7b08751
289. Han, X.G., Gong, Y.H., Fu, K.K., et al.: Negating interfacial impedance in garnet-based solid-state Li metal batteries. Nat. Mater. **16**, 572–579 (2017). https://doi.org/10.1038/nmat4821
290. Yan, P.F., Zheng, J.M., Liu, J., et al.: Tailoring grain boundary structures and chemistry of Ni-rich layered cathodes for enhanced cycle stability of lithium-ion batteries. Nat. Energy **3**, 600–605 (2018). https://doi.org/10.1038/s41560-018-0191-3
291. Tippens, J., Miers, J.C., Afshar, A., et al.: Visualizing chemomechanical degradation of a solid-state battery electrolyte. ACS Energy Lett. **4**, 1475–1483 (2019). https://doi.org/10.1021/acsenergylett.9b00816
292. Wang, B.Q., Liu, J., Sun, Q., et al.: Atomic layer deposition of lithium phosphates as solid-state electrolytes for all-solid-state microbatteries. Nanotechnology **25**, 504007 (2014). https://doi.org/10.1088/0957-4484/25/50/504007
293. Wang, B.Q., Liu, J., Norouzi Banis, M., et al.: Atomic layer deposited lithium silicates as solid-state electrolytes for all-solid-state batteries. ACS Appl. Mater. Interfaces **9**, 31786–31793 (2017). https://doi.org/10.1021/acsami.7b07113
294. Liu, J., Banis, M.N., Li, X.F., et al.: Atomic layer deposition of lithium tantalate solid-state electrolytes. J. Phys. Chem. C **117**, 20260–20267 (2013). https://doi.org/10.1021/jp4063302
295. Wang, B.Q., Zhao, Y., Banis, M.N., et al.: Atomic layer deposition of lithium niobium oxides as potential solid-state electrolytes for lithium-ion batteries. ACS Appl. Mater. Interfaces **10**, 1654–1661 (2018). https://doi.org/10.1021/acsami.7b13467
296. Wang, H.Y., Wang, F.M.: Electrochemical investigation of an artificial solid electrolyte interface for improving the cycleability of lithium ion batteries using an atomic layer deposition on a graphite electrode. J. Power Sources **233**, 1–5 (2013). https://doi.org/10.1016/j.jpowsour.2013.01.134
297. Kanno, R., Hata, T., Kawamoto, Y., et al.: Synthesis of a new lithium ionic conductor, thio-LISICON–lithium germanium sulfide system. Solid State Ion. **130**, 97–104 (2000). https://doi.org/10.1016/S0167-2738(00)00277-0
298. Seino, Y., Ota, T., Takada, K., et al.: A sulphide lithium super ion conductor is superior to liquid ion conductors for use in rechargeable batteries. Energy Environ. Sci. **7**, 627–631 (2014). https://doi.org/10.1039/C3EE41655K
299. Kozen, A.C., Pearse, A.J., Lin, C.F., et al.: Atomic layer deposition of the solid electrolyte LiPON. Chem. Mater. **27**, 5324–5331 (2015). https://doi.org/10.1021/acs.chemmater.5b01654
300. Perng, Y.C., Cho, J., Sun, S.Y., et al.: Synthesis of ion conducting $Li_xAl_ySi_zO$ thin films by atomic layer deposition. J. Mater. Chem. A **2**, 9566–9573 (2014). https://doi.org/10.1039/C3TA14928E
301. Hornsveld, N., Put, B., Kessels, W.M.M., et al.: Plasma-assisted and thermal atomic layer deposition of electrochemically active Li_2CO_3. RSC Adv. **7**, 41359–41368 (2017). https://doi.org/10.1039/c7ra07722j
302. Kazyak, E., Chen, K.H., Davis, A.L., et al.: Atomic layer deposition and first principles modeling of glassy Li_3BO_3-Li_2CO_3 electrolytes for solid-state Li metal batteries. J. Mater. Chem. A **6**, 19425–19437 (2018). https://doi.org/10.1039/c8ta08761j
303. Pearse, A.J., Schmitt, T.E., Fuller, E.J., et al.: Nanoscale solid state batteries enabled by thermal atomic layer deposition of a lithium polyphosphazene solid state electrolyte. Chem. Mater. **29**, 3740–3753 (2017). https://doi.org/10.1021/acs.chemmater.7b00805
304. Li, Y.F., Tan, Z.C.: Effects of a separator on the electrochemical and thermal performances of lithium-ion batteries: a numerical study. Energy Fuels **34**, 14915–14923 (2020). https://doi.org/10.1021/acs.energyfuels.0c02609
305. Sheng, L., Xu, R., Zhang, H., et al.: The morphology of polyethylene (PE) separator for lithium-ion battery tuned by the extracting process. J. Electroanal. Chem. **873**, 114391 (2020). https://doi.org/10.1016/j.jelechem.2020.114391
306. Liu, H.Y., Xu, J., Guo, B.H., et al.: Preparation and performance of silica/polypropylene composite separator for lithium-ion batteries. J. Mater. Sci. **49**, 6961–6966 (2014)
307. Hsu, W.D., Yang, P.W., Chen, H.Y., et al.: Preferential lattice expansion of polypropylene in a trilayer polypropylene/polyethylene/polypropylene microporous separator in Li-ion batteries. Sci. Rep. **11**, 1929 (2021). https://doi.org/10.1038/s41598-021-81644-3
308. Jang, J., Oh, J., Jeong, H., et al.: A review of functional separators for lithium metal battery applications. Materials (Basel) **13**, 4625 (2020). https://doi.org/10.3390/ma13204625
309. Shi, C., Dai, J.H., Li, C., et al.: A modified ceramic-coating separator with high-temperature stability for lithium-ion battery. Polymers **9**, 159 (2017). https://doi.org/10.3390/polym9050159
310. Jung, B., Lee, B., Jeong, Y.C., et al.: Thermally stable non-aqueous ceramic-coated separators with enhanced nail penetration performance. J. Power Sources **427**, 271–282 (2019). https://doi.org/10.1016/j.jpowsour.2019.04.046
311. Chao, C.Y., Feng, Y.F., Hua, K., et al.: Enhanced wettability and thermal stability of polypropylene separators by organic-inorganic coating layer for lithium-ion batteries. J. Appl. Polym. Sci. **135**, 46478 (2018). https://doi.org/10.1002/app.46478
312. Wang, X.R., Yushin, G.: Chemical vapor deposition and atomic layer deposition for advanced lithium ion batteries and supercapacitors. Energy Environ. Sci. **8**, 1889–1904 (2015). https://doi.org/10.1039/C5EE01254F
313. Lee, H., Yanilmaz, M., Toprakci, O., et al.: A review of recent developments in membrane separators for rechargeable lithium-ion batteries. Energy Environ. Sci. **7**, 3857–3886 (2014). https://doi.org/10.1039/C4EE01432D
314. Chen, H., Lin, Q., Xu, Q., et al.: Plasma activation and atomic layer deposition of TiO_2 on polypropylene membranes for improved performances of lithium-ion batteries. J. Membr. Sci. **458**, 217–224 (2014). https://doi.org/10.1016/j.memsci.2014.02.004
315. Shen, X., Li, C., Shi, C., et al.: Core-shell structured ceramic nonwoven separators by atomic layer deposition for safe lithium-ion batteries. Appl. Surf. Sci. **441**, 165–173 (2018). https://doi.org/10.1016/j.apsusc.2018.01.222
316. Chao, C.H., Hsieh, C.T., Ke, W.J., et al.: Roll-to-roll atomic layer deposition of titania coating on polymeric separators for lithium ion batteries. J. Power Sources **482**, 228896 (2021). https://doi.org/10.1016/j.jpowsour.2020.228896
317. Lee, J.W., Soomro, A.M., Waqas, M., et al.: A highly efficient surface modified separator fabricated with atmospheric atomic layer deposition for high temperature lithium ion batteries. Int. J. Energy Res. **44**, 7035–7046 (2020). https://doi.org/10.1002/er.5371
318. Nathan, M., Golodnitsky, D., Yufit, V., et al.: Three-dimensional thin-film Li-ion microbatteries for autonomous MEMS.

J. Microelectromechanical Syst. **14**, 879–885 (2005). https://doi.org/10.1109/JMEMS.2005.851860
319. Dudney, N.J.: Solid-state thin-film rechargeable batteries. Mater. Sci. Eng. B **116**, 245–249 (2005). https://doi.org/10.1016/j.mseb.2004.05.045
320. Long, J.W., Dunn, B., Rolison, D.R., et al.: Three-dimensional battery architectures. Chem. Rev. **104**, 4463–4492 (2004). https://doi.org/10.1021/cr0207401
321. Létiche, M., Eustache, E., Freixas, J., et al.: Atomic layer deposition of functional layers for on chip 3D Li-ion all solid state microbattery. Adv. Energy Mater. **7**, 1601402 (2017). https://doi.org/10.1002/aenm.201601402

Sina Karimzadeh is currently a Ph.D. candidate in Mechanical Engineering Science at the University of Johannesburg. His current research interest focuses on the development of solid-state Li-ion battery components including cathode, anode, solid-state electrolyte, and interface engineering by atomic layer deposition (ALD) technique. He has also been involved in a number of projects including Hydrogen Storage, Hydrogen Generation, Thin Films and Nanotechnology, Drug Delivery, Heat Transfer, Water Purification Membrane, Computational Modeling and Simulation. He is currently the Head of the ALD and innovation sub-research group and the Lead experimentalist at the JENANO ALD research center in the University of Johannesburg.

Babak Safaei currently is working as Associate Professor at the Department of Mechanical Engineering of Eastern Mediterranean University. Also, he has honorary position as Visiting Associate Professor at the University of Johannesburg since 2021. Presently, he is director of Nanotechnology and Multifunctional Structures Research Center (NMSRC) at Eastern Mediterranean University. He received his Ph.D. degree in Mechanical Engineering from the Department of Mechanical Engineering at Tsinghua University. His research interests focus on Computational Mechanics, Micro and Nano Mechanics, Advanced Manufacturing Technology, Design of Lightweight Structures, Composite and Nano Composite Materials, Lithium-Ion Batteries, Energy Storage Systems, and Renewable Energy.

Chris Yuan currently holds the Leonard Case Jr. Professorship in the Department of Mechanical and Aerospace Engineering at Case Western Reserve University. He is the Director of the Laboratory for Sustainable Energy Manufacturing at CWRU. His research interests are in sustainable manufacturing, scalable nanomanufacturing, lithium-ion batteries and electric vehicles.

Tien-Chien Jen is a Professor at the Department of Mechanical Engineering Science of University of Johannesburg and He is South Africa Research Chair of Innovation for Green Hydrogen (SARChI Chair). Before that he was a faculty member at the University of Wisconsin, Milwaukee. He is also the director of the newly established Atomic Layer Deposition Research Centre (JENANO) of the University of Johannesburg. He received his Ph.D. in Mechanical and Aerospace Engineering from UCLA. Moreover, he has received several competitive grants for his research, including those from the US National Science Foundation, the US Department of Energy, and the EPA. Furthermore, he has recently established a Joint Research Centre with Nanjing Tech University of China on the "Sustainable Materials and Manufacturing. In 2011, Prof. Jen was elected as a Fellow to the American Society of Mechanical Engineers (ASME), which recognized his contributions to the field of thermal science and manufacturing. In 2020, he was inducted to as the Academician of the Academy of Science of South Africa (AASAf) for his significant research contribution in the fields of thermal sciences and advanced manufacturing. His current research interests associated with developing ALD Thin Film Nanomaterials, Energy storage systems including Li-ion Batteries, Hydrogen Storage and Conversion, Sustainable Energy, Fuel Cells and Hydrogen Technology, Solar Cell, Cold Gas Dynamics Spraying, Heat and Mass Transfer, and Material Processing.